Signal Processing and Experimental Technology in Ultrasonic Flow Measurement

Department 12—Mechanical Engineering
University of Duisburg—Essen
Granted Dissertation for Acquisition of Academic Degree of

Doctor of Engineering

Submitted by M. Sc. Yaoying Lin
from Pingxiang, China

Date of oral examination: 30. November, 2004

Chariman: Prof. Dr.-Ing. D. Wissussek
Experts: Prof. Dr.-Ing. V. Hans
Prof. Dr.-Ing. R. Tracht
Prof. Dr.-Ing. L. Wang

Preface

This dissertation records all research work I have done in the past two years since I came to Germany and studied under the supervision of Professor Dr. Hans at the University of Duisburg-Essen.

First I must give special thanks to my supervisor, Professor Dr. Hans, for his help with my research work even after his retirement. That he is strict in research will be forever remembered by me and influence my future work. His optimistic character also helped me through the difficult period of time.

I'd like to thank Professor Dr. Tracht for taking time out of his tight schedule to review my dissertation. The discussion with him benefits both this dissertation and me myself so much that I will never forget. I must thank Professor Dr. Wang, at CDHK of Tongji University, Shanghai for his support and encouragement. It is he who gave me this chance to finish this dissertation in Germany.

I should also thank my colleagues in the Institute of Measurement and Control for their cooperation and friendly help.

Another special gratitude owes to my husband, from whom I always get support and understanding.

September 2004, in Essen

Yaoying Lin

Contents

Nomenclature

Value	Unit	Meaning
A	-	state matrix
A	m^2	pipe cross section area
a	V	amplitude
A_c	-	carrier amplitude
A_m	-	modulation signal amplitude
B	-	control matrix
C	-	observation matrix
C	-	carrier amplitude
D	m	pipe diameter
d	m	width of bluff body
d	m	distance between channels
E	V^2s	energy
E	-	expectation
F	-	transition matrix
F	-	Fourier transform
f_w	1/s	frequency of vortex shedding
f_s	1/s	sampling frequency
f_m	1/s	modulating frequency
$f_{sampling}$	1/s	sampling frequency
$f_{carrier}$	1/s	carrier frequency
f_H	1/s	Hilbert frequency
$\hat{f}(t)$	V	Hilbert transform of real signal
$f(t)$	V	real signal
G	-	weight matrix
H	-	Hilbert transform
H_n	-	weight function
$h(t)$	-	system weight function
Im	-	imaginary part of signal
j	-	complex prefix
Le	m	entrance length
LP	-	low pass filter

M	-	modulation amplitude
N	-	sampling number
n	-	speed dependent exponent
P	rad	initial phase angle
Q	-	covariance matrix of process noise
R	m	pipe radius
Re	-	Reynolds number
Re	-	real part of signal
r	m	velocity radius
r_{dev}	-	deviation factor
S_r	-	Strouhal number
s	V	voltage signal from the receiver
s	-	complex signal
sgn	-	signal function
t	s	time
T	s	sampling time
T	s	undersampling time
u_m	m/s	velocity of upstream
u	V	real part of signal
u(n)	-	initial state
$\overline{V}$	m/s	average flow velocity
v_{L}	m/s	linear average velocity
v_{meas}	m/s	measured velocity
v_{ref}	m/s	reference velocity
v(n)	-	noise vector
w	V	imaginary part of signal
w(n)	-	process noise
x	V	complex modulated signal
x	-	index number
X	-	analytic signal
x	-	real signal
$\hat{x}$	-	Hilbert transform of real signal
x(n)	-	input state vector

x(n+1)	-	following state
x(n)	-	current state
y(n)	-	system output
z	-	pipe length direction

Greek symbols

τ	s	transit time
Φ	-	correlation function
φ	rad	phase angle
α	-	absorption coefficient
ω_c	1/s	carrier frequency
ω_m‘	1/s	vortex shedding frequency

1 Introduction

The flow measurement plays a great role in the national domestic economy. A large amount of economy loss could be generated because of the inaccuracy of flow meter. For instance, in January of the year of 1999, 309.971 Terajoule natural gas was imported to Germany for 373 million DM. Among which, 3.7 million DM was more paid as a result of the inaccurate fluid measurement[48].

Ultrasonic flow measurement is gaining increasing popularity in the flowmeter market according to [42, 43]. This is partialy decided by the unique characteristics of ultrasonic flow measurement. Ultrasonic flow meters have such advantages as follows.

1. No pressure drop.
2. High frequency pulse rate of output minimizes errors from effects of pulsation and fluctuating flow.
3. Simple and inexpensive installation.
4. High sensitivity.
5. No moving parts in contact with flowing fluid.
6. Simple mechanical calibration easily checked without a throughout test.

In addition, ultrasound provides a key means to realize nonintrusive measurement for flow industry.

The ultrasonic meter category contains a number of different designs for measuring an average velocity in a flowing system. They are all based on an ultrasonic signal being changed by or reflected from the flowing stream velocity. Meter accuracy relates to the ability of the system to represent the average velocity over the whole stream passing through the meter body hydraulic area. This ability affects installation requirements and accuracy of results obtained.

Doppler flowmeter is a famous flowmeter which uses the ultrasonic system. It is used on liquids and gases with some type of entrained particles that are traveling at the same speed as the main body of flow. The ultrasonic signal is reflected from the stream, and the shift in the frequency is related to the average velocity of these particles over time.

The other kind of flowmeter using ultrasonic system is the cross correlation flowmeter which is one of the research key points in this work. It is principly based on stochastic signals. The transit

time is calculated from the cross correlation funtion of the two signals, upper stream and down stream respectively. In addition, the flow to be measured is assumed as Newtonian fluid which keeps its physical characteristic in a short time. The ultrasonic beam in the flow is modulated in amplitude as well as in phase. Hence, the so called complex modulated signal is proposed in this work. The previous works of several authors described much on the modulation which is called Quadrature Amplitude Modulation (QAM)[9,11,13]. In this work, the basic idea of complex modulation is inherited. But a different angle of view is taken. It intends to introduce analytic signal to model the complex modulation process. The analytic signal is obtained from the Hilbert Transform which was also referred to in the previous works but not so overall. Centering about the Hilbert Transform[16], a term, Undersampled Hilbert Transform is proposed in this work. The Hilbert Transform realized by software is also applied to the measurement. The results are displayed and discussed.

The demodulation of the complex modulated signal is always realized by Quadrature Amplitude Demodulation(QAD). The author Filips[11] tried using extended Kalman Filter to make phase demodulation in the flow measurement. Initial achievements were obtained. This work, based on that idea, developed other kinds of Kalman Filter to make both phase demodulation and amplitude modulation.

The other kind of flowmeter under research in this work is vortex flowmeter. Unlike the traditional vortex flowmeter, it is combined with ultrasonic system. First, an analog method of detecting vortex shedding frequency is described. What comes next is a method of calculating the transit time of the vortices. There are many factors influencing the sensitivity of the flowmeter. Some have been studied in previous works such as the different setups of bluff body, different shapes of bluff body and so on[10-12]. In this work, the inclination of bluff body with different ratios is studied in different setups. It aims to form a systematic knowledge to control the sensitivity and eventually the Strouhal number.

Almost all the flowmeters function well only in the fully developed flow. The measurement of the disturbed flow is a quasi-impenetratable problem for the flow industry. Previous authors also did some work on this branch but the result was not so systematic and clear. This work, in combination with different setups of bluff body, points out the better way to measure flow rate in

disturbed flow. It points out the better way to flatten and reshape the disturbed asymmetric flow profile so that it is closer to the well developed flow.

Chapter overview

This work, based on former works[9-13], describes the further research work on the flow measurment by means of ultrasound.

Chapter 2 elaborates on the technologies of the flow measurement both in history and in current days. Chapter 3 introduces the experimental setup based on which this research work is done. Chapter 4 introduces the analytic signal to model the complex modulated system. The different forms of Hilbert Transform are discussed. The measurement results both in cross correlation measurement and vortex measurement using different forms of Hilbert Transform are displayed and analyzed. Chapter 5 centers about improving the demodulation technique. Extended Kalman Filter[11, 18] is used to demodulate the complex modulated signals in cross correlation measurement as well as in vortex measurement. Chapter 6 deals with analog signal processing in the vortex flow measurement. Chapter 7 elaborated on the combination of vortex flow meter with cross correlation method. It ends up with the investigation of influence on modulation in vortex flow measurement by the size of bluff body. Chapter 8, by means of large amount of experimental data, displays the influence on the vortex measurement result caused by the inclination of bluff body. Chapter 9 taps into the disturbed flow measurement. Results are displayed under different types of pipe singularity.

2 Technologies in flow measurement

Flow measurement plays a great role in all aspects of social life. Flowmeter is the key element to flow measurement. For this reason, the different flowmeters are introduced in this section.

2.1 Classification of flowmeters

There are many flowmeters on the commercial market today, designed for a variety of industrial situations and employing several measurement methods. Different technologies are employed in different types of flowmeter. To understand the technologies in flow measurement, it is necessary to know the classification of flowmeters. For convenience, the concept of author Decarlo is borrowed in this work., that is, the flowmeters are divided into two categories according to the energy approch. They are: the extractive energy approach and the additive energy approach[1].

2.1.1 Extractive energy approach

This approach, just as its name implies, utilizes the energy of the flow itself. Therefore, there is always energy loss using this method. The differential-pressure-producing, or head-producing class of flowmeters belong to the oldest class of flowmeters in this range. There are many types of flowmeters in this class, the most conventional being the orifice, nozzle, and venturi flowmeters. Another class of flowmeters using this approach to flow measurement is the pulse-producing class. This class includes three basic types of flowmeters: positive-displacement type, current type, and fluid-dynamic type[1].

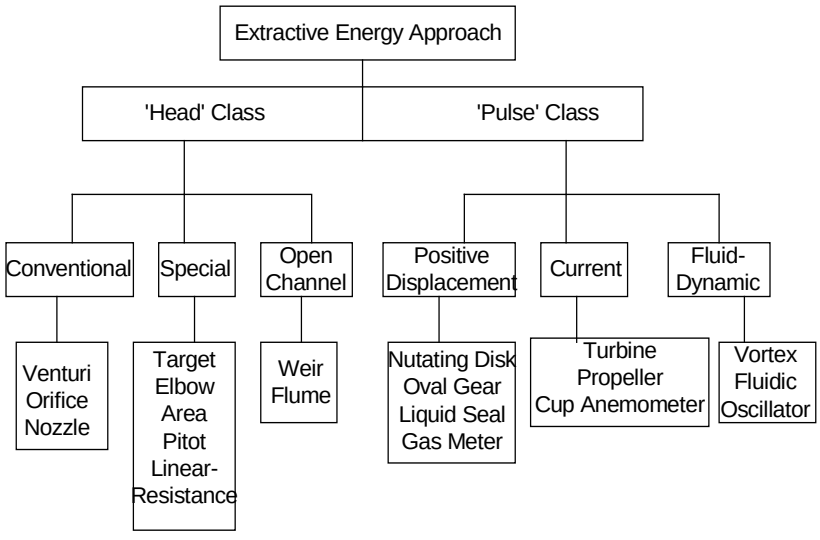

Fig. 2-1 Family tree of the Extractive Energy Approach to Flow measurement

The family tree of the head and pulse classes of flowmeters is provided in Fig.2-1. Two basic physical phenomena are employed in the fluid-dynamic-type flowmeter. They are vortex formation and the Coanda effect[1]. Both phenomena generate a digital or pulse output arising from the natural physics and dynamics of the fluid, hence the general category type fluid-dynamic flowmeters. Considering the current research, only the former will be discussed here.

The operating principle of the vortex meter is based on the natural phenomenon of vortex shedding. When a fluid flows past any obstacle, boundary layers of viscous, slow-moving fluid are formed along the outer surface. If the obstacle is unstreamlined, or it is a bluff body, the flow cannot follow the contours of the obstacle on the downstream side and the separated layers become detached and roll into eddies or vortices in the low pressure area behind the bluff body. The frequency of vortex shedding is directly proportional to the flow velocity, thus providing the basis of a flowmeter.

Vortex shedding is produced by the use of a blunt, normally flat-faced body placed perpendicular to the flowing fluid, as shown in Fig.2-2.

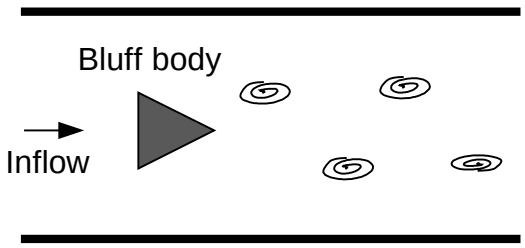

Fig. 2-2 Vortex shedding

As fluid passes blunt vortex generating element, the sharp corners cause a fixed point of fluid separation that forms a shear layer. In the shear layer, high-velocity gradients exist and the fluid whithin the layer is inherently unstable. After some length of travel, the fluid in the layer breaks down into well-formed vortices which is called vortex street. This phenomenon is von Karman vortex street phenomenon[21]. These vortices are formed and shed with a frequency linearly proportional to the flow rate. This fact had been known since 1878 when V. Strouhal observed that the frequency of eddies or vortices produced behind a bluff body increased with flowrate in

a linear fashion. The relation between the shedding frequency f_v and flow velocity u_m is described by

$$S_r = \frac{f_v \cdot d}{u_m}, \tag{2-1}$$

where S_r is Strouhal number[4] and d is the width of bluff body. The shedding frequency is generally measured by pressure sensors which has its own disadvantage[20, 24]. To overcome the disadvantage, ultrasonic is applied which is discussed in detail in this work[22].

2.1.2 Additive energy approach

The name of the approach itself indicates that this category of flowmeters use additional energy from outside in the flow measurement. Most often, the outside energy source is generated through the use of electrical power; however, nuclear power is used also. The three most

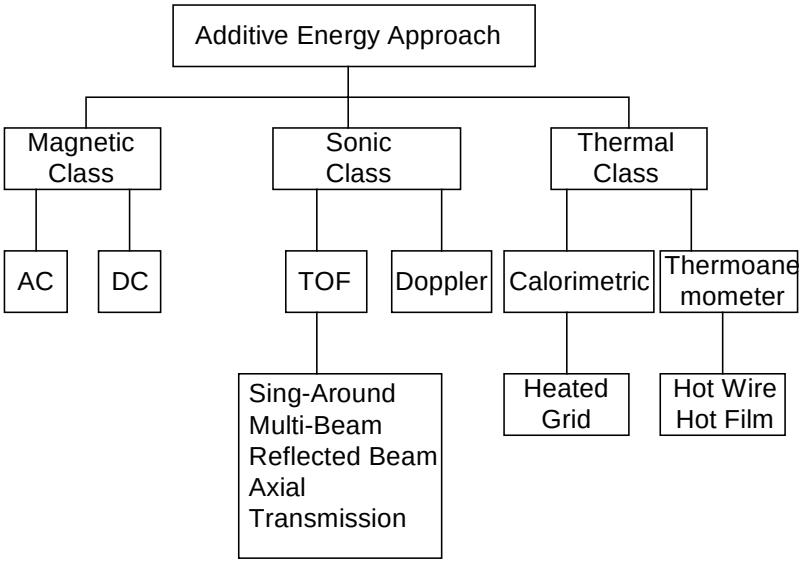

Fig. 2-3 Family tree of the additive energy approach to flow measurement (TOF=Time of flight)

prominent classes of flowmeters utilizing this approach to flow measurement are defined as the magnetic class, the sonic class, and the thermal class.

For a better review of the preceding discussion on the additive energy apporach to flow measurement, the family tree of the head and pulse classes of flowmeters is provided in Fig.2-3. There are two types of flowmeters in the magnetic class, the AC(alternating current type) and the

DC(direct current type). Both types use electricity to power an electromagnet which introduces the magnetic energy source into the flowing fluid.

In the thermal class of flow measurement, the flow rate is measured either by monitoring the cooling action of the flow on a heated body placed in the flow or by the transfer of heat energy between two points along the flow path. Here, the additive energy is heat, usually produced by an electrical source. Two types of flow measurement devices in the thermal class of flowmeters are the thermo-anemometer and the calorimetric flowmeter.

In the sonic class of flowmeters, there are two important types that deserve discussion: the time-of-flight(TOF), and the Doppler. For almost all of the sonic-class flowmeters, electrical energy is used to excite a piezoelectric or crystal-type material to its resonant frequency. This resonant frequency is transmitted in the form of a wave or pulse, travelling at the speed of sound, in the material the crystal is touching. If this wave is introduced into a fluid flowing in a pipe in such a way that the sound wave travels in opposite direction, shown in Fig.2-4, the difference in transit time of the wave is proportional to the fluid flow rate. This is because the velocity components of the fluid and of the ultrasound are superposed as vectors.

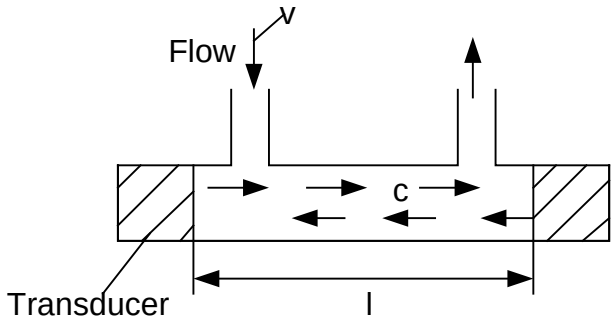

Fig. 2-4 One method of measuring transit time using ultrasonic beam

The Doppler effect, discovered in 1842 and commonly used today in radar systems and depth gauges(Sonar), is useful in medical and biological studies, some industrial pipeline applications, and marine applications. When an ultrasonic beam is projected into an inhomogeneous fluid, some acoustic energy is scattered back toward the transducer. Because the fluid is in motion with respect to the transducer and the scattered sound moves with the fluid, the received signal differs from the transmitted signal by a certain frequency referred to as the Doppler shift-frequency. This shift-frequency is directly proportional to the fluid flow rate. A schematic representation of the ultrasonic Doppler-type of sonic-class flowmeter is shown in Fig.2-5.

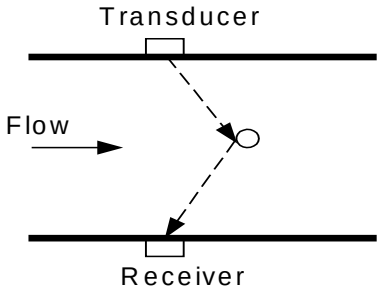

Fig. 2-5 Schematic of Doppler flowmeter

For both types of sonic class of flowmeters, electrical energy is used to excite a piezoelectric crystal type of material to a state of mechanical resonance. The crystal is either placed in contact with the fluid(wetted transducers) or mounted on the outside of the conduit containing the fluid(clamp-on transducers). As the crystal resonates, a sound wave traveling at the speed of sound of the media is generated and this sound wave is used to interrogate the flow field for the purpose of extracting the flow rate.

One of the first inventions of an acoustic contrapropagating transmission flow measurement apparatus for use in a pipe was patented in Germany by Rütten in 1928. In 1954, H. P. Kalmus measured flow velocity in a pipe using externally mounted transducers which he used for generating and detecting contrapropagating waves. However, it wasn't until the late 1970s that the ultrasonic flowmeter was introduced.

Several forms of the time-of-flight(TOF) ultrasonic flowmeter are shown in Fig.2-6, namely the axial transmission, multibeam, single-beam sing-around, reflected beam, and cross-beam forms[8].

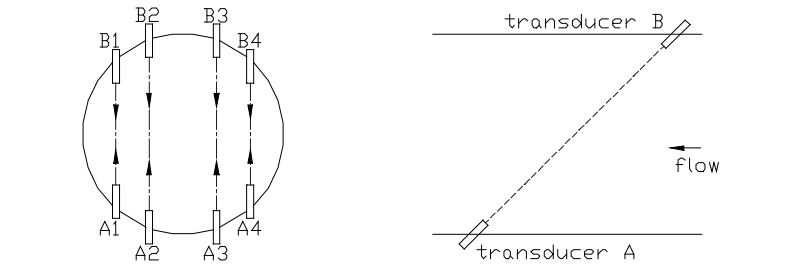

Multibeam contra-propagating type

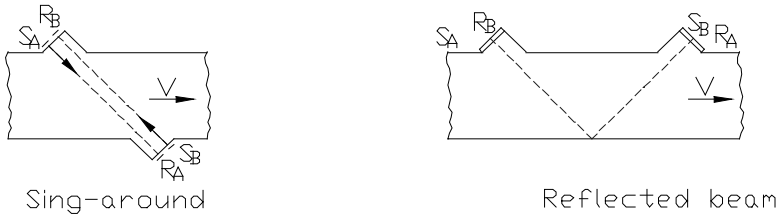

Fig. 2-6 Several forms of TOF ultrasonic flowmeters

Generally, the wetted transducer[33] devices are considered to be more accurate than the clamp-on flowmeters because of two factors, that is , the smaller angle of the sonic beam relative to the flow direction and lower transmission losses due to the absence of the pipe wall. In the wetted transducer arrangement, Fig.2-7, a 45° transmission angle is normally chosen to save the length of the pipe.

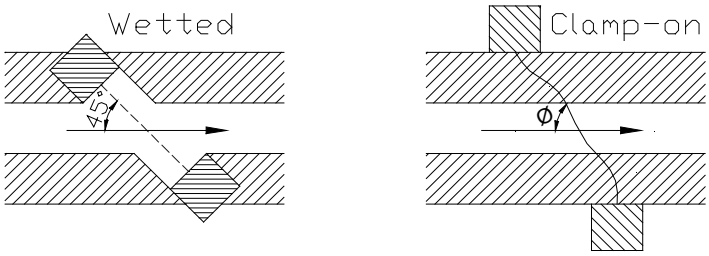

Fig. 2-7 Wetted and clamp-on transducer arrangement

Most common Doppler flowmeter configurations use the clamp-on arrangement because of the inherent advantages in being able to install or remove the device without interrupting the process and the fact that the transmission angle is not so critical as for the TOF flowmeters. To operate well, a Doppler flowmeter requires sufficient disturbances in the measured flow. A value of the

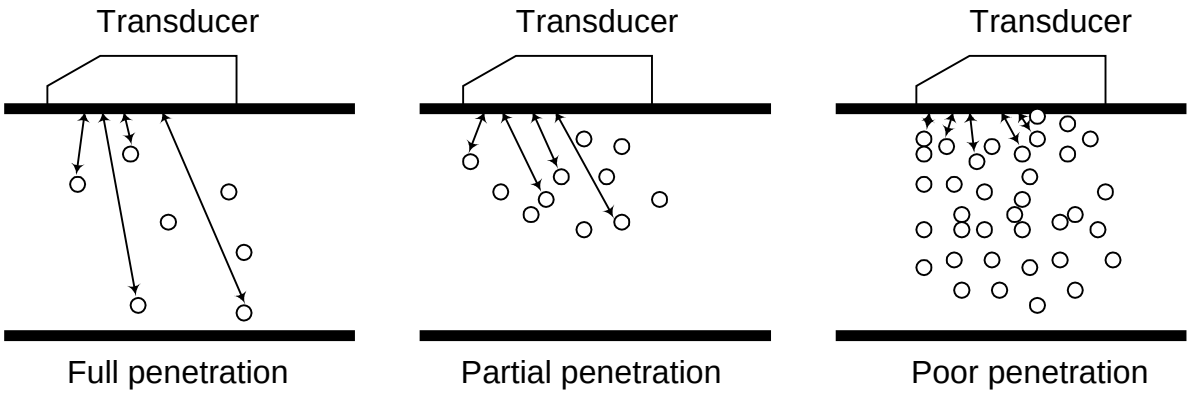

Fig. 2-8 Particle-concentration effect on Doppler sonic beam

minimum quantitiy of disturbance may be anywhere from 0.005% to 0.1% by volume depending on the fluid and type of particles present. The cross correlation measurement(CCF) using ultrasound studied in this work belongs also to the sonic class. The principle will be explained in detail in the next chapter.

2.2 Characteristics of ultrasonic flowmeters

Doppler and TOF ultrasonic flowmeters are in essence complimentary due to the fact that the former requires sufficient particles in the flow to reflect the ultrasonic beam while the latter requires a clean fluid to prevent the beam from being too much diverted. CCF requires that the characteristics of the flow to be measured does not change much in a short time.

Clamp-on or the wetted approach to sound transmission may be used in the above three flowmeters; however, clamp-on, although preferable from an application‘s point of view, may be less accurate as a flowmeter.

As to the accuracy, it is important to mention the sensitivity of three types of ultrasonic flowmeters to velocity profile changes. The TOF type, when a single transmission path is used, is line-averaging the velocity along the path of the sound transmission. Any velocity-profile change outside of the transmission path is not felt by the sonic beam. For greater accuracy in flows of changing asymmetric profiles, multiple beams may be used. CCF type has also the similar problem as for the TOF type. If the profile changes too much, the peak in the cross correlation function will be very small. That indicates the two signals have less similarity, which is a disadvantage for the precise measurement. Doppler flowmeter performance is normally affected by velocity-profile changes because the receivers normally detect multiple frequencies, the low frequencies coming from particles near the wall, and the high frequencies coming from particles in the center of the pipe. Signal processing techniques are used to weight each frequency to arrive at an integrated velocity. This works well for a homogeneous particle distribution, however, if particle concentration varies, severe errors may be incurred. For example, as shown in Fig. 2-8, an accurate flow-rate average is obtained if the beam penetrates the flow field; however, if signals are reflected primarily from particles in the center of the pipe, a high flow reading results, and if signals are reflected from particles near the wall, a low flow rate reading results. Consequently, the Doppler-type flowmeter performance is affected not only by profile shape as is the TOF, but also by the particle concentration distribution.

Because ultrasonic flowmeters are relatively new to such flowmeter standards as the orifice plate or venturi, there is a great deal of evolution at present in the technology. With the advent of sophisticated electronics and greater application experiences, no doubt overall performance in these devices will be improved on in the future.

3 Experimental setup and basic principle

The cross correlation measurement and vortex measurement combined with ultrasonic technique are thoroughly studied in this work based on the former research achievements[9-13]. Before describing the detailed problems such as signal processing and so on, it is better to briefly introduce the experimental setup and basic measurement principle.

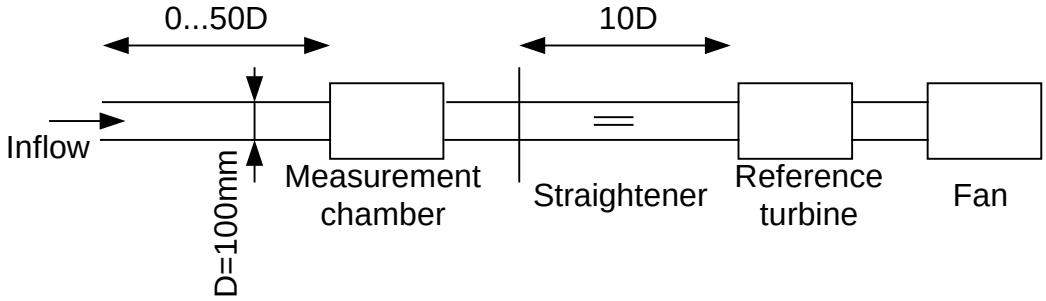

Fig. 3-1 Construction of the measurement equipment for ultrasonic flow measurement

For both kinds of ultrasonic flowmeters, the measurement equipment is constructed as shown in Fig.3-1. The pipe has a diameter of 100mm and is made of plexiglas. The fan at the end of the pipe can make the flow velocity reach maximum 35m/s. The turbine flowmeter, working as a reference, maintains its high precision up to 25m/s. The straightener straightens the disturbances in the flow before it flows into the reference. The measurement chamber which can be reconstructed for the aim of different flowmeters is installed between 0 and 50D behind the inflow. The distance of 50D is enough for a fully developed flow. In addition, other connections such as 90° bends with the pipe are also possible in order to form disturbed flow which will be detailedly discussed in chapter 9.

3.1Cross correlation measurement

3.1.1Setup

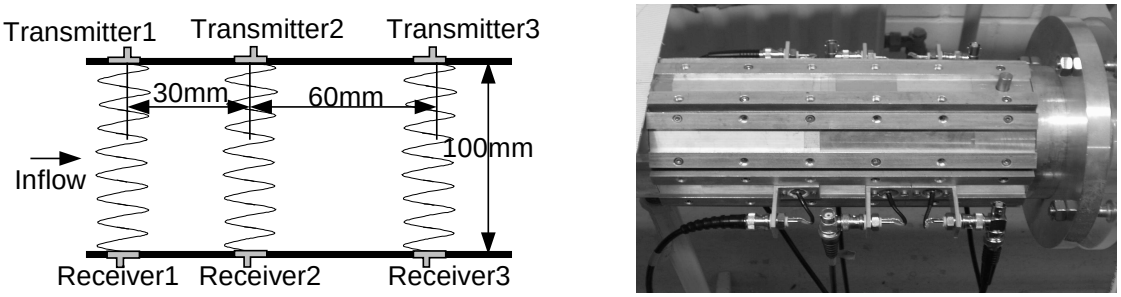

Fig. 3-2 Schematic and picture of measurement chamber for cross correlation measurement

Wetted transducers are applied to sense the modulation of the fluid which is air in a pipe in the present research. The pipe diameter is 100mm. The basic frequency of the ultrasonic beam is 220kHz. At least two pairs of sensors are required for the aim of cross correlation, but considering the dissipation of flow which influnces the cross correlation function of signals, three pairs of piezoelectric ultrasonic sensors are installed along the pipe wall axially. The sensor pairs are called channel 1, 2, 3 respectively from left to right. The correspondingly received signals are called s1,s2 and s3. The distances between each two channels are 30mm, 60mm respectively. The schematic and picture of the measurement chamber for cross correlation measurement is shown in Fig.3-2.

The point of maximum similarity between two signals from each of two channels is computed by using the mathematical cross-correlation function(CCF) Φ_{s1s2}[25,31]

$$\Phi_{s1s2} = \lim_{T\to\infty} \frac{1}{2T} \int_{-T}^{T} s_1(t) s_2(t-\tau) dt \tag{3-1}$$

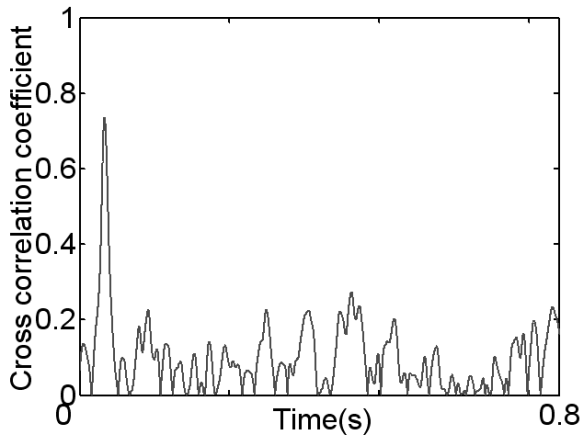

Fig. 3-3 Normalized result of the CCF between s1 and s2. The abscissa of the peak represents the transit time(velocity=2m/s, distance between channels is 90mm)

and the result can be directly read from the abscissa of the extremum of the CCF(Fig.3-3). With a known distance *d* between the barriers the average axial speed can be calculated by

$$\bar{v} = \frac{d}{\tau} \tag{3-2}$$

The ultrasonic beam with a frequency of 220kHz is emitted by a transmitter sensor. After being modulated by pipe flow, the received signal is first amplified and then transferred further to A/D converter. Sampling is carried out at the same time with the result of storing the sampled data in

the hard disk where cross correlation function can be calculated. The signal-flow diagram for the cross correlation flowmeter is shown in Fig.3-4.

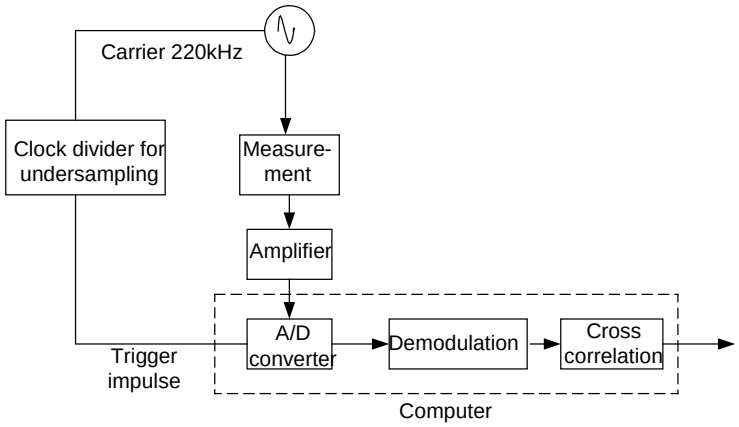

Fig. 3-4 Signal-flow diagram for the cross correlation measurement

3.1.2 Complex modulation

When a signal is modulated both by amplitude and phase, it is called complex modulation. The ultrasonic beam passing through the turbulent fluid is modulated in such a complex way. The complex modulated signal can be expressed by

$$x(t) = a(t)\cos(\omega_c t + \varphi(t)) \tag{3-3}$$

where a(t) reprensents the amplitude modulation while φ(t) represents the phase modulation[10]. According to Euler equation, this signal is the real part of the following complex function

$$s(t) = a(t) \cdot e^{j\varphi(t)} \cdot e^{j\omega_c t} \quad . \tag{3-4}$$

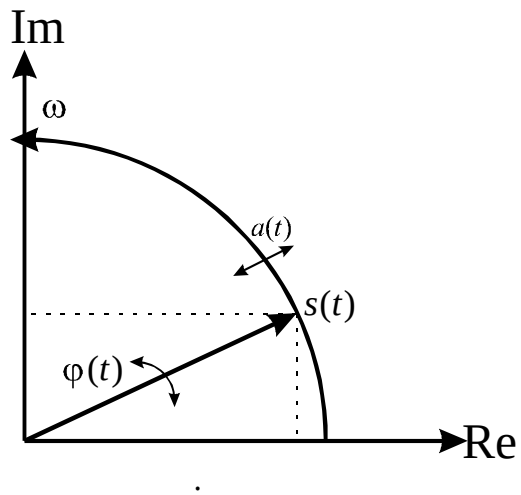

.

Fig.3-5 Pointer of the complex function s(t)

In the complex area this function can be described as a pointer rotating with the carrier frequency as shown in Fig.3-5. The original signal is the projection of the real axis. By undersampling with integer submultiples of the carrier frequency, the rotation of the pointer with the carrier frequency is stopped. The remaining changing of the angle corresponds with the phase modulation and the changing of the length of the pointer is the amplitude modulation.

To determine the length and the angle of the pointer, the signal must be sampled at two points with 90 degrees shifted. The real part of the first value is identical with the imaginary part of the second one, see Fig.3-6.

With this information the amplitude and the phase modulation can be calculated as

$$a(t) = \sqrt{u(t)^2 + \quad w(t)^2} \tag{3-5}$$

and

$$\varphi(t) = \arctan\left(\frac{w(t)}{u(t)}\right) \quad . \tag{3-6}$$

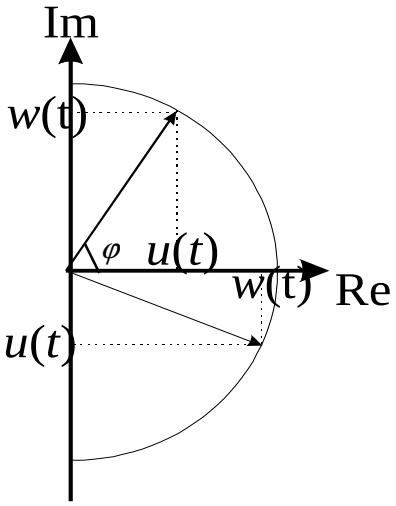

Fig.3-6 Complex bandpass sampling

3.1.3 Demodulation

The ultrasonic beam passing through the pipe flow is complex modulated by the fluid. Further signal processing can only be done when the modulated signal is correctly demodulated. Consequently, as indicated in section 3.1.2, this signal restoration is performed in two steps: the suppression of the carrier (stopping the rotation of pointer with carrier frequency) and the separation of independent parts in the signal(sampling the signal at two points with 90 degrees shifted).

Supression of the carrier frequency

In order to suppress the carrier frequency, the undersampling technique is applied according to Shannon theorem saying

$$f_s >= 2f_m \tag{3-7}$$

where f_s is the sampling frequency, f_m is the maximum frequency of the signal to be sampled. Only if the above requirement is met can the signal be reconstructed from the sampled signal. This sampling method is called oversampling method. It is called undersampling when the sampling frequency f_s is smaller than two times of the highest signal frequency. According to theoretical signal definition“ information decreases with an increasing predictability of a signal“[36,38], there are plenty of reasons to neglect the carrier which is a determined sinusoidal signal without falsifying the final result.

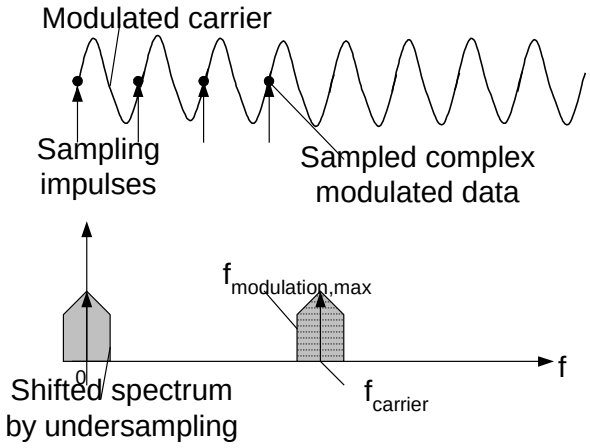

Fig. 3-7 Suppression of carrier by undersampling in time(upper picture) and frequency domain(lower piture)

Fig.3-7 shows the suppression of carrier by undersampling both in time and frequency domain. More precisely speaking, the undersampling frequency should be integer submultiples of the carrier frequency so as to eliminate the carrier frequency. That is,

$$f_{sampling} = \frac{f_{carrier}}{x}, \quad x=\{1,2,3...\}[36] \quad . \tag{3-8}$$

By using this undersampling method, a Shannon frequency according to the bandwidth of the modulation has to be selected which reduces the number of sampled data and the computing data.

Separation of demodulated signal

Although a result has been obtained by undersampling one has to be aware of the fact that this so-called signal still represents a combination of single independent influences which have to be

separated as far as possible. The next step of signal analysis is still a very fundamental consideration about signal theory and can easily be seen from the general equation describing modulated signals shown in equation (3-3). The phase modulation and amplitude modulation can at least theoretically be obtained according to equation (3-5) and (3-6). But the imaginary part, denoted as $u(t)$, cannot be measured in reality and has to be reconstructed by other means. A very simple method, displayed in Fig. 3-7, for function with $f_{carrier} >> f_{signal}$, needs a second sample taken with a phase shift of 90° relative to the first sample according to the carrier frequency. By this way, the local phase and amplitude modulation is reconstructable from each measurement pair. The frequency between the measurement pair is called Hilbert frequency in this work. The basic Hilbert frequency in this research is 880kHz due to the fact that the carrier frequency is 220kHz.

3.2 Vortex measurement

Vortex flowmeter combined with ultrasonic beam is also studied in this work. For convenience, the experimental setup is necessary to be described first as shown in Fig.3-8. The measurement chamber is identical with that in cross correlation measurement. Theoretically, only one channel is needed. But in practice, three channels with the distribution shown in Fig.3-2 are installed to see the dissipation of the vortices.

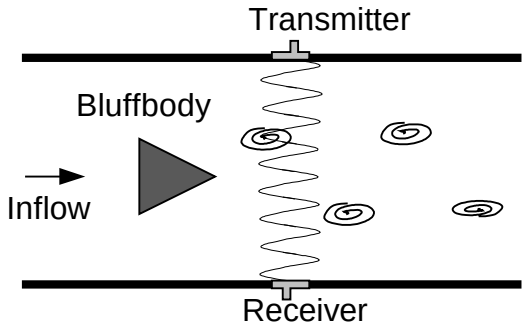

Fig. 3-8 Schematic of vortex measurement

The received modulated signal, after demodulation through the same method discussed in the section of cross correlation measurement, is analysed in its frequency domain. The abscissa of the peak of its spectrum shown in Fig.3-9 as an example corresponds to the vortex shedding frequency.

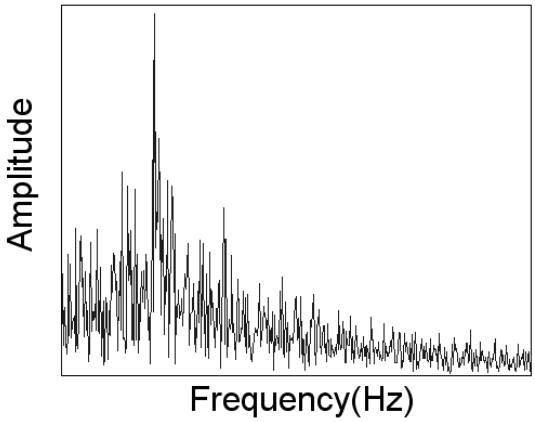

Fig. 3-9 Principle spectrum of the phase demodulated signal in vortex measurement

As pointed out already, there are two types of modulation in the flow measurement. So both can be chosen for analysis and compared, through which the essence of modulation under different conditions can be investigated.

4 Hilbert Transform

4.1 Negative and positive frequencies

The spectrum of a signal shows the amplitude of different frequencies contained in this signal. Normally it is symmetric to the *y* axis where the origin is zero. Therefore, it contains not only the frequencies which are bigger than zero but also those which are smaller than zero.

4.2 Analytic signal

As is known, every real signal contains equal amount of positive frequencies and negative frequencies in its spectrum. A signal which has no negative-frequency components is called an analytic signal[35]. An analytic signal can be generated from a real signal suppressing the negative frequency components while preserving the positive components. Given a real signal x(t), a complex analytic signal can be expressed as $z(t)=x(t)+j\cdot y(t)$, where y(t) is the 90 degrees phase shift of x(t). Now it can be seen that an analytic signal consists of real part and imaginary part, among which only the real part can be measured in real life. To get the imaginary part of the analytic signal, Hilbert Transform is introduced.

The use of analytic signals to model amplitude and phase modulated signals is only applicable when the modulation sidebands do not overlap over zero frequency[16], as illustrated in Fig.4-1.

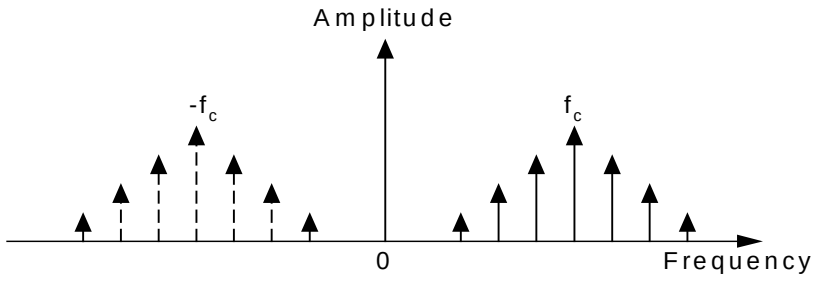

Fig. 4-1 Modulation sidebands without overlapping over zero frequency

In practice this means that for amplitude modulation, the carrier frequency must be greater than the highest modulating frequency. For frequency modulation it must be greater than both $4f_m$ and $2\Delta f$, where f_m is now the highest modulating frequency, and Δf is the maximum frequency deviation corresponding to the maximum modulating signal amplitude. For combined amplitude

and phase(or frequency) modulation, the lowest sideband from the phase modulated part must be higher than the highest frequency in the amplitude modulation signal.

4.3 Concept of Hilbert Transform

For a real signal

$$f(t) \qquad -\infty < t < +\infty \quad ,$$

its Hilbert Transform is strictly defined as

$$\hat{f}(t) = H\{f(t)\} = \frac{1}{\pi}\int_{-\infty}^{+\infty}\frac{f(\tau)}{t-\tau}d\tau = f(t) * h(t), \tag{4-1}$$

where the integral is the principal value of the integral and

$$h(t) = \frac{1}{\pi t}. \tag{4-2}$$

The inverse transform is defined as

$$f(t) = H^{-1}\{\hat{f}(t)\} = -\frac{1}{\pi}\int_{-\infty}^{+\infty}\frac{\hat{f}(t)}{t-\tau}d\tau \quad . \tag{4-3}$$

The Fourier Transform of $h(t)$ is

$$F(\frac{1}{\pi t}) = -j\,\mathrm{sgn}\,\omega \quad , \tag{4-4}$$

so, the Fourier Transform of the Hilbert Transform is

$$\hat{F}(\omega) = \tilde{H}[f(t) * h(t)] = -j\,\mathrm{sgn}\,\omega F(\omega) \tag{4-5}$$

which indicates that a Hilbert Transform can be obtained when processing the signal with an ideal 90 degree's shifter[16]. At the same time, it also indicates that the Hilbert Transform can be realized by software according to the above algorithm.

The real part by undersampling technique is obtained and the real part is processed with Hilbert Transform from which a new analytic signal is generated as

$$X = x + j \cdot \hat{x} \tag{4-6}$$

where the imaginary part $\hat{x}$ is the Hilbert Transform of the measured real part while x is exactly the real part.

4.4 Electronic Hilbert Transform

The arrangement of electronic Hilbert Transform[15, 23, 26, 27, 32] is shown in Fig.4-2, where the output *u*' and *w*' are Hilbert Transform pairs with *u*' as real part and *w*'

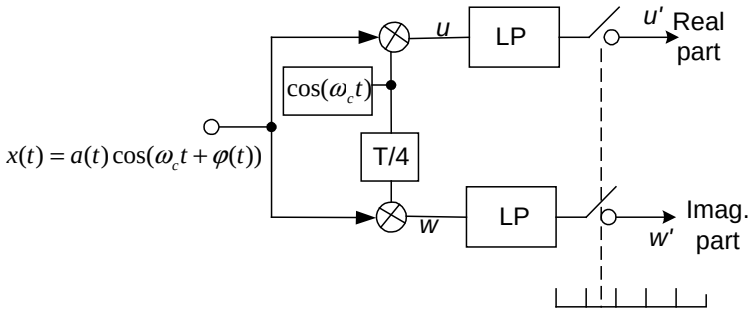

Fig. 4-2 Electronic Hilbert Transform

imaginary part behind a low pass filter LP. *u*' is in fact proportional to the input *x*(t), which is a real signal. This realization has been described in chapter 3 but in another different way of expression. As pointed out, the Hilbert Transform of a real signal can be obtained by a 90° shifter.

Hilbert Transform in ultrasonic flow measurement is realized by sampling the signal at two points with a 90° phase shift from each other. The two measured points form a combination which is an analytic signal as defined in equation (4-6). The 90 degrees' phase shift is calculated on the basis of carrier frequency[28].

4.5 Software realization of Hilbert Transform

Hilbert Transform can be calculated in two ways[35]. One way is to use a Hilbert filter. The other is to perform FFT-based frequency domain convolution. Fig.4-3 shows the FFT approach. According to the diagram of the weight function H_n, it can be expressed in the mathematic form as

$$H_n = \begin{cases} 0 + j \cdot 0 & n = 0, N/2 \\ 0 + j \cdot 1.0 & 1 \le n \le N/2 - 1 \\ 0 - j \cdot 1.0 & N/2 + 1 \le n \le N - 1 \end{cases} . \qquad (4\text{-}7)$$

The input x_n in the diagram is the measured real part while the output y_n is the Hilbert Transform of x_n. It can be described as

$$y_n = \text{Hilbert}(x_n) \tag{4-8}$$

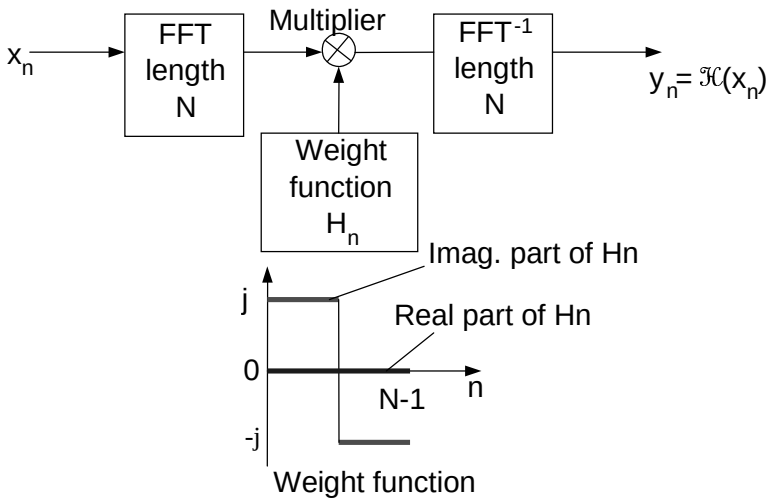

Fig. 4-3 Diagram of Hilbert Transform using FFT

By means of Matlab, this algorithm can be easily realized. The code is described in the appendix.

4.6 Results of the software

The following pictures are from the data measured in the cross correlation measurement. All three velocities are from the same channel.

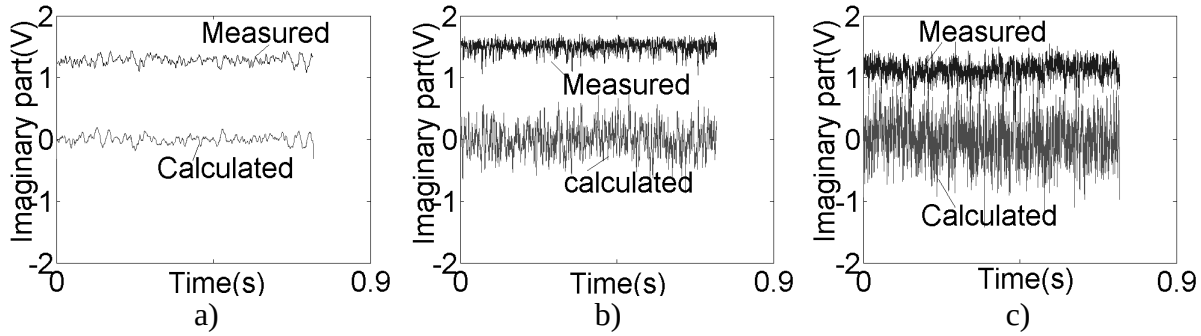

Fig.4-4 Measured imaginary part and calculated imaginary part
a) velocity=2m/s b) velocity=10m/s c) velocity=20m/s

The comparison between the calculation and the measured value is shown in Fig.4-4. Then the cross correlation method is applied to the newly formed analytic signal. The results are shown in Fig.4-5, Fig.4-6.

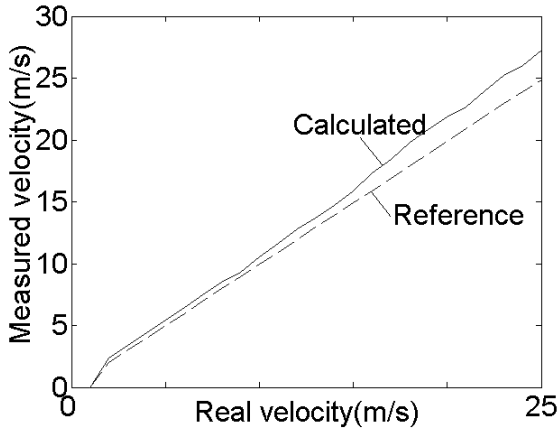

Fig. 4-5 Measured velocity

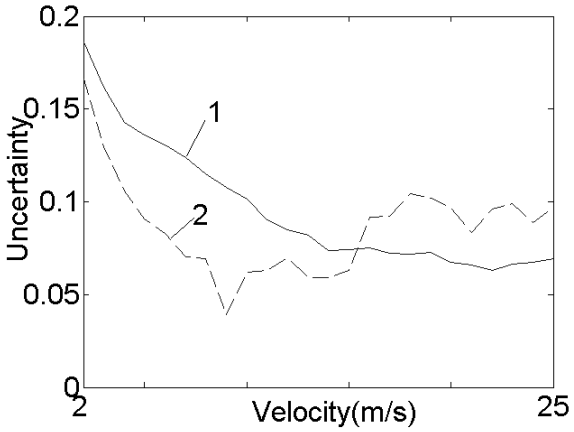

Fig. 4-6 Uncertainty (f_H=880kHz)
1—hardware 2--software

The calculated velocity based on the software Hilbert Transform is shown in Fig.4-5. The dash line stands for the real velocity and the solid line is the calculated velocity. From Fig.4-6, it can be seen that the uncertainty resulted from software is much smaller than the digital method at low velocities which are of high interest. That's because an ideal Hilbert Transform realizes a 90 degree's shift of all frequencies in a signal, while the digital method realizes this only according to the carrier frequency. The results at the lower velocities are even better than at higher velocities. This may be partly due to the different characteristics of modulation frequencies between low and high velocities.

4.7 An improved CCF of amplitude demodulation by Hilbert Transform software

The former experiments indicate that the cross correlation function of amplitude has no obvious peak, which doesn't benefit further signal processing[10, 11]. For this reason phase-CCF is always applied instead of amplitude-CCF.

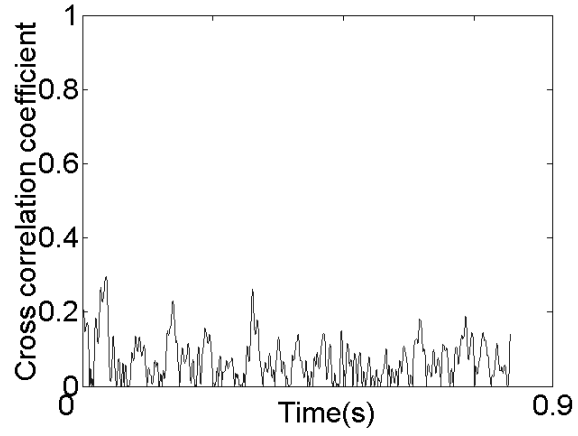

a)

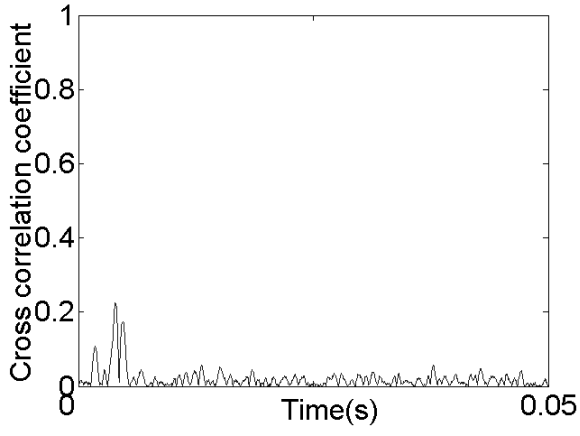

a)

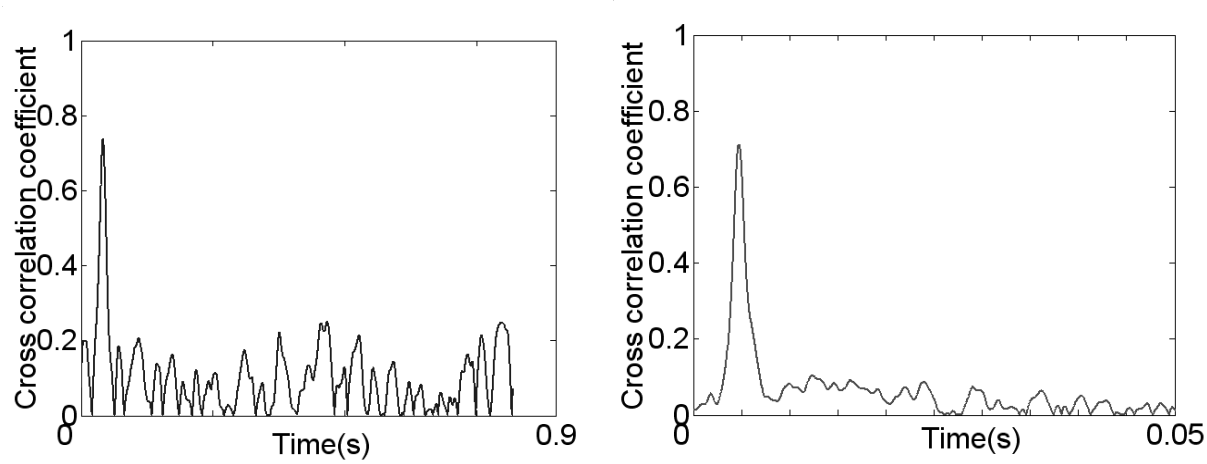

Fig. 4-7 Amplitude-CCF at 2m/s(left) and 20m/s(right)
a)—Old method b)—Using Hilbert Transform software

Amplitude-CCF is calculated again on the basis of the results of Hilbert Transform software and compared with measurement results as shown in Fig.4-7.

It can be easily seen that the amplitude-CCF based on Hilbert Transform software has much higher peak than that from digital Hilbert Transform. In addition, it has high similarity with the phase-CCF especially at low velocity as shown in Fig.4-8. This similarity indicates the convergence of the measurement results of velocity using both CCFs and presents a clear progress in relation to methods applied up to now.

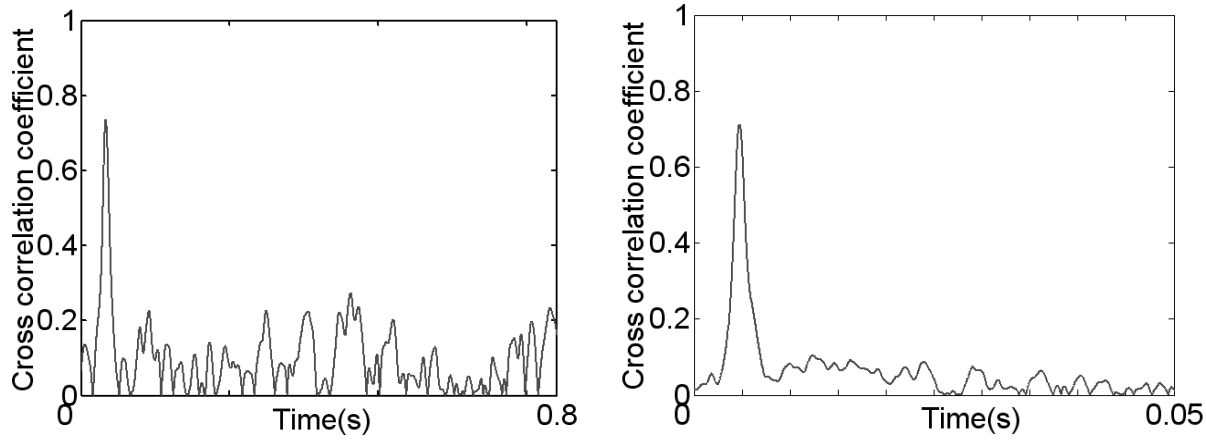

Fig.4-8 Phase-CCF using old method at 2m/s(left) and 20m/s(right)

From the above figures, it can be seen that the measured results using the software Hilbert Transform or ideal Hilbert Transform is better than the results obtained by digital method. But how does such a surprising result come out? Next, an explanation is given as follows.

The accuracy of the approximated Hilbert Transform operator can be measured by comparing the energy of the signals between the real signal and the signal obtained from Hilbert Transform.

$$E_f = \int_{-\infty}^{+\infty} |f(t)|^2 dt = \frac{1}{2\pi} \int_{-\infty}^{+\infty} |F(\omega)|^2 d\omega \tag{4-9}$$

$$E_{\hat{f}} = \int_{-\infty}^{+\infty} |\hat{f}(t)|^2 dt = \frac{1}{2\pi} \int_{-\infty}^{+\infty} |-j\,\mathrm{sgn}(\omega) F(\omega)|^2 d\omega \tag{4-10}$$

theoretically, (4-9) equals (4-10)[44].

The Parseval equation for discrete signals[46] is

$$\sum_{n=0}^{N-1} x^2(n) T_{sampling} = \sum_{k=0}^{N-1} |T_{sampling} X(K)|^2 \Delta f = T^2_{sampling} \frac{1}{NT_a} \sum_{k=0}^{N-1} |X(K)|^2 . \quad [\mathrm{V^2/Hz}] \tag{4-11}$$

In the present case, the real part forms the real signal. The digital method realizing the Hilbert Transform by turning 90 degrees according to carrier frequency can be regarded as approximate Hilbert Transform. The difference between the energy of the two constructed signals will be displayed.

The following three energies are calculated results from measured data according to equation (4-11).

E_f=1.1521e+004/20000=0.576 V² /Hz energy of real signal

E_{fd}=3.9066e+004/20000=1.953 V²/Hz energy of approximate Hilbert Transformed analytic signal

E_{fs}=1.1586e+004 /20000=0.579V² /Hz energy of software Hilbert Transformed analytic signal

Obviously, the approximate Hilbert Transform caused bigger error than the software. This is part of the reason that ccf-amplitude from software Hilbert Transform works much better than the normal Hilbert Transform.

4.8 Undersampled Hilbert Transform

4.8.1 Cross correlation measurement

For a specific real part, its imaginary part can be measured at the point of 90 degrees shifted on the signal as shown in Fig.4-9. It is self-evident that the same result is obtained even if the pointer is turned with 360 degrees around. Then the angle between the two points is 90 degrees plus 360 degrees. If the pointer is turned with *n* times 360 degrees, the result is also always the

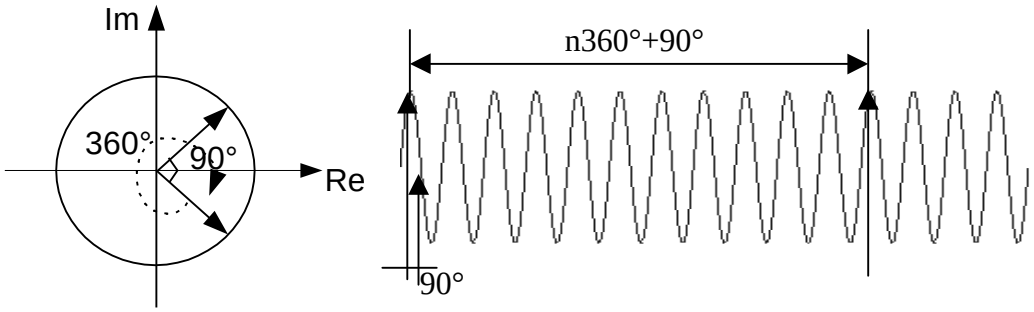

Fig.4-9 Undersampled Hilbert Transform

same. That means the distance between the two points can be lengthened, as shown by Fig.4-9. This idea shall be called undersampled Hilbert Transform.

On account of the fact that the gas fluid changes little during a short time which according to the experiment is the time corresponding to *n*=5 in Tab.1. n=5 corresponds to the sampling frequency 41.9kHz, from which the time can easily be calculated as 1/41.9kHz=23.86μs. This very short time corresponds to a distance of 596.5μm of the fluid at a velocity of 25m/s. It can be taken for granted that the fluid does not change its properties within this time.

Tab.4-1 Different f_H (kHz) f_c=220kHz f_s=20kHz

n	f_H =1/(n+0.25) f_c	n	f_H =1/(n+0.25) f_c
0	880	6	35.2
1	176	7	30.3
2	97.8	8	26.7
3	67.7	9	23.8
4	51.8	10	21.5
5	41.9		

The sampling period can be extended without big influence on the measurement. When the undersampling frequency is fixed at 20kHz, the Hilbert frequency f_H can be changed according to Tab.4-1. Here the Hilbert frequency shall be defined as the frequency between the two sampling trigger points causing 90° or n·360°+90° phase shift.

A lot of measurements are made using the above frequencies. The measured velocities with different Hilbert frequency listed in Tab.1 are shown in Fig.4-10. Due to the small difference between the measurements, only the frequency 41.9kHz is displayed for a better view.

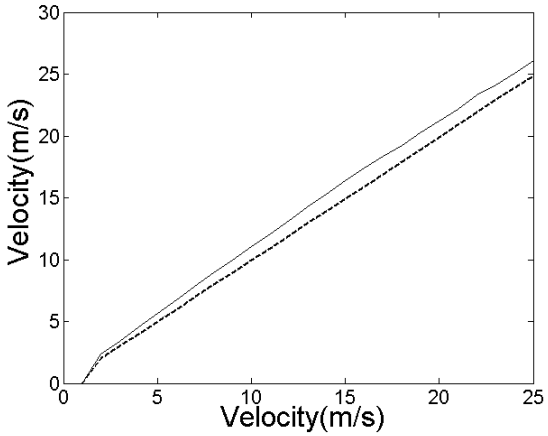

Fig. 4-10 Measured velocity using different f_H (the frequency in the picture is 41.9kHz)

The dashline in Fig.4-10 is the reference velocity while the other solid lines stand for the measured velocities using different Hilbert frequencies from 880kHz to 41.9kHz. This figure indicates that the undersampled Hilbert Transform can also yield comparable measured results as the normal Hilbert Transform. The uncertainty of each is illustrated in Fig.4-11.

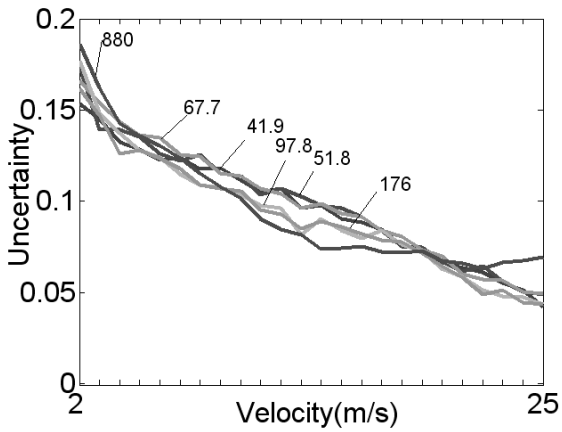

Fig.4-11 Measurement relative error of different f_H

As can be seen in the Fig.4-11, the difference between the measured velocities using different suitable f_H is small. These frequencies are from 41.9kHz to 880kHz. The frequencies lower than 41.9kHz give not so good results. The reason of this phenomenon will be explained later in this chapter.

4.8.2 Vortex measurement

The undersampled Hilbert Transform is also applied to vortex measurement. As explained, the gas fluid changes little during a short time. For n=5 and f_H=41.9kHz, this time is 23.86μs. The sampling period can be extended without big influence on the measurement. When the undersampling frequency is fixed at 20kHz, the f_H can be changed according to the Tab.4-1.

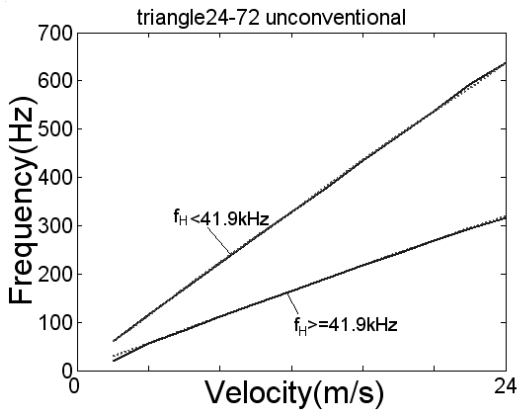

Fig. 4-12 f-v relation with f_H<41.9kHz and f_H>=41.9kHz

From f_H=41.9kHz to f_H=880kHz, the detected vortex shedding frequency is almost the same as shown in Fig.4-12. The difference comes up when the Hilbert frequency f_H is lower than 41.9kHz(i.e., more than 5 periods later than the normal Hilbert Transform) as illustrated in Fig.4-12. It can be clearly seen that the detected vortex shedding frequency is seemingly twice that with the Hilbert frequency higher than 41.9kHz.

According to the former research in this field, the smaller the bluff body is, the higher shedding frequency is. The smallest bluff body is 4mm wide, which causes the highest frequency of not more than 2kHz when the flow velocity is not more than 25m/s. As a result, the undersampling frequency f_s can be reduced to 4kHz which still meets the Shannon Sampling Theorem[38]

$$f_s >= 2 f_m \ .$$

On this basis, an undersampled Hilbert Transform is also applied as shown in Tab.4-2.

Tab.4-2 Different f_H (kHz) f_c=220kHz f_s=4kHz

n	f_H =1/(n+0.25) f_c	n	f_H =1/(n+0.25) f_c
0	880	...	...
1	176	27	8.07
2	97.8	28	7.79
3	67.7	...	...
4	51.8	45	4.86
5	41.9	52	4.21

As in the case of sampling frequency of 20kHz, from 880kHz until 8.07kHz, the detected vortex shedding frequency is the same shown in Fig.4-13.

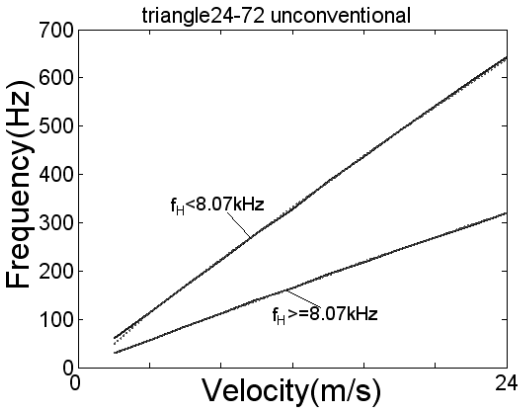

Fig. 4-13 *f-v* relation with f_H<8.07kHz and f_H>=8.07kHz (right)

The convergence of the characteristic lines using different Hilbert frequencies between 8.07kHz and 880kHz indicates that the frequency range is suitable for the measurement. The Hilbert frequency in this range leads to correct results. However, when the Hilbert frequency is even lower, i.e., when the delayed periods number is larger than 27, the detected vortex shedding frequency doubles as illustrated in Fig.4-13.

The above figures are measured results in vortex flow measurement using undersampled Hilbert Transform. When the Hilbert frequency is not lower than half the undersampling frequency, the measured vortex shedding frequency is the same as that using normal Hilbert Transform. But so long as the Hilbert frequency is lower than half the undersampling frequency, the detected vortex shedding frequency doubles, which is wrong.

Similarly, in the cross correlation measurement, when using undersampled Hilbert Transform, the lowest Hilbert frequency is exactly half the undersampling frequency. The results measured with lower Hilbert frequency are not good. This phenomenon is substantiated by the Shannon theorem.

With sampling the spectrum of the sampled signal is repetitive with the sampling frequency. When the sampling frequency is lower than two times of the maximum signal frequency, the repetitive spectrum of the sampled signal overlaps with each other, which leads to error. In the current case, the signal with the undersampling frequency is the one to be sampled with a Hilbert frequency which is equivalent to the sampling frequency. Therefore, the Hilbert frequency should be at least two times the undersampling frequency. That is $f_H \geq 2f_s$.

5 Kalman Filter

5.1Theoretical model description

Generally, complex systems can not be expressed in easy mathematical functions. They are easily expressed as differential equations which include observation equation and state equation. The observation model is illustrated in Fig.5-1[30,31].

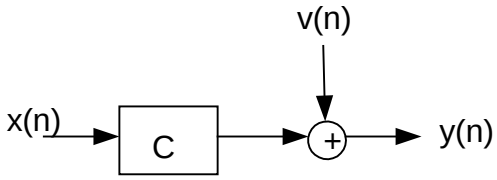

Fig. 5-1 Observation model

The model above, as clearly seen, consists of an unkown input state vector x(n), an observation matrix C, a measurement noise vector v(n) and the observation vector y(n) as the output of the system. The noise of the system should be assumed as white noise which meets Normal distribution. The observation model can be written as the following equation in a discrete time form

$$y(n) = Cx(n) + v(n). \tag{5-1}$$

The second part, the state model is shown in Fig.5-2.

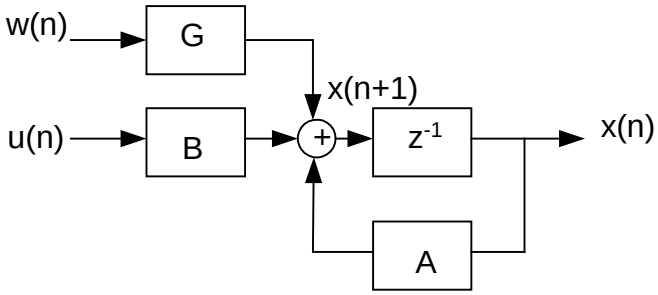

Fig. 5-2 State model

In this figure, u(n) is the known input value. W(n) is the process noise. G is the weight matrix which decides the influence of the forward process noise. A is the state matrix. B is the control matrix. The expression z^{-1} contains the relation between the current state x(n) and the following state x(n+1). In formular, the model can be described as[31]

$$x(n+1) = A \cdot x(n) + B \cdot u(n) + G \cdot w(n) \quad . \tag{5-2}$$

Combining the two parts, a whole complex system is established as illustrated in Fig.5-3.

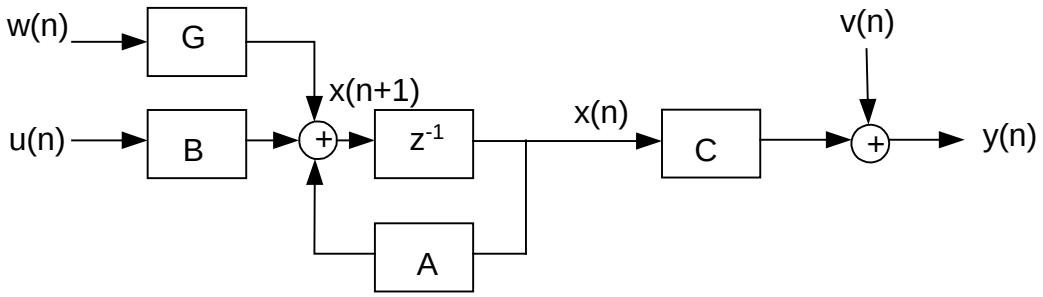

Fig. 5-3 Complete model

The corresponding state-space equation of the above system is as follows

$$y(n) = C \cdot x(n) + v(n),$$

$$x(n+1) = A \cdot x(n) + B \cdot u(n) + G \cdot w(n) \ . \tag{5-3}$$

5.2 Kalman Filter

A distinctive feature of a Kalman filter is that its mathematical formulation is described in terms of state-space concepts which are described in the former section[30]. Consider a simple linear, discrete-time dynamic system described by the signal-flow graph shown in Fig.5-4. Considering the unkown input value, the control matrix B is set zero matrix.

The notation of state plays a key role in this formulation. The state vector, denoted by x(n) in the

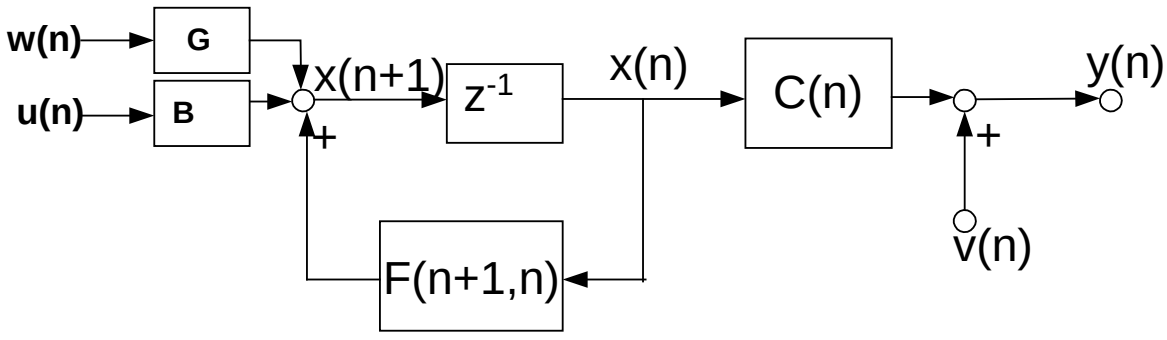

Fig. 5-4 Signal-flow graph representation of a linear, discrete-time dynamic system

Fig.5-4, is defined as any set of quantities that would be sufficient to uniquely describe the unforced dynamical behavior of the system. Typically, the state vector, assumed to be of

dimension M, is unkown. To estimate it, a set of observed data is used, denoted by the vector y(n) in Fig.5-4. The observation vector y(n) is assumed to be of dimension N.

In mathematical terms, the signal-flow graph of Fig.5-4 embodies the following pair of equations[18].

1) A process equation

$$x(n+1) = F(n+1,n)x(n) + w(n) \quad , \tag{5-4}$$

where F(n+1,n) is a known M-by-M state transition matrix relating the state of the system at times n+1 and n. The M-by-1 vector w(n) represents process noise. The vector w(n) is modeled as a zero-mean, white-noise process whose covariance matrix is defined by

$$E[w(n)w^{H}(k)] = \begin{cases} Q(n), n = k \\ 0, n \neq k \end{cases} \quad . \tag{5-5}$$

2) A measurement equation, describing the observation vector as

$$y(n) = C(n)x(n) + v(n) \quad , \tag{5-6}$$

where C(n) is a known N-by-M measurement matrix. The N-by-1 vector v(n) is called measurement noise. It is modeled as a zero-mean, white-noise process whose covariance matrix is

$$E[v(n)v^{H}(k)] = \begin{cases} R(n), n = k \\ 0, n \neq k \end{cases} \quad . \tag{5-7}$$

It is assumed that x(0), the initial value of the state, is uncorrelated with both v_1(n) and v_2(n) for n>=0. The noise vectors w(n) and v(n) are statistically independent, so it may be written as

$$E[w(n)v^{H}(k)] = 0 \qquad \text{for all n and k} \quad . \tag{5-8}$$

The question which is addressed by the Kalman Filter is this: Given the kowledge of the behaviour of the system and given the measurements, what is the best estimate of the system state. We can do better than just take the measurement especially when we suspect there is a lot of measurement noise.

5.3 Extended Kalman Filter

The Kalman filter considered up to this point in the discussion has addressed the estimation of a state vector in a linear model of a dynamic system. If the model is nonlinear, the use of Kalman filter may be extended through a linearization procedure. The resulting filter is naturally referred to as the Extended Kalman Filter(EKF). Such an extension is feasible by virtue of the fact that the Kalman filter is described in terms of differential equations or difference equations.

The alternative state-space model in the case of nonlinear system is given as

$$x(n+1) = F(n, x(n)) + w(n) \quad , \tag{5-9}$$

and

$$y(n) = C(n, x(n)) + v(n) . \tag{5-10}$$

where, as before, w(n) and v(n) are uncorrelated zero-mean white-noise processes with correlation matrices Q(n) and R(n), respectively. Here, F(n,x(n)) denotes a nonlinear transition matrix function that is possibly time-variant. In the linear case, simply there is

$$F(n, x(n)) = F(n+1, n)x(n) \ . \tag{5-11}$$

The basic idea of EKF is to linearize the state-space model of equations (5-9) and (5-10) at each time instant around the most recent state estimate, which is taken to be either $\hat{x}(n \mid y_n)$ or $\hat{x}(n \mid y_{n-1})$, depending on which particular function is being considered. Once a linear model is obtained, the standard Kalman filter equations are applied.

The nonlinear model can be simplified by determination of the derivatives which can be obtained by the first-order Taylor approximation[18]

$$F(n+1, n) = \left. \frac{\partial F(n, x(n))}{\partial x} \right|_{x=\hat{x}(n|y_n)} \quad , \tag{5-12}$$

$$C(n) = \left. \frac{\partial C(n, x(n))}{\partial x} \right|_{x=\hat{x}(n|y_{n-1})} \quad . \tag{5-13}$$

5.4 EKF in phase demodulation

The algorithm of Kalman filter in phase demodulation

The initial application of EKF in phase demodulation is used in the speech signals in the field of telecommunication [5].

The imaginary part and the real part are obtained by bandpass undersampling and digital Hilbert transform. The measurement equation can be written as the following[5]

$$\begin{gathered} y(n) = C[x(n)] + v(n), \\ \begin{pmatrix} \mathrm{Re}(y(n)) \\ \mathrm{Im}(y(n)) \\ \arctan(\dfrac{\mathrm{Im}(y(n))}{\mathrm{Re}(y(n))}) \end{pmatrix} = \begin{pmatrix} \cos(2\pi\alpha \cdot x_1(n)) \\ \sin(2\pi\alpha \cdot x_1(n)) \\ 2\pi\alpha x_1(n) \end{pmatrix} + \begin{pmatrix} v_1(n) \\ v_2(n) \\ v_3(n) \end{pmatrix}, \end{gathered} \tag{5-14}$$

and the process equation as follows:

$$\begin{pmatrix} x_1(n+1) \\ x_2(n+1) \end{pmatrix} = F(n, x(n)) + Bu(n) + Gw(n), \\ = \begin{pmatrix} x_1(n) + T \cdot x_2(n) \\ x_2(n) \end{pmatrix} + \begin{pmatrix} 0\,0 \\ 0\,1 \end{pmatrix} \begin{pmatrix} w_1(n) \\ w_2(n) \end{pmatrix}, \tag{5-15}$$

where $v(n)$ and $w(n)$ are respectively the measurement noise and process noise which are of a dimension of 3 by 1 and 2 by 1. $v(n)$ and $w(n)$ are assumed to be zero-mean, white noise whose covariance matrix are defined respectively by R(n) and Q(n). They are in this application chosen to be the following matrices.

$$Q(n) = \begin{pmatrix} 0.1 & 0 \\ 0 & 0.1 \end{pmatrix} \\ R(n) = \begin{pmatrix} 1 & 0 & -0.1\sin(x_1(n)) \\ 0 & 1 & 0.1\cos(x_1(n)) \\ -0.1\sin(x_1(n)) & 0.1\cos(x_1(n)) & 0.1 \end{pmatrix} \tag{5-16}$$

These two noise signals are also mutually uncorrelated. The input u(n) is not specified, so it is assumed to be zero, so is the matrix B. $x_1(n)$ corresponds to the actual phase position in the system and $x_2(n)$ corresponds to the frequency. α is an absorption coefficient, or modulation index and ***T*** is the undersampling time. The measurement y(n) is obtained from the digital Hilbert Transform. Re(y(n)), Im(y(n)) and arctan(Re(y(n))/Im(y(n))) stand for the real part, imaginary part and angle of the measured complex signal through QAD. For further resolution to the demodulation, the nonlinear state transition matrix F(n,x(n)) and nonlinear measurement matrix C(n,x(n)) should be linearized according to equations (5-12) and (5-13). Therefore, the linearized state transition matrix F(n+1,n) and measurement matrix C(n) are

$$F(n+1, n) = \begin{pmatrix} 1 & T \\ 0 & 1 \end{pmatrix} \tag{5-17}$$

$$C(n) = \begin{pmatrix} -2\pi\alpha \cdot \sin(2\pi\alpha \cdot x_1(n)) & 0 \\ 2\pi\alpha \cdot \cos(2\pi\alpha \cdot x_1(n)) & 0 \\ 2\pi\alpha & 0 \end{pmatrix}, \tag{5-18}$$

Unlike the author in [11], here another input is added which is the phase angle of the measured signal resulting in three observations and two states. For this reason it is called EKF32 while that provided by author in [11] is called as EKF22. This has its own advantage over EKF22(the one discussed in [11]), which will be elaborated next.

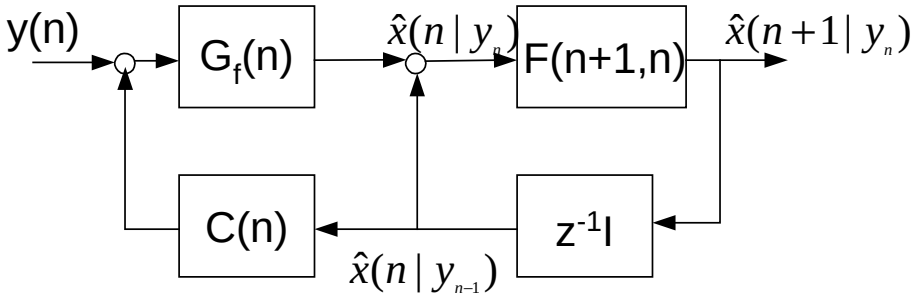

Fig. 5-5 One-step predictor for the EKF

A set of observed data denoted by y(n) in Fig.5-5, in this case, includes three parts referred to above in equation(5-14). $G_f(n)$ is the Kalman Gain. F(n+1,n) and C(n) are respectively linearized state transition matrix and linearized measurement matrix.

The algorithm is listed as follows. Matlab program is applied to realize this algorithm whose code can be seen in the appendix.

Input vector process includes

observations={y(1),y(2).....y(n)}.

Known parameters include

nonlinear state transition matrix=F(n,x(n)),

nonlinear measurement matrix=C(n,x(n)),

covariance matrix of process noise vector=Q(n),

and covariance matrix of measurement noise vector=R(n).

Next are computation formulae, where n=1,2,3,.....

$$G_f(n) = K(n, n-1)C^H(n)[C(n)K(n, n-1)C^H(n) + R(n)]^{-1},$$

$$\alpha(n) = y(n) - C(n, \hat{x}(n \mid Y_{n-1})),$$

$$\hat{x}(n \mid Y_n) = \hat{x}(n \mid Y_{n-1}) + G_f(n)\alpha(n),$$

$$\hat{x}(n+1 \mid Y_n) = F(n, \hat{x}(n \mid Y_n)),$$

$$K(n) = [I - G_f(n)C(n)]K(n, n-1),$$

$$K(n+1, n) = F(n+1, n)K(n)F^H(n+1, n) + Q(n).$$

The initial conditions are

$$\hat{x}(1 \mid Y_0) = E[x(1)],$$

$$K(1,0) = E[(x(1) - E[x(1)])(x(1) - E[x(1)])^H] = \Pi_0.$$

5.5 The result of demodulation using EKF32

5.5.1 Fully developed flow

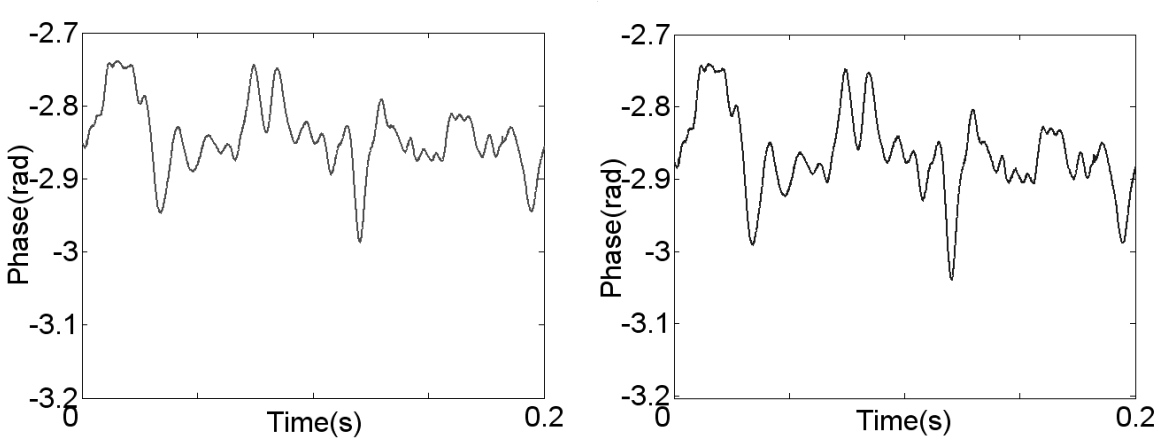

Fig.5-6 Phase demodulation through QAD(left) and EKF32(right) in undisturbed flow at 2m/s

A comparison of the phase demodulation by QAD and EKF32 shows that the above two pictures in Fig.5-6 are almost the same. At low velocities, the two phase demodulation methods are identical which can also be clearly seen in their figures showing cross correlation functions illustrated in Fig.5-8. But as the velocity increases, the difference between these two methods becomes more obvious.

As is shown in Fig.5-7, the demodulated phase signal through EKF32 is much more clear than that through QAD. EKF32 effectively rules out some unnecessary noise which comes out of

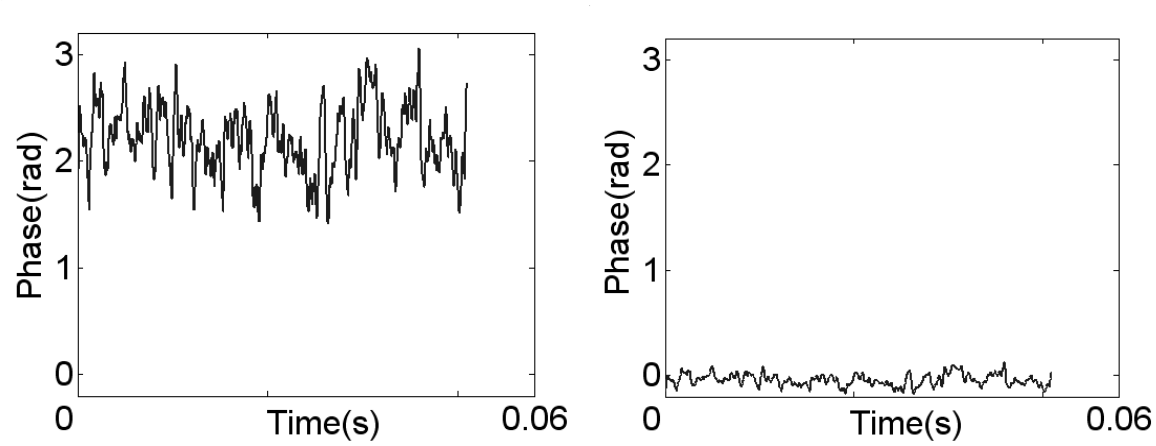

Fig.5-7 Phase demodulation through QAD(left) and EKF32(right) in undisturbed flow at 25m/s

the system. Besides, from the demodulated phase signal, the EKF32 itself possesses the function of zero phase correction which is normally provided by another specific function when QAD is applied.

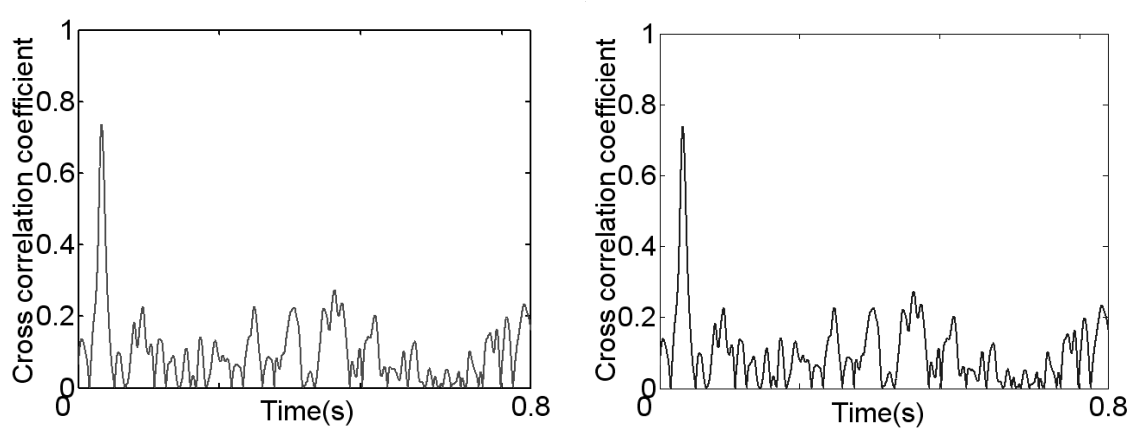

Fig.5-8 Cross correlation function of the phase signal demodulatied by QAD(left) and EKF32(right) in undisturbed flow at 2m/s

At low flow velocities, the cross correlation functions shown in Fig.5-8 through two different demodulation methods have no difference. This further proves that the two methods are identical in dealing with lower flow velocities. The difference, or the advantage of EKF32 over QAD is displayed when dealing with higher velocities which is shown in Fig.5-9.

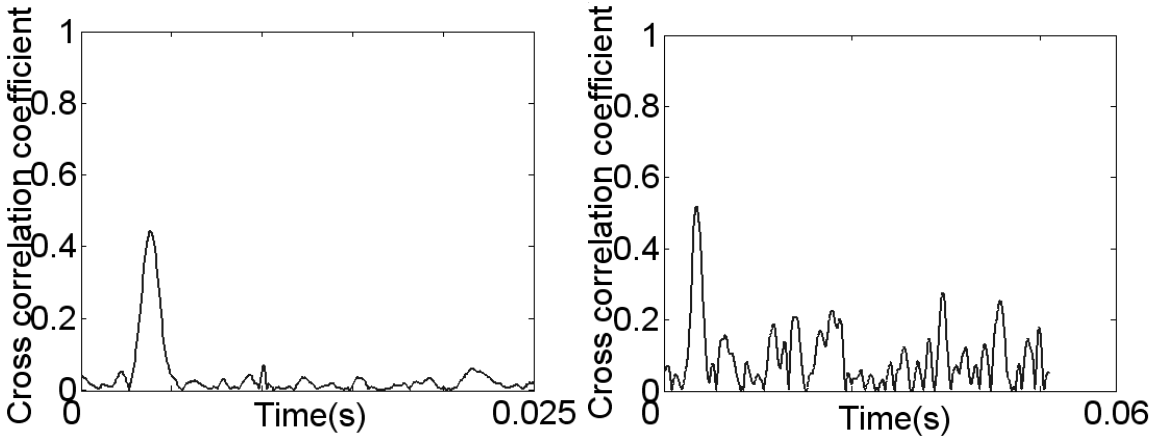

Fig. 5-9 Cross correlation function of the phase signal demodulatied by QAD(left) and EKF32(right) in undisturbed flow at 25m/s

Fig.5-9 indicates clearly that the cross correlation function got through EKF32 has a much higher peak than that through QAD, which is certainly an advantage in cross correlation measurement.

5.5.2 Disturbed flow

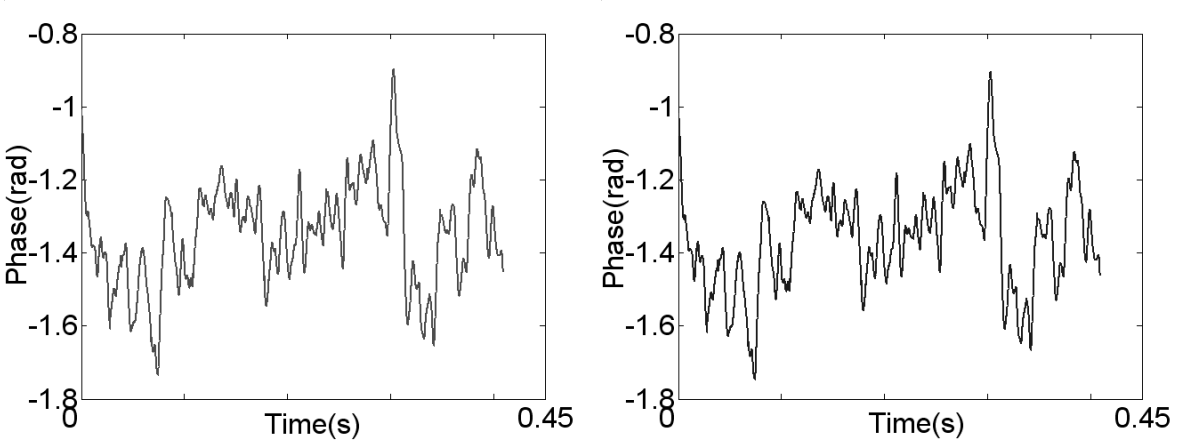

Fig.5-10 Phase demodulation through QAD(left) and EKF32(right) in disturbed flow at 2m/s

In this section, the disturbed flow is caused by a 90° bend. Fig.5-10 shows the phase demodulation in disturbed flow at velocity of 2m/s through EKF32 and QAD respectively. The difference between the two methods is not easily seen in the demodulated phase. The visible difference will be displayed later in their cross correlation functions.

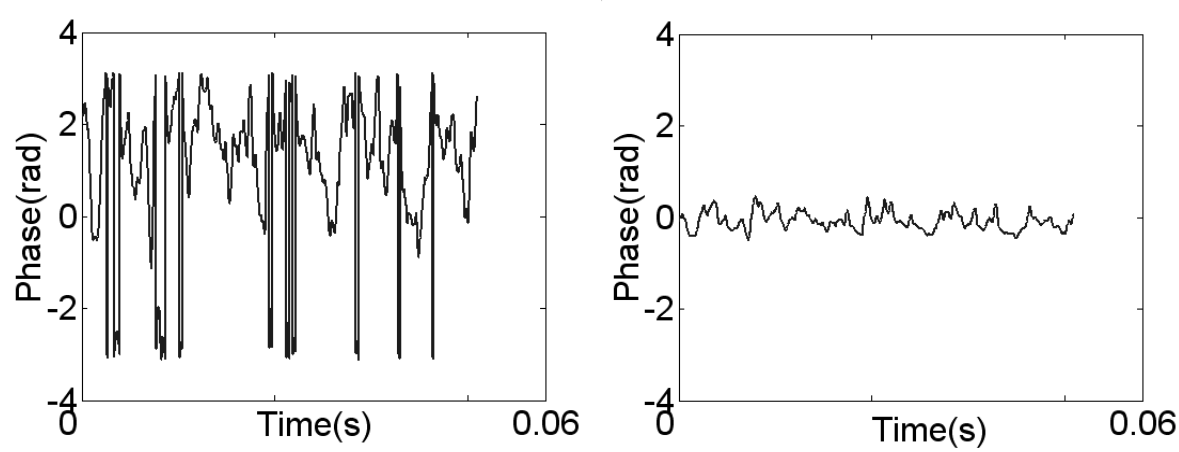

Fig.5-11 Phase demodulation through QAD(left) and EKF32(right) in disturbed flow at 25m/s

The big difference between EKF32 and QAD dealing with disdurbed flow at high velocity is clearly displayed in Fig.5-11. There exists no big phase jump caused by strong modulation when EKF32 is applied. Like what referred to in the undisturbed flow section, the demodulated phase signal through EKF32 has less noise and the filter possesses the function of zero phase correction[10].

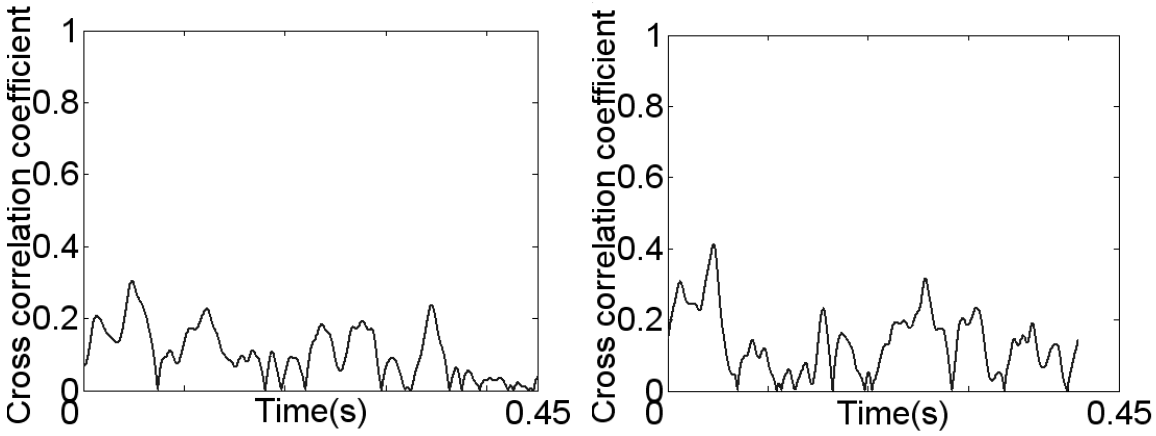

Fig.5-12 Cross correlation function of the phase signal demodulated by QAD(left) and EKF32(right) in disturbed flow at 2m/s

The advantage that EKF32 takes over QAD in phase demodulation in disturbed flow is also displayed by the cross correlation function shown in Fig.5-12 and Fig.5-13.

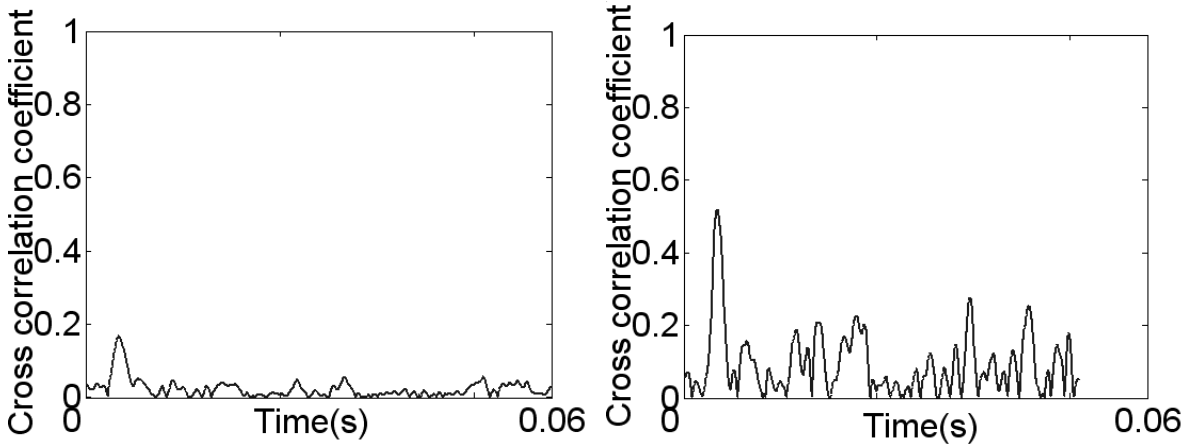

Fig.5-13 Cross correlation function of the phase signal demodulatied by QAD(left) and EKF32(right) in disturbed flow at 25m/s

Fig.5-12 and Fig.5-13 provide a strong evidence for the advantage of EKF32 in phase demodulation in disturbed flow. The cross correlation function, at low velocity or high velocity, has a higher peak value than that obtained through QAD, which benefits the precise calculation of flow transit time.

5.6 The algorithm of EKF24

In the EKF32 discussed in the former section, the observation is composed of the phase(phase demodulation) or amplitude(amplitude demodulation) information except for the directly measured signal. The phase or amplitude information can be obtained by specific sensors or

equipment, but in present case, they are calculated from the quadrature amplitude modulation method. So, strictly speaking, the EKF32 does not completely eliminate the effect of QAD but is dependent on that method. Here in this section, a Kalman Filter called EKF24 which is totally independent of QAD is elaborated. The imaginary part and the real part are obtained by bandpass undersampling and digital Hilbert Transform. The measurement equation is

$$\begin{aligned} y(n) &= C[x(n)] + v(n), \\ \begin{pmatrix} \mathrm{Re}(y(n)) \\ \mathrm{Im}(y(n)) \end{pmatrix} &= \begin{pmatrix} \cos(2\pi\alpha x_1(n)) + x_3(n) \\ \sin(2\pi\alpha x_1(n)) + x_3(n) \end{pmatrix} + \begin{pmatrix} v_1(n) \\ v_2(n) \end{pmatrix}, \end{aligned} \tag{5-19}$$

and the process equation is

$$\begin{aligned} \begin{pmatrix} x_1(n+1) \\ x_2(n+1) \\ x_3(n+1) \\ x_4(n+1) \end{pmatrix} &= F(n, x(n)) + Bu(n) + Gw(n), \\ &= \begin{pmatrix} 1 & samplingrate^{-1} & 0 & 0 \\ 0 & 1 & 0 & 0 \\ 0 & 0 & 1 & samplingrate^{-1} \\ 0 & 0 & 0 & 1 \end{pmatrix} \begin{pmatrix} x_1(n) \\ x_2(n) \\ x_3(n) \\ x_4(n) \end{pmatrix} + Gw(n). \end{aligned} \tag{5-20}$$

In the above two equations, the phase demodulation part is denoted as x_1 and amplitude demodulation part is denoted as x_3. x_2 is the change of phase and x_4 is the change of amplitude. The other symbols in the equations are the same as described in EKF32.

5.7 Amplitude demodulation

Phase demodulation in the fully developed flow can be realized by this Kalman filter whose result is as good as that from EKF32. This will not be discussed in this section. The emphasis of this section lies in the amplitude demodulation of the signal. What is of highest interest is the cross correlation function of the signals in cross correlation measurement. For this reason, the result of cross correlation functions at different velocity are displayed in this section.

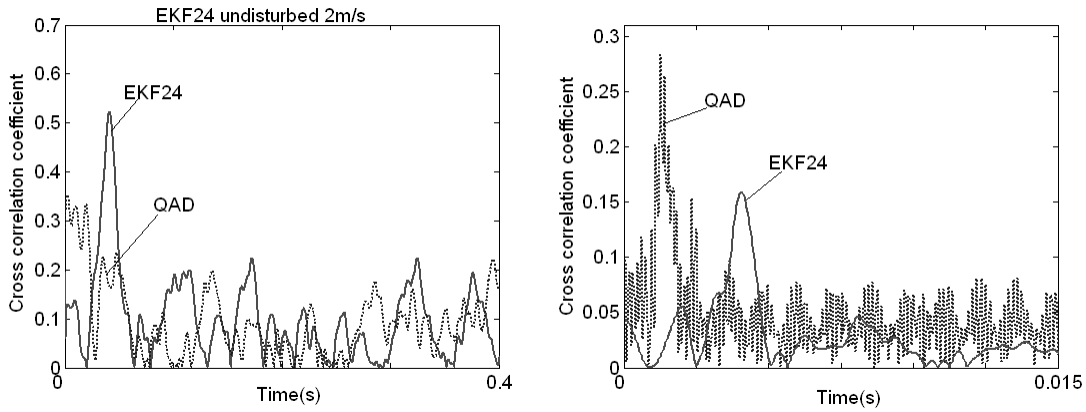

Fig.5-14 Cross correlation function of the amplitude signal demodulatied by QAD and EKF24 in fully developed flow at 2m/s(left) and 25m/s(right)

Fig.5-14 shows the cross correlation function of the amplitude signal demodulated by QAD and EKF24 in undisturbed flow at 2m/s and at 25m/s. There is no obvious peak in the cross correlation function obtained using QAD amplitude demodulation at low velocity. At high velocity, although the peak in the cross correlation function obtained from EKF24 is smaller than that in QAD cross correlation function, yet it is not difficult to find the transit time calculation is more precise. The distance between the cross correlated two channels is 100mm, the transit time acquired by EKF24 is 0.004s. Therefore, the velocity is exactly 25m/s. However, the velocity measured by QAD is much higher.

Mathematically, the Kalman Filter can be developed into different kinds of filter by expanding the observation or the state. But with the expanding matrices defined in the measurement equation and process equation, the burden of the computer increases. This makes the demodulation far more slowly.

5.8 Vortex measurement

Up till now, all the work done with Kalman Filter EKF32 is limited to cross correlation measurement. It is also applied to make demodulation in vortex measurement. EKF32 has some obvious advantages over EKF22 in phase demodulation applied in vortex measurement. Some results are shown in the next.

5.8.1 Fully developed flow

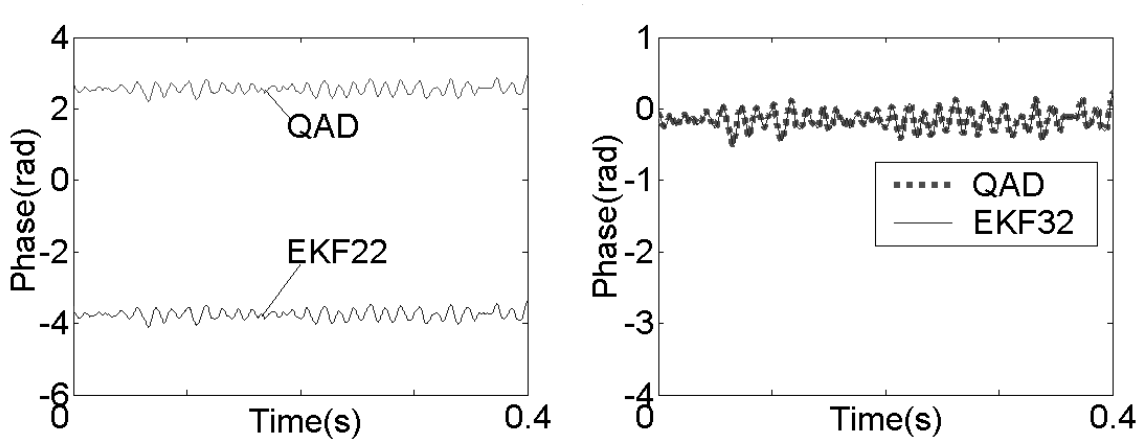

Fig.5-15 Phase demodulation using QAD, EKF22 and EKF32 in fully developed flow at low velocity

Fig.5-15 shows the phase demodulation in fully developed flow at a velocity of 2m/s with a conventional-set triangular bluff body whose width is 4mm and length is also 4mm. The left picture displays the result of QAD and EKF22. There is a phase shift caused by EKF22 which originates from the algorithm. But in the right picture showing the result of QAD and EKF32, there is none. The two results converge very well.

Fig.5-16 shows the result of phase demodulation in fully developed flow at a velocity of 24m/s with a conventional-set triangular bluff body whose width is 4mm and length is also 4mm. The left picture displays the result of QAD and EKF22. There is irrevocable phase climbing in the result obtained through EKF22, which leads to mistakes in the subsequent signal processing. But in the right picture showing the phase demodulation using QAD and EKF32, it can be seen the two correspond to each other very well without any constant phase climbing.

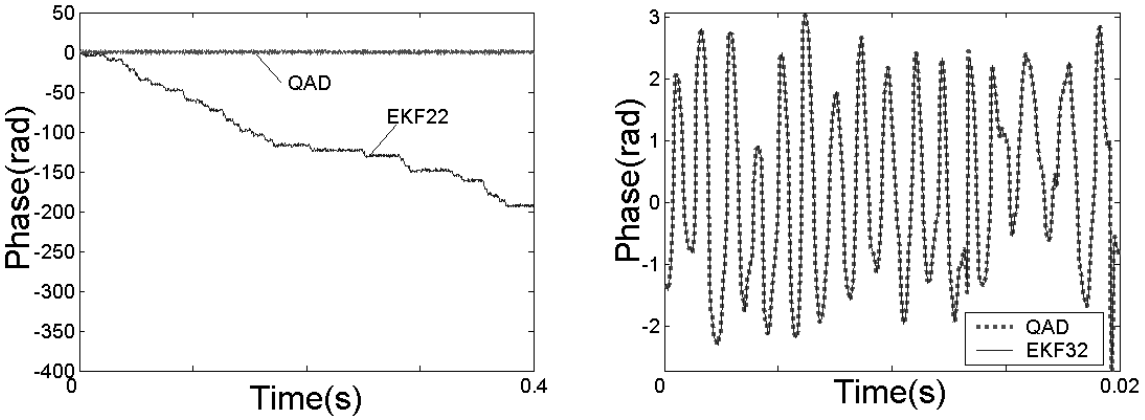

Fig.5-16 Phase demodulation using QAD, EKF22 and EKF32 in fully developed flow at high velocity

5.8.2 Disturbed flow

The phase demodulation in disturbed flow is also tested by QAD, EKF22 and EKF32. The result of low velocity is shown in Fig.5-17. Exactly like the situation in fully developed flow, the phase demodulated signal by means of EKF22 has a constant phase shift relative to QAD while EKF32 eliminates this shift.

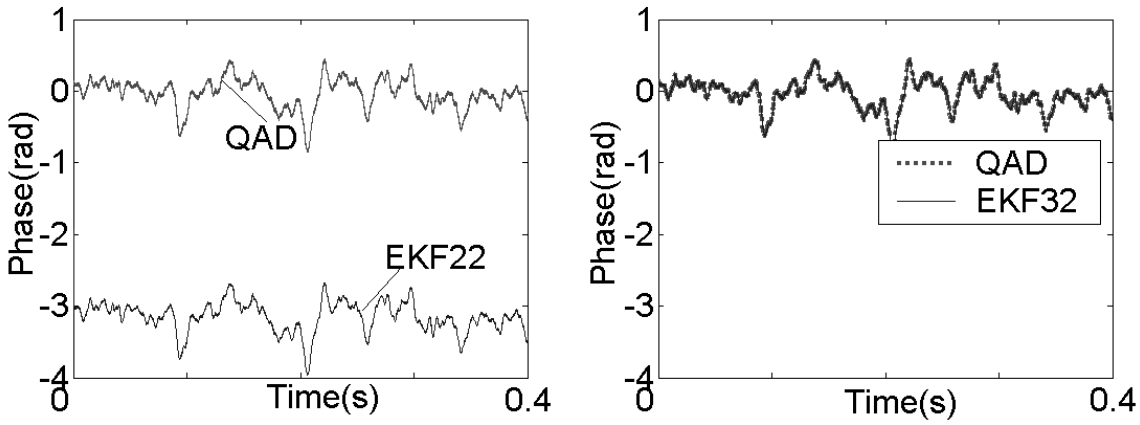

Fig.5-17 Phase demodulation using QAD, EKF22 and EKF32 in disturbed flow at low velocity

The demodulation result at high velocity is shown in Fig.5-18 where the left picture displays clearly that EKF22 brings out a phase climbing in the demodulation while EKF32 shown in right picture does not.

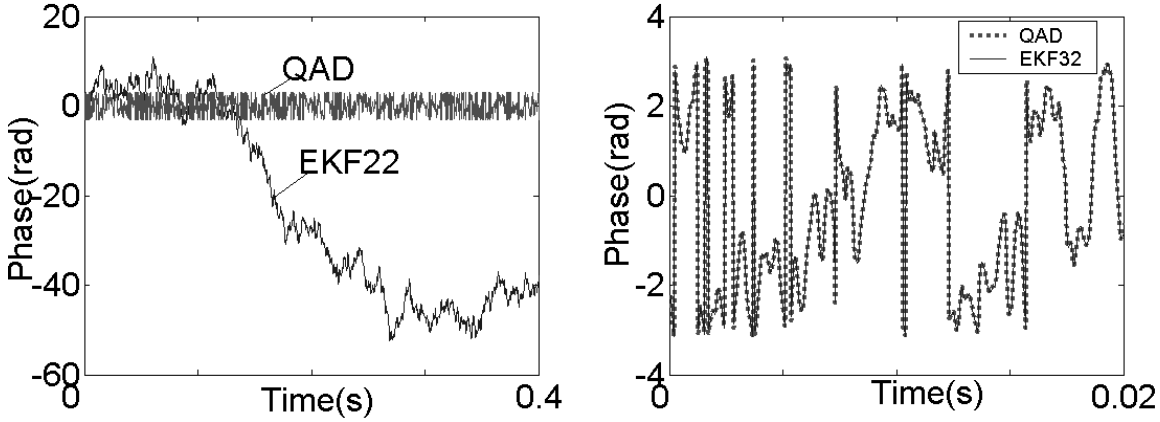

Fig.5-18 Phase demodulation using QAD, EKF22 and EKF32 in disturbed flow at high velocity

Phase climbing at high velocity in vortex measurement using EKF22 is a common problem which is also confirmed by Fig.5-19 which is the result of another unconventional-set triangular bluff body whose width is 24mm and length is 72mm.

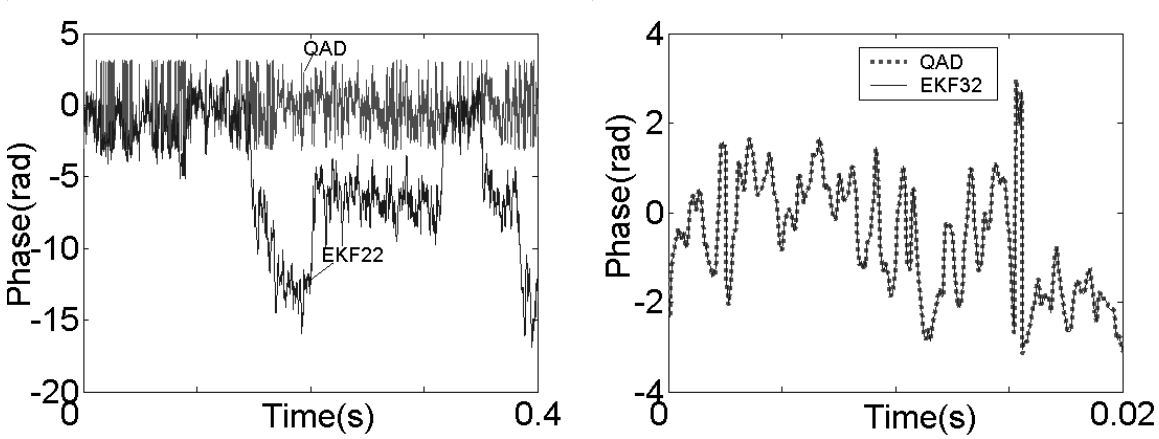

Fig.5-19 Phase demodulation using QAD, EKF22 and EKF32 in disturbed flow at high velocity

From the above discussion, a conclusion can be drawn that EKF22 functions well only in cross correlation measurement as is shown in[11] while EKF32 is also suitable for vortex measurement.

Fig.5-20 shows the frequency velocity characteristic using different methods in fully developed flow and disturbed flow. The disturbed flow is generated by two 90° bends in plane. The bluff body in it is unconventional-set triangle24-72. Conventional set bluff body triangle4-4 is used in the fully developed flow.The third filter EKF24 is not listed below because it shows no good results in vortex measurement. EKF32 has advantages over EKF22 which

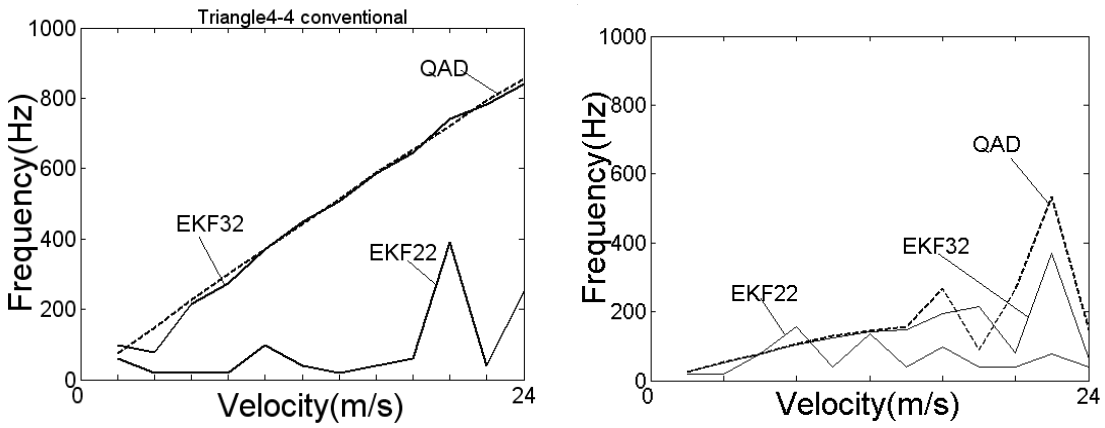

Fig. 5-20 f-v characteristic using different methods in fully developed flow(left) and disturbed flow(right)

can be clearly seen from Fig.5-20. But there is no obvious advantage of EKF32 over traditional QAD. QAD and EKF32 both function well for the low velocity range but not good for high velocity range.

From the discussion of this whole chapter about the application of Kalman filter in ultrasonic flow measurement, a conclusion may be drawn that EKF32 is good for the phase demodulation in cross correlation measurement especially at high velocity by filtering the noise and supressing the natural phase jumping. Both EKF22 and EKF32 are good for the phase demodulation in cross correlation measurement, with EKF32 being a little more advantageous. EKF24 is good only for the amplitude demodulation in undisturbed flow in cross correlation measurement.

6 Analog signal processing in flow measurement

The undersampling technique eliminates or reduces the burden of the converter in the digital signal processing. But it is not so well-known in practical application. Analog signal processing methods are more prefered therefore. In this section, a new analog signal processing method in ultrasonic flow measurement is discussed.

6.1 Frequency shifting

Suppose a real signal *f*(*t*)multiplied by a cosinusoidal signal $\cos\omega_0 t$ as expressed by

$$f(t)\cos\omega_0 t\,,$$

where *f*(t) is the modulating signal and the cosinusoidal signal is the carrier signal. According to Euler equation, it can be described as

$$f(t)\cos\omega_0 t = \frac{1}{2}(f(t)e^{j\omega_0 t} + f(t)e^{-j\omega_0 t}) \quad . \tag{6-1}$$

When applying Fourier Transform to the two sides of the above equation, the Fourier transform of the left side can be obtained as follows

$$\frac{1}{2}[F(\omega+\omega_0)+F(\omega-\omega_0)]. \tag{6-2}$$

This shows that multiplication of a signal *f*(t) by a sinusoid frequency ω_0 shifts the spectrum F(ω) by $\pm\omega_0$. This is the frequency shifting caused by multiplication.

6.2 Mathematic justification

$$\begin{aligned} A_c\sin(\omega_c t)\cdot A_m\cos(\omega_m t) &= A_c\cdot A_m\cdot\frac{1}{4j}(e^{j\omega_c t}-e^{-j\omega_c t})(e^{j\omega_m t}+e^{-j\omega_m t}),\\ &= A_c\cdot A_m\cdot\frac{1}{4j}[e^{jt(\omega_c+\omega_m)}+e^{jt(\omega_c-\omega_m)}-e^{-jt(\omega_c-\omega_m)}-e^{-jt(\omega_c+\omega_m)}], \qquad (6\text{-}3)\\ &= A_c\cdot A_m\cdot\frac{1}{2}[\sin((\omega_c-\omega_m)t)+\sin((\omega_c+\omega_m)t)]. \end{aligned}$$

In the equation (6-3), A_C and A_m are the amplitudes of the carrier and the modulating signal respectively. ω_C and ω_m are the corresponding frequencies. Equation(6-3) indicates the spectrum of the product of two sinusoidal signals has two sidebands around the carrier frequency.

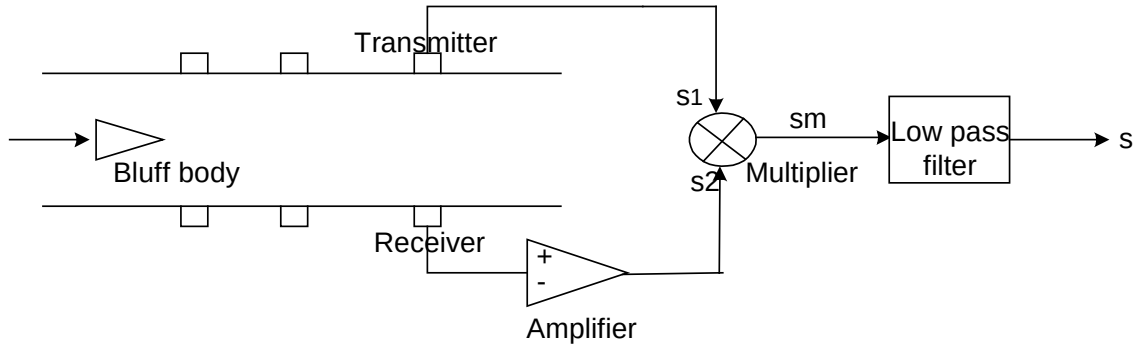

Fig. 6-1 Analog signal processing in vortex flow measurement

In the present case, that is vortex measurement which is shown in Fig.6-1, the modulating signal is the modulated signal caused by the vortex which contains also the carrier frequency, that is the ultrasonic sound frequency. For convenience, ω_m in equation(6-3) is written as

$$\omega_m = \omega_c + \omega_m', \tag{6-4}$$

where ω_m' is the modulating frequency of the vortex. According to equation(6-2), the spectrum of the multiplication of transmitter signal by the amplified receiver signal, that is sm in Fig.6-1, should have two parts of frequency. They are ω_m' and $2\omega_c+\omega_m$' respectively. With the following Low Pass filter, the vortex frequency ω_m' is obtained.

6.3 Amplitude modulation

This generation of sideband is similar to that generated from the amplitude modulation which will be described again in the next for reference.

Suppose the carrier signal described by

$$c(t) = C \cdot \sin(\omega_c t) \cdot \tag{6-5}$$

The modulating signal is

$$m(t) = M \cdot \sin(\omega_m t + P) \cdot \tag{6-6}$$

As is known, amplitude modulation is simply adding $m(t)$ to C, then the amplitude modulated signal is

$$y(t) = (C + M\sin(\omega_m t + P)) \cdot \sin(\omega_c t) \cdot \tag{6-7}$$

According to the trigonometric formulae, it can be written as

$$y(t) = C\sin(\omega_c t) + M\cos(P + (\omega_c - \omega_m)t)/2 - M\cos(P + (\omega_c + \omega_m)t)/2\,. \tag{6-8}$$

This means the amplitude modulation causes a pair of side bands in the spectrum of the modulated signal, which is completely the same with the multiplication of two sinusoid signals. This is shown in Fig.6-2.

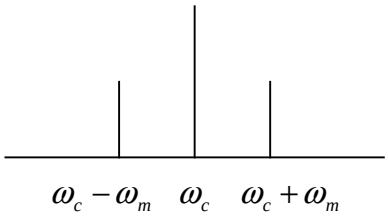

Fig. 6-2 Side bands from amplitude modulation

From the above analysis, it can be seen that multiplication of two sinusoidal signals is in essence a kind of amplitude modulation.

6.4 Application in vortex measurement and ccf measurement

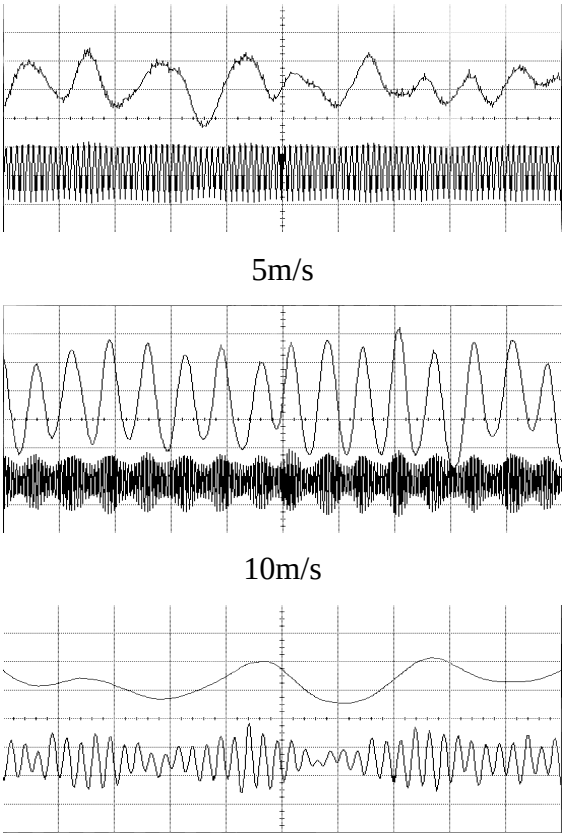

5m/s

10m/s

20m/s

Fig. 6-3 Photos from the oscilloscope in vortex measurement (unconventional set-up)
Upper signal: filtered multiplication Lower signal: receiver signal

The pictures in Fig.6-3 are from the bluff body with a width of 4mm and length of 12mm. The distance between receiver(channel 1) and bluff body is 45mm.It would be pointed out that in vortex measurement, the amplitude modulation is more dominant which can be clearly observed by the oscilloscope. Especially at high velocities, the amplitude modulation can be clearly seen from the lower signals in Fig.6-3. This amplitude modulated signal is multiplied by the carrier signal afterwards. According to the analysis above, the carrier signal will also be modulated by the amplitude whose information is contained in the receiver signal, that is, the modulating signal caused by the vortices generated behind the bluff body.

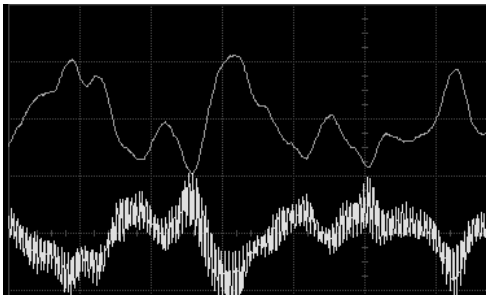

Fig. 6-4 Product(lower) of two signals and filtered product(upper)

In Fig.6-4, the lower signal is the product of the carrier signal and the modulated signal while the upper signal is the output of the analog method shown in Fig.6-1. Except the 180 degrees phase shift caused by the analog method itself, it can be seen that the product is strongly amplitude modulated. The upper signal in Fig.6-4 is exactly the demodulated signal or the modulating signal.

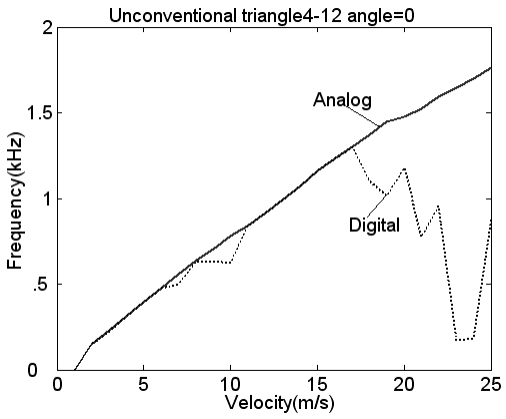

Fig. 6-5 Measurement results using analog and digital method

Fig.6-5 shows part of the measurement results from the analog method and compares it with that from digital method. Obviously the analog method has advantage. The frequency velocity characteristic line is more linear and has less deformation. This should owe to the low pass filter

which also filters the noise in the flow. However, in the cross correlation measurement, the amplitude modulation is not so strong as phase modulation according to the experience from the measurement. Fig.6-6 shows the photos from the oscilloscope which display the receiver signals at different flow velocities.

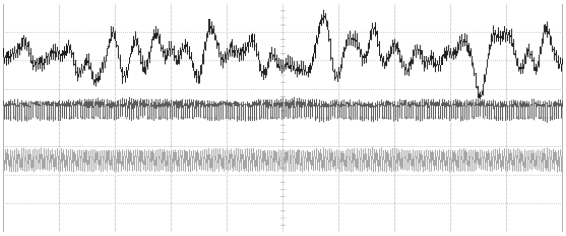

5m/s

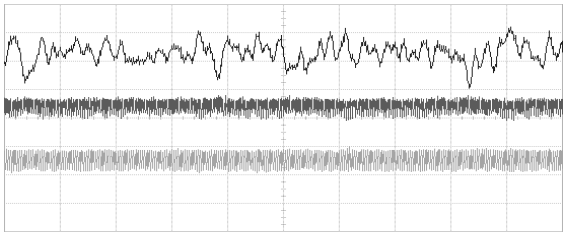

10m/s

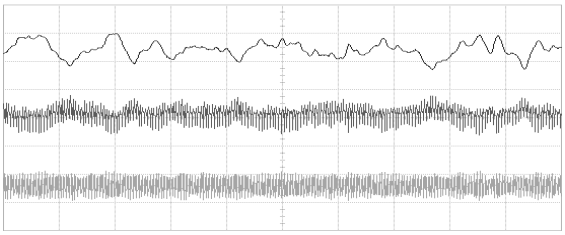

20m/s

Fig. 6-6 Signal photos from oscilloscope in ccf measurement
Upper: analog output Middle: product Lower: receiver signal

From Fig.6-6 which shows the photos of different signals in cross correlation flow measurement, it can be clearly seen that amplitude modulation is not dominant in this method. Some experiences have been obtained in the cross correlation measurement that the result is not so good when using amplitude modulation signal in this case. Just as pointed out above, the analog method is in fact a kind of amplitude modulation which uses the amplitude information contained in the receiver signal, so it can not be expected that the analog method functions well because of the weak amplitude modulation part in the receiver signal in the case of cross correlation measurement.

7 A combination of vortex flow meter with cross correlation method

7.1 Theoretical background

In flow measurement, the cross correlation method is based on the assumption that the flow belongs to Newton fluid which does not change within a short time. Cross correlation methods are applied especially to stochastic signals.

As mentioned above, the peak in the cross correlation function represents the transit time of the flow through the two barriers. Cross correlation functions can also be used to detect the periodic signal hidden in the stochastic background. The vortex flow meter is combined with cross correlation method to realize such a goal[29]. The measurement setup is shown in Fig. 7-1.

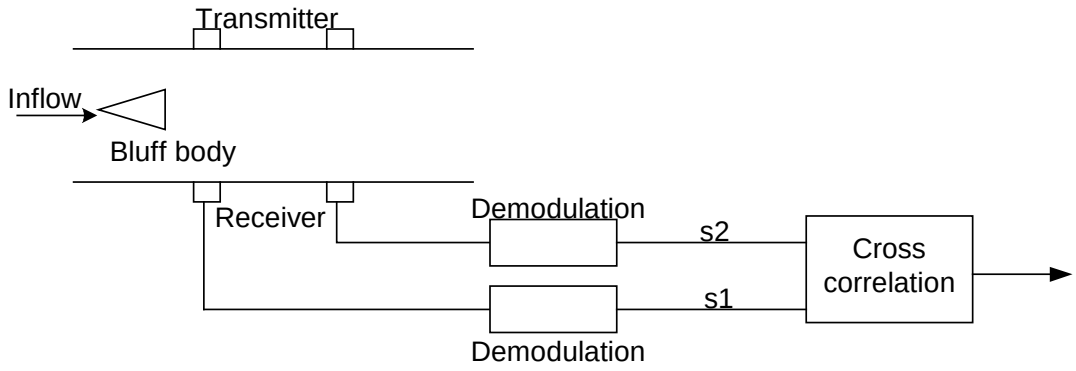

Fig. 7-1 Combination of vortex with ccf

The difference from the normal cross correlation method is that a bluff body is put in the pipe flow so that the signals s1 and s2 after demodulation from the receiver sensors are not dominated by stochastic signal but periodic signal. In this case, a sinusoidal signal due to the von Karman vortex street is generated.

The vortices generated by the bluff body can be regarded as a certain pattern[15, 37] which of course will pass through the second barrier in the downstream. Fig.7-2 displays the principle of the measurement. Because the signal is sampled from both channels not only for a time instant but for a period of time, therefore, the carrier signal is not modulated by only one vortex but by a group of vortices which is described as p in the upstream, and the same group, after certain time, goes to the downstream sensors which is described as p‘ in Fig.7-2. The transit time of this group from upstream to downstream is also the flow transit time which can be calculated from

the cross correlation function between the two channels. Given distance between the two channels, the flow velocity can be easily obtained.

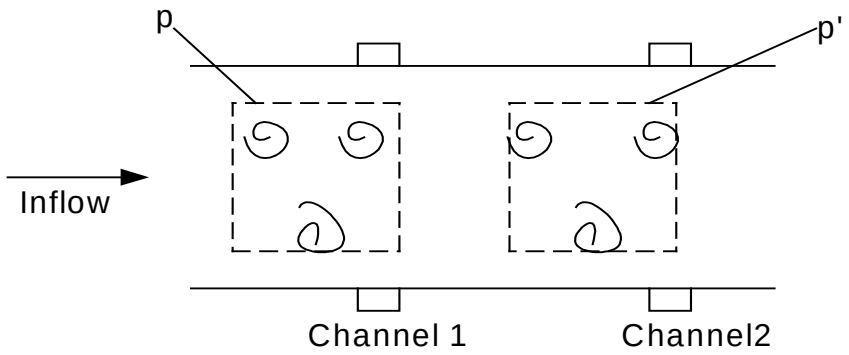

Fig.7-2 Pattern shift

As well known there is dissipation in the flow, so the distance between the channels should ensure the vortices will not dissipate much. This distance depends on such factors as size of the bluff body, flow velocity and so on. The dissipation amount through the distance can be displayed by the cross correlation coefficient between the two receiver signals. As shown in the next, the bluff body with relative smaller size is preferred in this measurement because of the small pipe-wall effect. It is self-evident that small bluff bodies generate smaller vortices which dissipate more quickly. That is, at a fixed flow velocity, they dissipate more in a short distance. Therefore the suitable distance must be ensured. To put it in an exact way, for a triangular bluff body with width of 4mm and length of 12mm, the longest distance between the shedding point of bluff body and the sampling sensors is 130mm.

As to how many vortices are sampled, an example is given. The distance between the two channels is 30mm. The triangular bluff body has a width of 4mm and a length of 12mm. The sampling time lasts for 0.8192 second. Taking velocity of 2m/s for an instance, the transit time for a vortex through the two channels is 0.015 second. Hence, there are altogether $0.8192/0.015=54\pm1$ vortices to be sampled. To see the influence of the vortex number sampled on the measurement results, only the sampling time should be shortened or extended.

7.2 Measurement results

Using this method, the cross correlation functions between the two channels are partially shown in Fig.7-3. The left side is for flow velocity of 2m/s and the right side is for 25m/s. In order to

study the influence of distance between channels on the cross correlation function, three channels are assembled whose distances from each other are 30mm, 60mm and 90mm respectively. The first channel is very near where the vortices are generated from the bluff body. From the figures of cross correlation function, it can be clearly seen the cross correlation coefficient decreases with the increasing distances between the channels. It is self-evident that the vortices dissipate with flow. After a long distance, the vortices will disappear. But they do not change within a relatively short distance. Bigger coefficient is undoubtedly an advantage, hence the distance between the channels should be shortened. In this case, 30mm is the best.

The cross correlation function in measurement without bluff body is also displayed in Fig.7-3, represented by the dashline. In comparison with the cross correlation measurement with bluff body, it has larger cross correlation coefficient at low velocity but smaller cross correlation coefficient at high velocity.

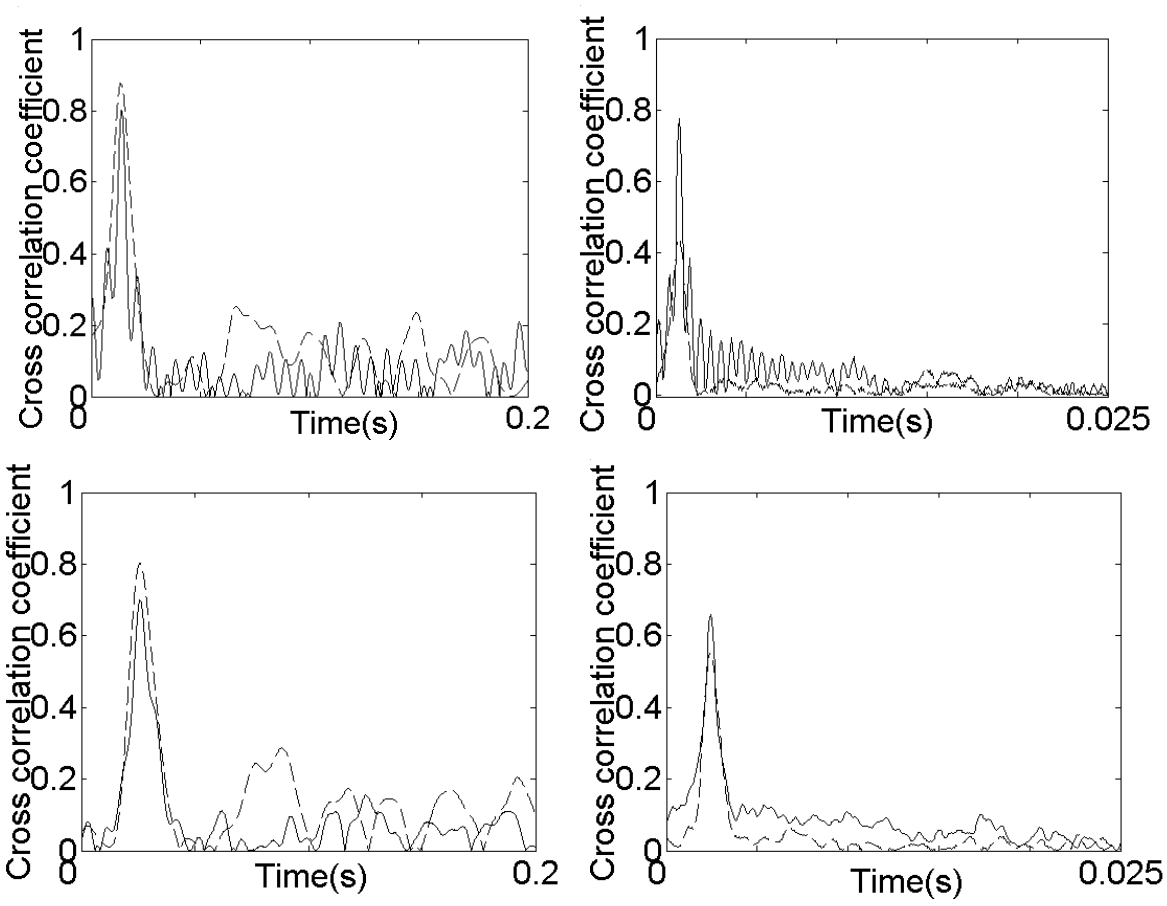

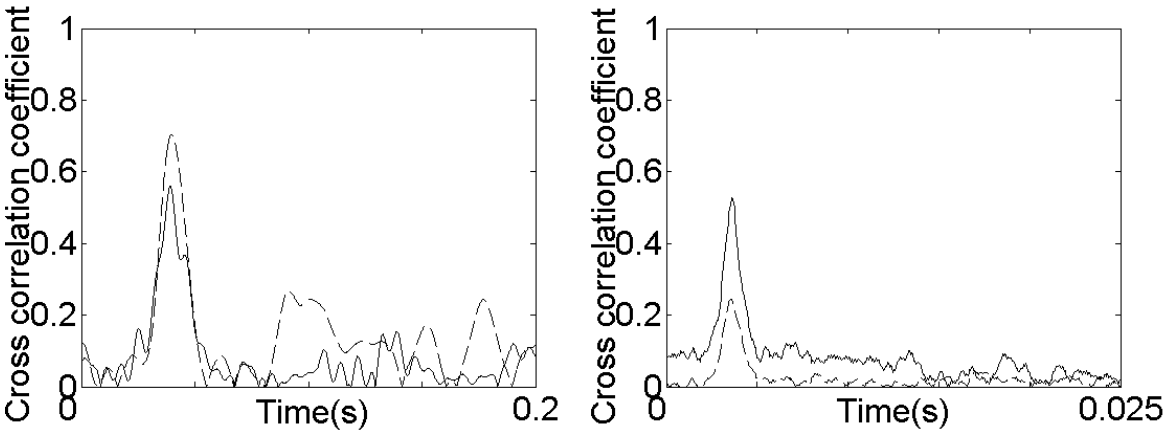

Fig. 7-3 Cross correlation function with vortex 2m/s (left) 25m/s (right)
30mm(upper) 60mm(middle) 90mm(lower)
dash line: without bluff body solid line: with bluff body

Next the flow velocity through different methods will be calculated and displayed.

Fig.7-4 shows the calculated results from this method and compares with the results from pure cross correlation method. It can be seen this method yields quite good results.

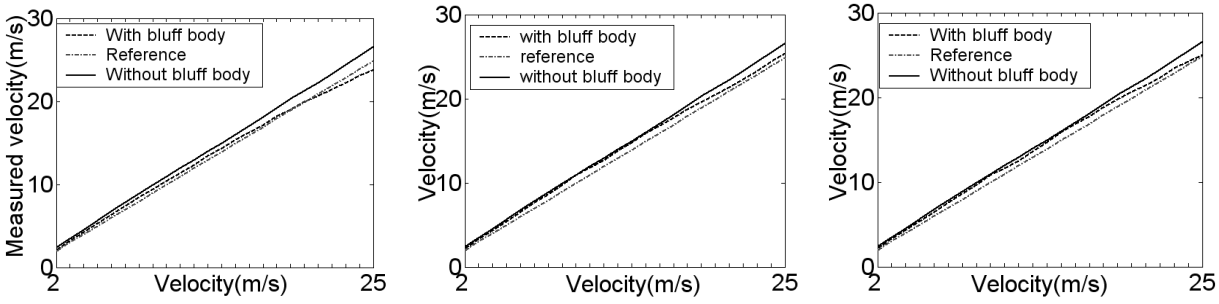

a) b) c)

Fig. 7-4 Calculated velocity
Distance between sensor pairs a)30mm b)60mm c)90mm

To better compare with the normal method so that the advantage of this method can be clearly seen, the corresponding uncertainty of the measured result is illustrated in Fig.7-5. The uncertainty of the measured velocity with bluff body is obviously smaller than that without bluff body. This is because of the different measurement principles in the two kinds of cross correlation measurement. In the both figures, Fig.7-4 and Fig.7-5, 30mm, 60mm and 90mm stand for the distances between sensor pairs.

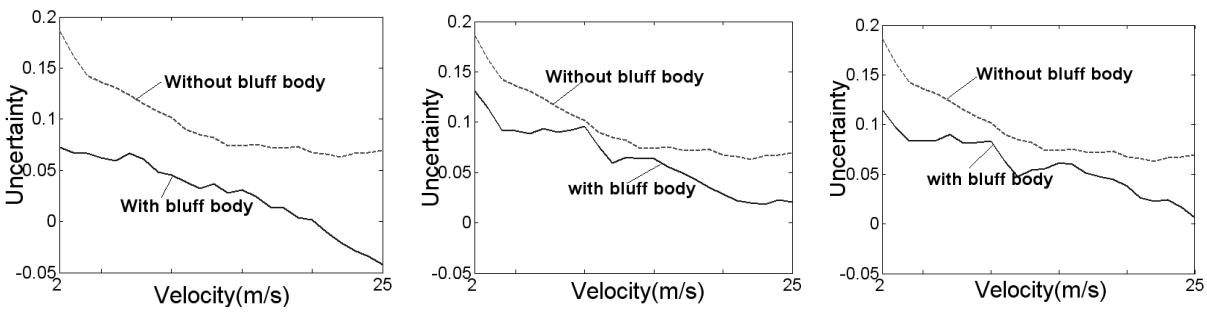

a) b) c)

Fig. 7-5 Uncertainty of measured velocity
Distance between sensor pairs a)30mm b)60mm c)90mm

7.3 Analysis

Principly, the cross correlation method measures the most probable velocity element in the flow[34]. This most probable velocity is regarded as average velocity. This conclusion is drawn because of an assumption is made about the fluid in cross correlation method. That is, the velocity element across the flow pipe section area meets the normal distribution as shown in Fig.7-6. In this case, the average velocity $\bar{v}$ is exactly the velocity v_p possessing the largest probability[34]. If the practical flow is like this, then there exists no systematic error caused by the measurement principle. However, the flow in practice does not precisely meet this assumption. The velocity element across the pipe section area does not meet the normal distribution but some other distribution somehow similar to normal distribution as illustrated in Fig.7-7. As is shown in Fig.7-7, the real distribution of the flow velocity element is not symmetric any more like in normal distribution. It is skewed normal distribution. As a result, the average velocity $\bar{v}$ does not equal the most probable velocity

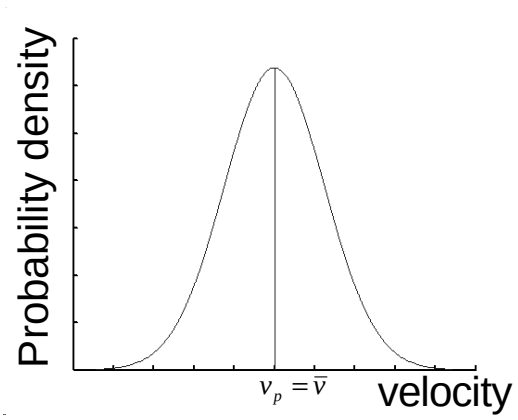

Fig.7-6 Normal distribution

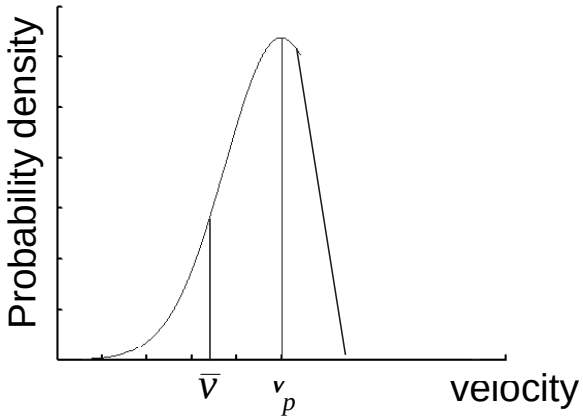

Fig.7-7 Actual distribution

v_p. But it is still regarded that the two velocities are the same, from which the systematic error undoubtedly generated. Therefore, the uncertainty of the pure cross correlation method is composed of both systematic and random uncertainty.

When a bluff body is put in the pipe flow, the signal to be measured is not random any more but periodic sinusoidal signal. So the assumption used in pure cross correlation method is not necessary. The systematic error is therefore eliminated. For this reason, the relative error of the cross correlation method with bluff body is smaller than that without bluff body.

The deviation factor should be taken into account in pure cross correlation measurement to rule out the systematic error caused by the measurement principle. This can be eliminated by putting a bluff body in the pipe flow. From other respect, the cross correlation measurement with bluff body is a self monitoring system. Firstly if one channel of sensor goes wrong, the cross correlation method will not work. But the vortex meter still runs. Secondly with the time passing by, the vortex meter displays a changing result because of the changing shape of the bluff body but the cross correlation meter maintains. When this happens the bluff body should be changed or the vortex meter should be recalibrated.

This method is only applicable for bluff bodies with relatively small size. In this case, the biggest width of bluff body is 8 mm. Bluff bodies of bigger width lead to bad results. This can be explained below.
The principle is based on the vortex group passing through the ultrasonic beam in a specific time. The signal received and sampled is generated by fairly large amount of vortices. With bigger bluff bodies, the number of vortex in a fixed distance decreases. So the signal can not so well carry the information of the flow when the sampling time is fixed as that for smaller bluff bodies. Theoretically, distance between channels can be lengthened or sampling time can be prolonged so that the number of vortices increases in order to better the final signal.

However, with the increasing size of bluff body, the size of vortices also increases. This will result in the known pipe-wall effect. Not only the naturally generated vortices but also those reflected by the pipe wall will modulate the ultrasonic beam, which leads to the counting error. What is more, the pressure loss of using bigger bluff body is always a problem which should be avoided.

7.4 Influence of bluff body size on the characteristic of the modulation in the vortex flow measurement

In the research done by Windorfer[12], it was pointed out that amplitude modulation is more dominant in the conventional vortex flow measurement than phase modulation. However, when applying the unconventional setup as shown in Fig.7-8, something interesting happens. It has been found that the size of the bluff body may to a certain extent affect the modulation characteristic. Therefore, the amplitude modulation part can not be taken all the time to be processed.

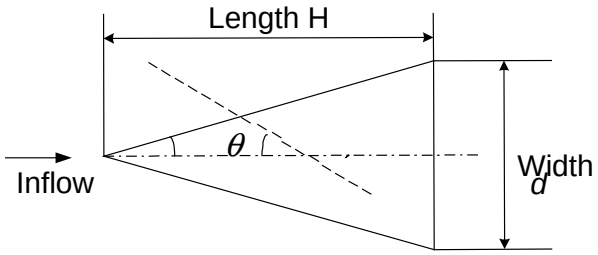

Fig.7-8Unconventional bluff body setup

Two bluff bodies with different sizes are used to detect this problem. Each was tried with different modulation signal part to get the f-v relation to compare with each other. Fig.7-9 and Fig.7-10 are the results of bluff body whose width is 4mm and length is 12mm. Fig.7-9 shows the f-v characteristic obtained through the amplitude modulation. Fig.7-10 shows the result through phase modulation. Obviously amplitude modulation is better or stronger than phase modulation.

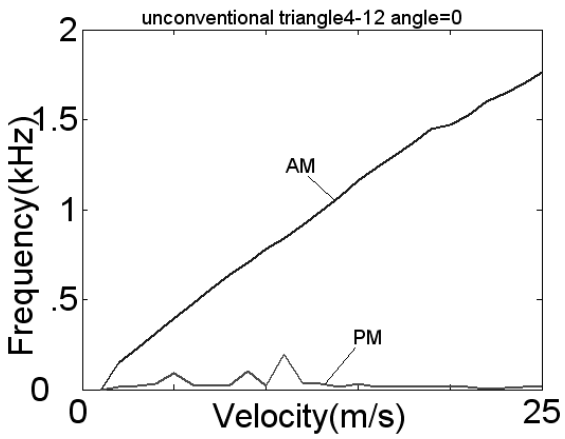

Fig.7-9 f-v characteristic measurement by amplitude modulation and by phase modulation

As to the other bigger bluff body whose width is 12mm and length is 36mm, Fig.7-10 shows the corresponding results. Obviously, phase modulation is better or stronger than amplitude modulation. This is just contrary to the smaller bluff body.

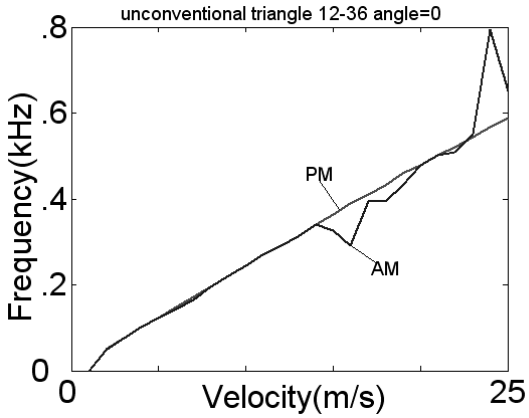

Fig. 7-10 f-v characteristic measurement by AM and by PM of big triangle

This phenomenon can be explained as follows. It is known that phase modulation is mainly caused by the superposition of vortex radial velocity on the ultrasonic beam, which leads to the phase shift of the carrier. The bigger the vortex, the bigger the vortex linear velocity.

As shown in Fig.7-11, $V_b > V_s$. For this reason, the bigger vortex causes more phase shift to the

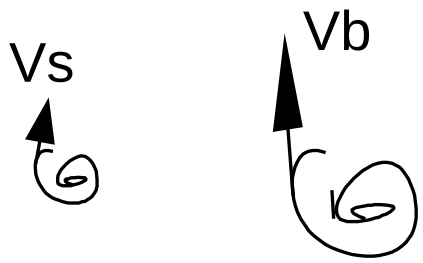

Fig. 7-11 Vortex of different size

carrier while the smaller one causes less phase shift. And it is undoubtable that big bluff bodies result in bigger vortices and small ones result in smaller vortices. The bigger vortices have more inertia so that they are more stable. For this reason, the vortices from the big bluff body can be measured at far instance but nothing or very little can be measured at the same distance in the case of smaller bluff body. The vortices, once shed from the bluff body, begin to dissipate with the flow direction. It is self-evident that smaller ones dissipate more quickly. From this respect, this problem can be relatively well explained.

The two bluff bodies are turned every time with one degree to see if it corresponds to the explanation given above.

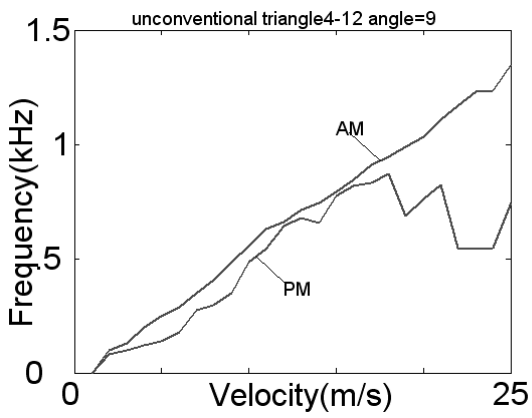

Fig.7-12 f-v characteristic measurement by AM and by PM (triangle4-12 angle=9°)

Fig.7-12 displays the corresponding results of the small bluff body at θ=9°. They even further indicate that in the case of smaller bluff body, amplitude modulation is more dominant.

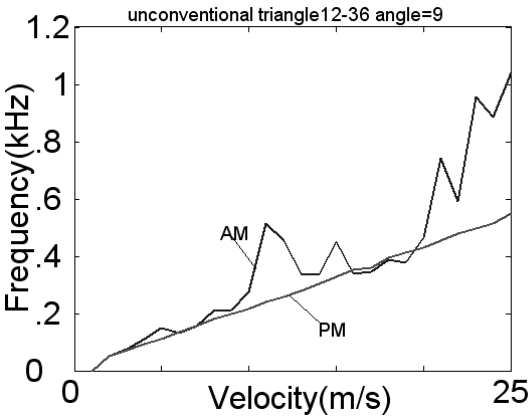

Fig.7-13 f-v characteristic measurement by AM and by PM

Fig.7-13 is the corresponding result of the big bluff body at θ=9°. It can be seen clearly that the phase modulation in this case is much more dominant in this case.

Two other bluff bodies with different sizes are also tested. The widths are 8mm and 24 mm. A conclusion can be drawn that for a bluff body whose width is smaller than 10mm, amplitude modulation is more dominant. For the bluff body whose width is bigger than 10mm, phase modulation is more dominant. This statement is related to a pipe diameter of 100mm.

8 Inclination of bluff body in vortex flow measurement

This chapter studies another factor which might influence the Strouhal number, that is, the inclination of the bluff body. The inclination of the bluff body happens in flow industry when the bluff body is inclined relative to its pipe parallel axis. Triangular bluff bodies are thoroughly discussed in this chapter. Normally, the flat side is facing the inflow which is called conventional setup, see Fig.8-3. It is turned around with 180 degrees facing the sharp side to the inflow, which is called unconventional setup[39, 40] in this chapter, see Fig.8-4. The inclination of bluff body has different influences in each setup. It is shown in this chapter that the flowmeter with bluff body in conventional setup results in lower Strouhal number but has more robustness to the inclination. On the contrary, it leads to higher Strouhal number but less robustness. With fixed width, the different length of the triangular bluff body also causes influence to the Strouhal number, which is described in detail in the next. In addition, the inclination of rectangular plate bluff bodies is also studied at the end of this chapter.

8.1 Measurement background

As explained in section 2.1.1, the frequency of vortex shedding is directly proportional to the flow velocity, thus providing the basis of a flowmeter[19]. The relation between the shedding frequency f_v and flow velocity u_m is described by equation (2-1).

Experiments indicate that the dimensionless number S_r depends only on the Reynolds number *Re*, which is shown in the Fig.8-1[21].

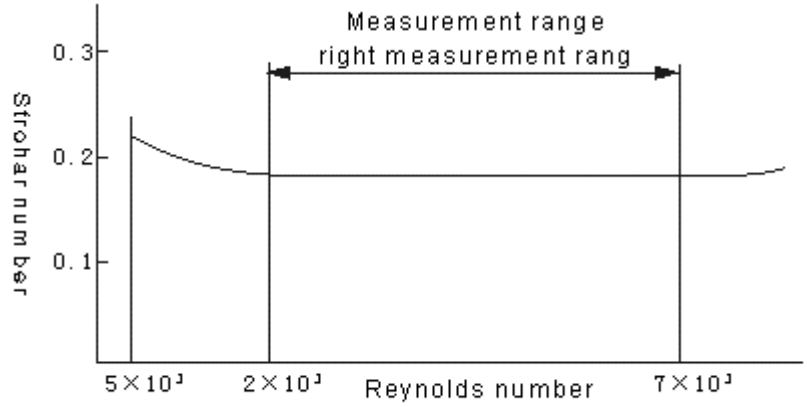

Fig.8-1 Relationship between Strohar number and Reynolds number

It can be seen that the Strouhal number almost maintains constant within a wide range of Reynolds number. For a specific bluff body, the width *d* is also a constant, so the vortex shedding frequency is linear with the upstream velocity. This is the main principle of vortex flow meter based on Karman vortex Street effect.

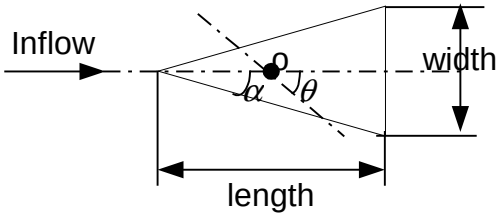

Fig.8-2 Bluff body

The width of the bluff body is defined normaly as shown in the Fig.8-2. In the vortex flow measurement, the position of the bluff body in the pipe flow will certainly influence to some extent the sensitivity[11] of the flow meter, among which the rotation of the bluff body is a normal problem due to the production tolerance and installation tolerance. In this section, the research results with experimental results on this problem are displayed so that some specific laws in this field can be found out. Considering the specific research condition in the laboratory, only the triangle bluff bodies and rectangle plates are studied.

As shown in Fig.8-2, the bluff body is rotated around the point *O* with a certain angle until $\theta=\alpha$ for triangle bluff bodies so that one side is parallel to the flow. Point *O* is the middle point of the symmetrical axis of the bluff body. During this process, it is found that the frequency of the vortex changes even at the same velocity. Since the width *d* is constant for the same bluff body, the vortex frequency should be always the same according to the above formular. But measurements do not confirm this.

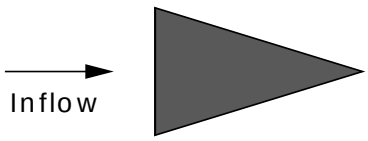

Fig.8-3 Conventional setup

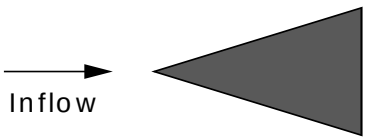

Fig.8-4 Unconventional setup

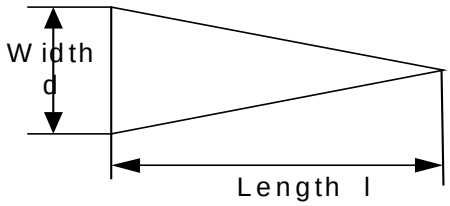

Fig. 8-5 Definition of ratio *l*/*d*

Triangle bluff bodies with different ratios between width and length defined in Fig.8-5 are tested. The ratios studied in this work are *l*/*d*=1, 2, 3, respectively. The performances in both conventional setup and unconventional setup shown in Fig.8-3 and Fig.8-4 are also initially studied which will be described in the next. The vortex shedding frequency is researched in this chapter. For convenience, the concept of sensitivity is inherited from Filips[10]. It is defined as

$$sensitivity = \frac{f_v}{u_m} \ . \tag{8-1}$$

It can be deduced that the unit of sensitivity is m^{-1}. That physically means sensitivity stands for the number of vortices in the distance of one meter. Theoretically, it keeps constant for a specific bluff body. It does not change with the flow velocity as the frequency does.

8.2 Ratio=1

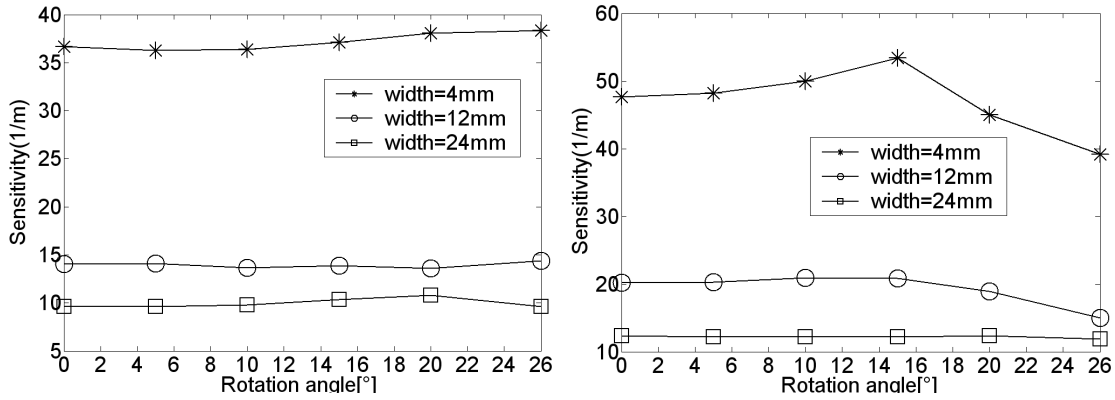

Fig. 8-6 Changes of sensitivity with rotation of bluff body of ratio 1 in conv. setup(left) and unconv. setup(right)

The marked measuring points are average values of a set of 20 measurements. Left picture in Fig.8-6 shows that the sensitivity fluctuates around a certain value during the bluff body rotation. This indicates the robustness of the conventional-set bluff body with ratio 1. The bluff body with width of 4mm seems to be an exception. The sensitivity has more upward tendency than

fluctuation around a certain value. This could be explained by the characteristic width of the bluff body defined by d1 and d2 in Fig.8-7. With the rotation,

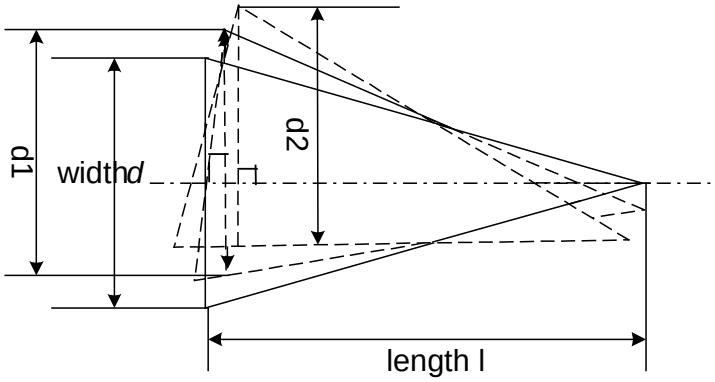

Fig.8-7 Characteristic width of triangular bluff body during rotation

the characteristic width decreases so that the sensitivity eventually increases. At around 15°, there is a transition period of the vortex shedding point. For bluff bodies with other bigger width, there exists also characteristic width. But due to the large size, the characteristic width plays a smaller role here than the asymmetric flow profile caused by the rotation. Therefore, the sensitivity does not go upward. At the same time, the well known pipe wall effect makes the changes in sensitivity undetectable. So it keeps almost constant. From this aspect, the conventional setup seems to be the ideal situation according to the pictures in Fig.8-6 because the sensitivity tends to be constant even if the relative bigger bluff body rotates with a big angle. In this case, the rotation of the bluff body does not have to be worried about by virtue of the robustness.

Right picture in Fig.8-6 indicates that when the width of the bluff body is relatively small, the rotation has a relatively big influence on the sensitivity of the flow meter. In the present case, the width of 4 mm and 12mm have the same tendency of sensitivity changing with the rotation of the bluff body. From 0° to about 15°, the sensitivity increases, it decreases from 15° on. The characteristic width plays undoubtedly a role in the increasing process like in conventional setup. The subsequent decreasing process is caused by the shifting of vortex shedding side from side d1 to side d2 as shown in Fig.8-8. Side l2, which is the long side of the triangular, is longer than d1, which leads to the decreasing sensitivity.

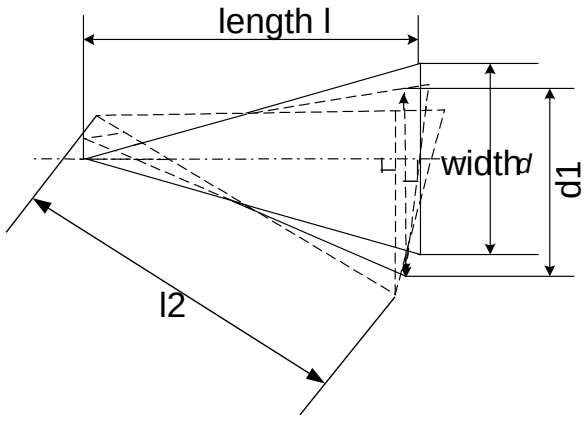

Fig. 8-8 Changing of vortex shedding side

But in the case of width 24 mm, it seems to be very robust. The sensitivity does not change much even with same degree of bluff body rotation. From mathematical view, the sensitivity at angle=26 degree in the case of width 4mm decreases to 82.1% of that at angle=0 degree. But the bluff body with width of 24mm does not decrease. This can be well explained by the pipe wall effect.

8.3 Ratio=2

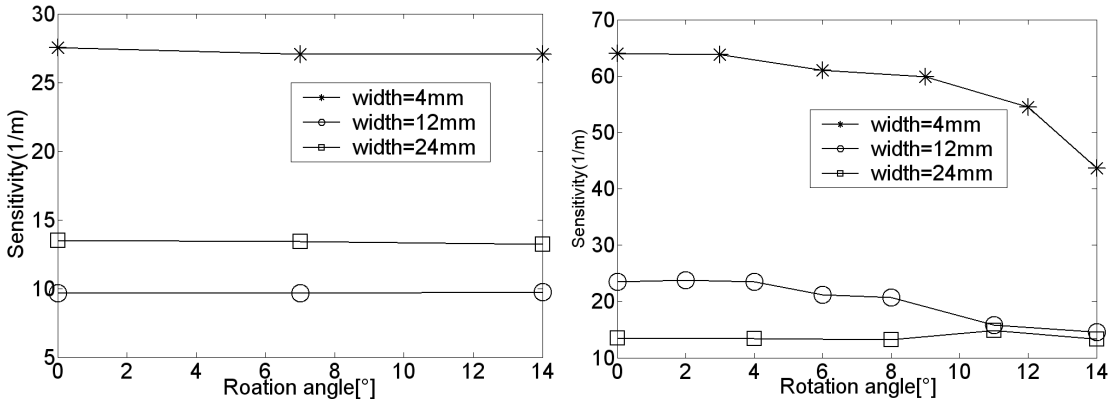

Fig. 8-9 Changes of sensitivity with rotation of bluff body of ratio 2 in conv. setup(left) and in unconv. setup(right)

In the left picture of Fig.8-9, only three measurement points are shown in the figure. This is, according to the former measurement experience, enough to represent the tendency of the sensitivity without deviation. The figures clearly indicate that the sensitivity is almost constant in conventional setup. But in the case of bigger bluff body, the sensitivity fluctuates more. This is

mainly because of the stronger wall effect. The vortices are reflected from the pipe wall leading to the counting error or modulation error.

In the right picture of Fig.8-9, when the width of the bluff body is relatively small, the rotation has a relatively big influence on the sensitivity of the flow meter. And in present case, the width of 4 mm and 12mm have the same tendency of sensitivity changing with the rotation of the bluff body. With the rotation, the shape relative to the inflow changes correspondingly. That is the reason why the sensitivity changes. But in the case of width 24 mm, it seems to be very robust. The sensitivity does not change much even with the same degree of bluff body rotation. From mathematical view, the sensitivity at angle=14 degree in the case of width 4mm decreases to 68.2% of that at angle=0 degree. For the width of 12mm, it decreased to 61.2% of that at angle=0 degree. But the bluff body with width of 24mm does not decrease.

8.4 Ratio=3

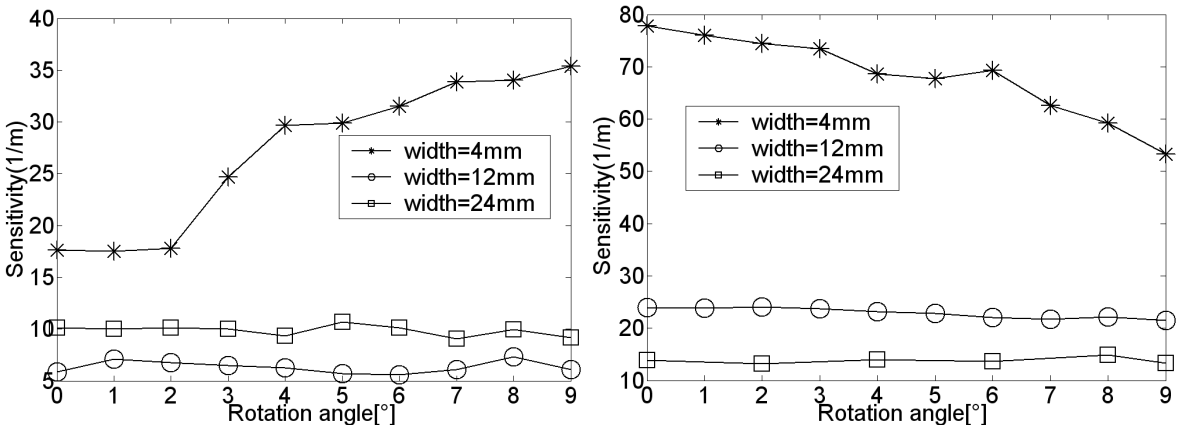

Fig. 8-10 Changes of sensitivity with rotation of bluff body of ratio 3 in conv. setup(left) and in unconv. setup(right)

The bluff body with width 4mm shows a special characteristic in the left picture of Fig.8-10. Its sensitivity increases dramatically with the rotation. Characteristic width can account partly for this, but the increasing amount is too large for the characteristic width. The real reason for this change needs to be further researched. The other two bigger bluff bodies display more stable characteristic.

In the right picture of Fig.8-10, when the width of the bluff body is relatively small, the rotation has a relatively big influence on the sensitivity of the flow meter. And in this case, the width of 4

mm and 12mm have the same tendency of sensitivity changing with the rotation of the bluff body. But in the case of width 24 mm, it seems to be very robust. The sensitivity does not change much even with same degree of bluff body rotation. From mathematical view, the sensitivity at angle=9 degree in the case of width 4mm decreases to 67.9% of that at angle=0 degree. For the bluff body with width 12mm, it decreases to 89.6% of that at angle=0 degree. But in the case of bluff body with width of 24mm it does not decrease.

Besides, it has been discovered from experiments that for a fixed width, different length leads to the difference in sensitivity. The sensitivities of bluff body with different ratios at

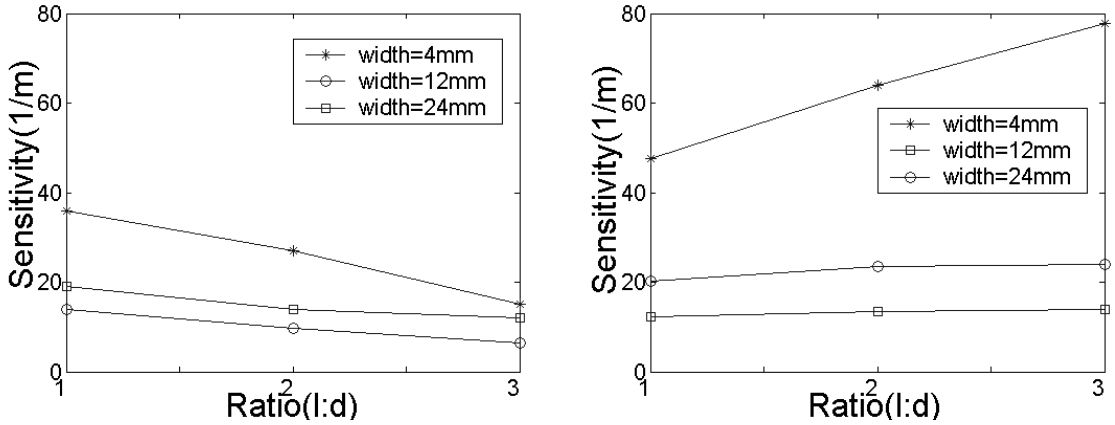

Fig. 8-11 Sensitivity changes with the width of bluff body in conventional setup(left) and unconventional setup(right)

angle=0 degree both in conventional setup and unconventional setup are compared and the result is shown in Fig.8-11. From the above figure, it can be seen that the smaller the width of the bluff body is, the stronger influence of the length on the sensitivity is. But the influence of the length on different setup is quite different. In unconventional setup, for a fixed width, the sensitivity increases with the increasing length of the bluff body. While in conventional setup, the tendency is completely contrary. The sensitivty decreases with the increasing length of the bluff body for a fixed width. The change of the sensitivity due to the different length is mainly caused by the difference in Strouhal number because with different ratio, the shape of the bluff body is different. Strouhal number is a function dependent on the Reynolds number. In addition, it is dependent on the shape of the bluff body. Hence, the sensitivity will change.

8.5 Rectangular bluff body

The rectangle bluff body is installed in the pipe as shown in Fig.8-12. The rectangle whose

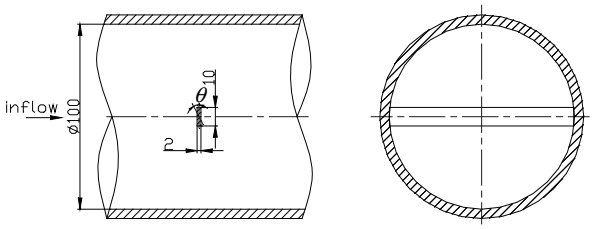

Fig.8-12 View from front and view from left (unit: mm)

width is 10mm and length is 2mm rotated from 0 degree to 90 degrees to see the changes in sensitivity. From the Fig.8-13, it can be seen that the rotation causes strong influence on the sensitivity which can be explained by the form of characteristic width defined in Fig.8-13 where θ is the rotation angle. α is the angle between diagonal and the vertical symmetrical axis of the rectangular bluff body which can be calculated as α=arctan(1/5)=11.3°. With the rotation, the characteristic width decreases so that the

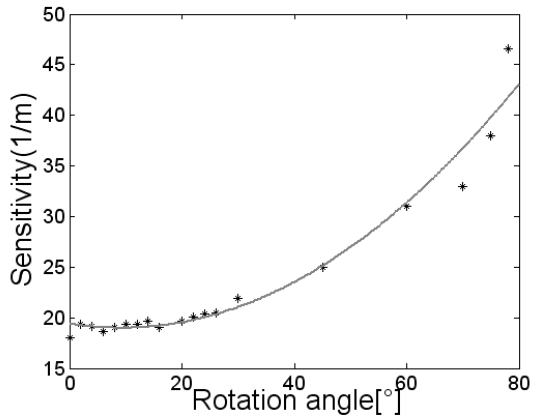

Fig. 8-13 Sensitivity

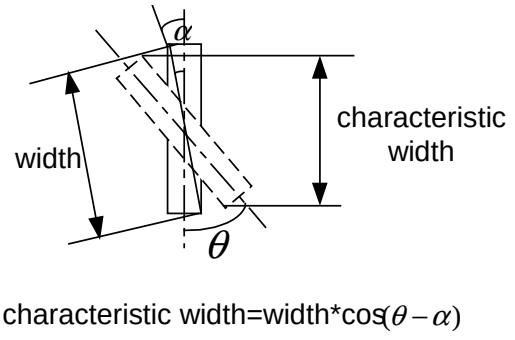

Fig. 8-14 Definition of characteristic width

sensitivity increases according to equation (2-1) in chapter 2. In fact, the characteristic width is the actual wake of the vortices. Only the angles from 0 to 75 degrees are listed because the bigger angles show no stability. The sensitivity decreases dramatically due to the much too small characteristic width, defined in Fig.8-14, of the bluff body.

A set of rectangular bluff bodies have been investigated. They all possess the ratio 5 of width to length. Their sizes are displayed in Tab.8-1.

Tab.8-1 Sizes of rectanglular bluff bodies investigated in inclination

Characteristic width mm(θ=0°)	24	20	16	12	10	8	6	4
Length (mm)	4.8	4	3.2	2.4	2	1.6	1.2	0.8

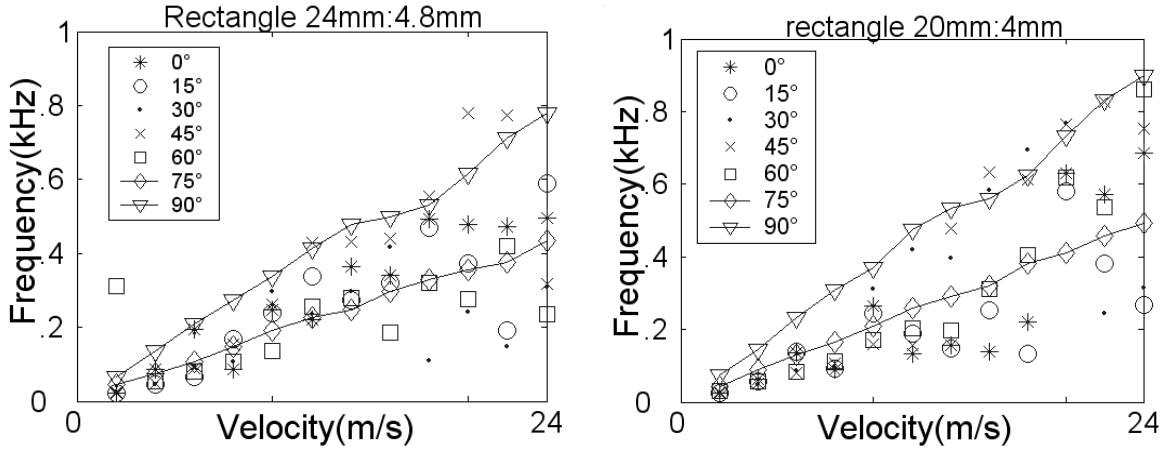

Fig. 8-15 f-v characteristic lines for rectangle at different angles

Fig.8-14 displays the frequency and velocity characteristic for rectangle at different angles. For the rectangle with width of 24mm, the characteristic line begins to show stability since 75°, which corresponds to the characteristic width of 10.8mm. The right picture in Fig.8-15 also possesses this feature. For this rectangle, the characteristic width at 75° is 9.04mm. Rectangle with a width of 16mm and length of 3.2mm beginns to show stable frequency velocity characteristic since 54° at which the chracteristic line is 12mm. This can be also proved with the rectangle with a width of 12mm and length of 2.4mm shown in Fig.8-16.

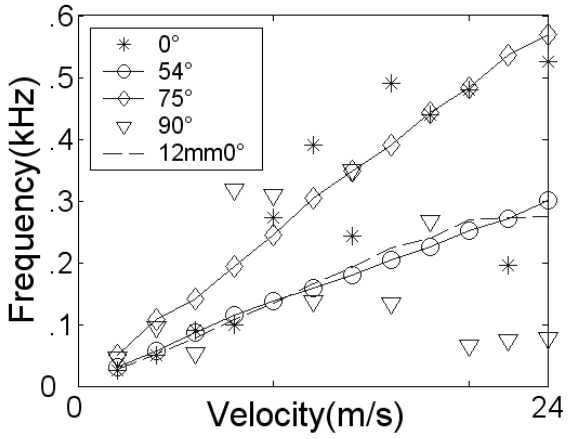

Fig.8-16 f-v characteristic for rectangle 16mm at different angles

After a large amount of investigations, a conclusion can be followed. Only if the characteristic width is equal to or smaller than 12mm the vortex flow meter using rectangular bluff body works well. The characteristic width must not be smaller than 4mm. The vortices generated by bluff bodies are too small and not stable in the streaming fluid.

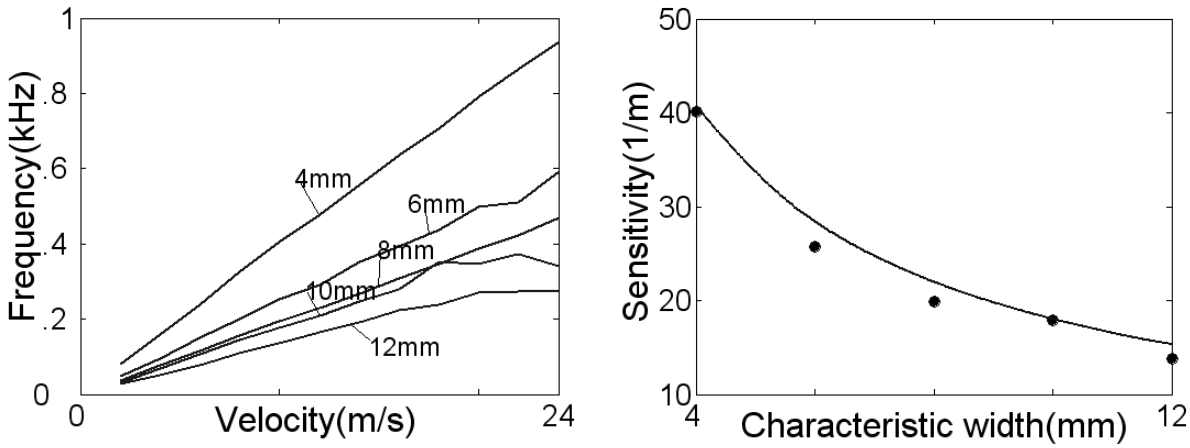

Fig.8-17 f-v relation for different size of rectangles at 0° and corresponding sensitivity

Fig.8-17 shows the frequency velocity characteristic lines and the corresponding sensitivity for the suitable rectangle bluff bodies at angle=0°. It could be shown that the charcteristic width is independent off the natural size of the bluff body. Only the characteristic width counts. The sensitivity characteristic line can be expressed by equation $S=140 \cdot d^{-0.89}$, where d is the characteristic width of the rectangular bluff body whose unit is mm.

Proof of the existence of characteristic width

Cross correlation method in the case of rectangle is applied to prove the existence of the characteristic width. The result is shown in the following figures. The rectangle whose width is 10mm, length is 2mm is taken as a description example to prove this existence.

From the angle of 60 degrees on, the cross correlation method works very well which can be seen in the above figure. When the angle equals 60 degrees, the characteristic width is 6.73mm according to its definition. This width is suitable for the pipe flow as the vortex flow meter is combined with cross correlation method.

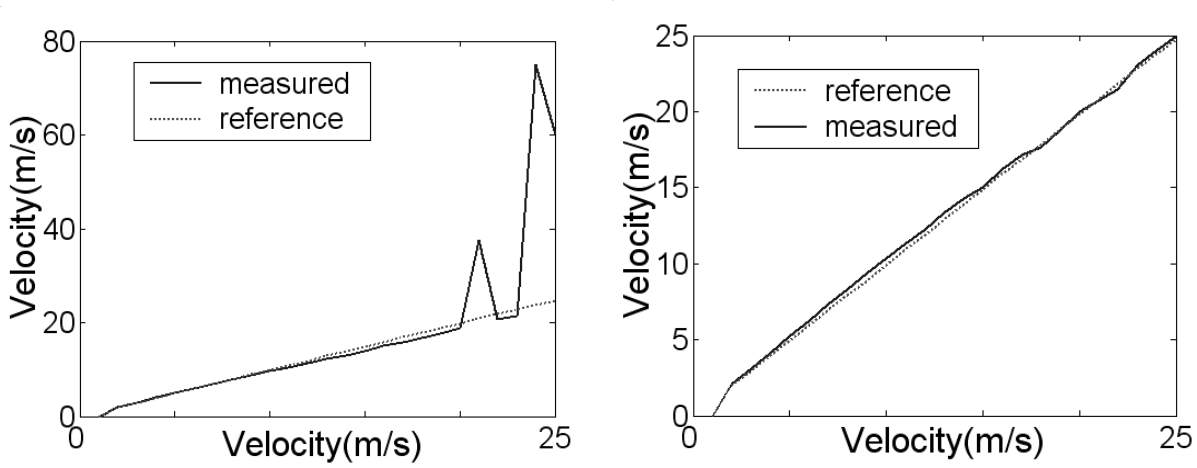

Fig. 8-18 CCF combined with vortex at angle=60°(left) and angle=80°(right)

The right picture in Fig.8-18 shows the measured result at the angle of 80 degrees. At this angle, the characteristic width is 3.7mm which is too small for pure vortex flow meter but good for the cross correlation method.

It has been discussed in Chapter 7 that the vortex flow meter combined with cross correlation method works well for the bluff bodies with a width smaller than 8mm. This is further proved by the rotation of rectangular bluff bodies. Only when the rectangular bluff body is inclined with a certain angle at which the characteristic width is smaller than 8mm can this method work well. It is clear that the natural width of the bluff body does not change. What has changed is the vortex generation point. That is also the width of the von Karman vortex street, or the width of the wake which is called characteristic width in this work.

According to the above discussion and research, although there is still a lot to be further proved, yet the following conclusion can be drawn. That is, bigger bluff body has higher robustness against the rotation; bigger bluff body in conventional setup is more robust than in unconventional setup.

Large amount of investigations display both the advantages and the disadvantages for each kind of bluff body. No doubt the resolution of the measurement will be improved with the higher sensitivity which can be brought by unconventional-set bluff body. So unconventional setup should be the ideal choice for vortex measurement. The inclination of bluff body in practical flow industry is very small, which causes little influence on the sensitivity despite that the

smaller bluff body is more sensitive to the inclination. Therefore, smaller bluff body should be considered as the first option compared with bigger bluff body because there is larger pressure loss with bigger bluff body than with smaller one. All in a word, the unconventional-set small bluff body is the most suitable for ultrasonic vortex flow measurement.

9 Disturbed flow measurement

Fully developed flow is the counterpart of disturbed flow which is always required in practical flow measurement. They are two states of flow according to their disturbance. They can be changed into each other by means of the singularities of pipe setting and so on. The entrance length is also critical for the distinguishment of both states. For better understanding, the concept of fully developed flow and disturbed flow will be discussed in detail in the next.

9.1 Fully developed flow and disturbed flow

An effect of viscosity is evident at the entrance to a pipe as illustrated in Fig.9-1. Flow is uniform at the entrance, but as the fluid travels downstream, the effect of zero wall velocity propagates throughout the cross section. The flow is divided into a viscous region and a core region. Particles in the core do not sense that a wall is present. Eventually, the core disappears, and the velocity distribution becomes fully developed. A fully developed profile does not change with further increases in length. Mathematically it is written as

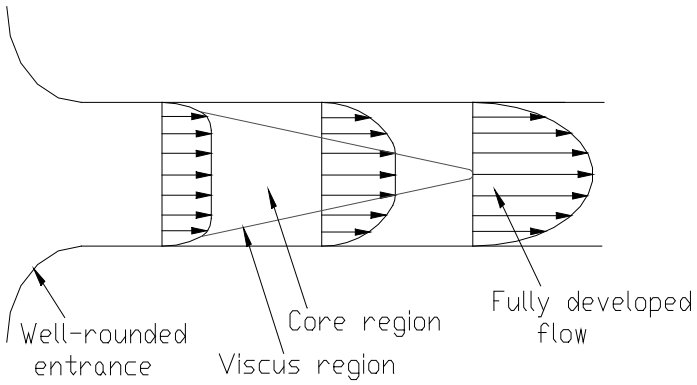

Fig. 9-1 Laminar flow near a pipe inlet

$$\frac{d(V_z)}{d(z)} = 0 \qquad \text{(fully developed laminar flow)} \tag{9-1}$$

$$\frac{d(\overline{V}_z)}{d(z)} = 0 \qquad \text{(fully developed turbulent flow)} \ . \tag{9-2}$$

The distance *Le* is called the entrance length whose magnitude is dependent upon the forces of inertia and viscosity. It is in fact the length in a tube or duct until the flow velocity profile is fully developed after obstructions. It has been determined from numerous experimental and analytical investigations that the entrance length can be estimated with

$$Le=0.06D(\mathrm{Re}) \quad \text{(for laminar flow)} \tag{9-3}$$

$$Le=4.4D(\mathrm{Re})^{1/6} \quad \text{(for turbulent flow)} \tag{9-4}$$

where $\mathrm{Re}=\rho VD/\mu=VD/\nu$. For laminar flow, it can be seen that the entrance length varies directly with the Reynolds number. For the largest Reynolds number encountered in laminar flow of 2100, equation (9-3) predicts

$$Le=0.06D(2100)=126D .$$

Thus, 126 diameters is the maximum length that would be required for fully developed conditions to exist in laminar flow.

For turbulent flow, the entrance length varies with the one sixth power of the Reynolds number. Conceptually, there is no upper limit for the Reynolds number in turbulent flow, but in many engineering applications, $10^4<\mathrm{Re}<10^6$. Over this range, it can be calculated with equation (9-4)

$$20<Le/D<44.$$

So in turbulent flow, the entrance length values are considerably less than the 126 diameters required at a Reynolds number of 2100. The reason that a shorter length is required in turbulent flow is the mixing action. For abrupt or sharp-edged entrances, additional turbulence is created at the inlet. The effect is to further decrease the entrance length required for fully developed flow to exist[43].

9.2 Technologies in disturbed flow measurement

Most of the flowmeters only work fairly well under a fully developed flow as discussed above. In practice, due to the spatial limitations, the entrance length can not be met. At this moment, the flow is in a disturbed state. Disturbed flow measurement is a difficult problem in flow measurement field. A lot of research work has been done about this problem.

Griswold Control's "Disturbed Flow Measurement"[2] means engineers can specify to ±1% accuracy and locate the valve with less than four pipe diameters entry piping, or adjacent to an elbow or temperature control. A patented Piezo Ring and dual chamber[2] enable accurate measurement in the smallest footprint, ensuring quality comfort conditioning and lowering operating costs for owners. The McCrometer V-Cone Flowmeter[3], shown in Fig.9-2, is a patented technology that accurately measures flow over a wide range of Reynolds numbers, under all kinds of conditions and for a variety of fluids. This flowmeter is introduced in detail for better understanding of the unconventional-set triangular bluff body applied in disturbed flow

which is going to be later described. It operates on the same physical principle as other differential pressure-type flowmeters, using the theorem of conservation of energy in fluid flow through a pipe. The V-cone's remarkable performance characteristics, however, are the result of its unique design. It features a centrally-located cone inside the tube. The cone interacts with the fluid flow, reshaping the fluid's velocity profile and creating a region of lower pressure immediately downstream of itself. The pressure difference, exhibited between the static line pressure and the low pressure created downstream of the cone, can be measured via two pressure sensing taps. One tap is placed slightly upstream of the cone, the other is located in the downstream face of the cone itself. The pressure difference can then be incorporated into a derivation of the Bernoulli equation to determine the fluid flow rate. The cone's central position in the line optimizes the velocity profile of the flow at the point of measurement, assuring highly accurate, reliable flow measurement regardless of the condition of the flow upstream of the meter.

Pipe flow is rarely ideal. Practically any change to the piping can disturb even a well-developed flow. The contoured shape and location of a suspended cone in the V-Cone Flowmeter overcomes this by reshaping the velocity profile upstream. As the flow

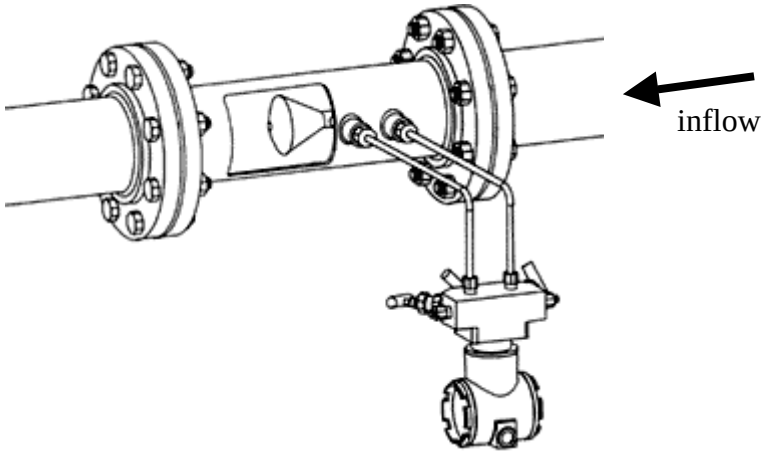

Fig.9-2V-cone flowmeter [3]

approaches the cone, the flow profile "flattens" toward the shape of a fully-developed profile even in extreme flow conditions.

9.3 Forms of disturbed flow

In this research, three kinds of pipe singularity are used to generate disturbed flow. They are one 90° bend, two 90° bends in plane and two 90° bends out of plane, respectively. The schematic and disturbance characteristics of each singularity will be discussed in the next.

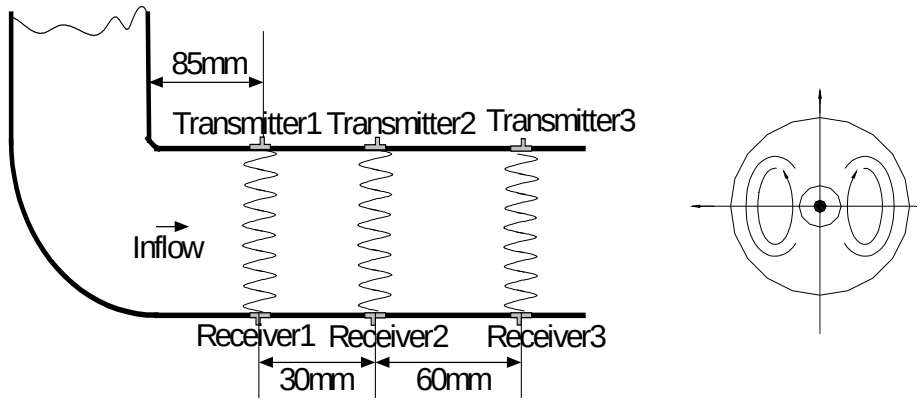

Fig. 9-3 One 90° bend or two 90° bends in plane

As shown in Fig.8-3, the downstream of the bend the flow is severely disturbed. The two main characteristics of the perturbation are[17]:

- a pair of strong counter-rotating vortices, indicated by the streamlines in a cross section
- a strong deformation of the former well-developed laminar velocity profile.

Due to viscous effects, the swirl as well as the non-uniform axial profile decreases in strength in the straight pipe section downstream of the bend. The two 90° bends in plane has the same characteristics with one 90° bend.

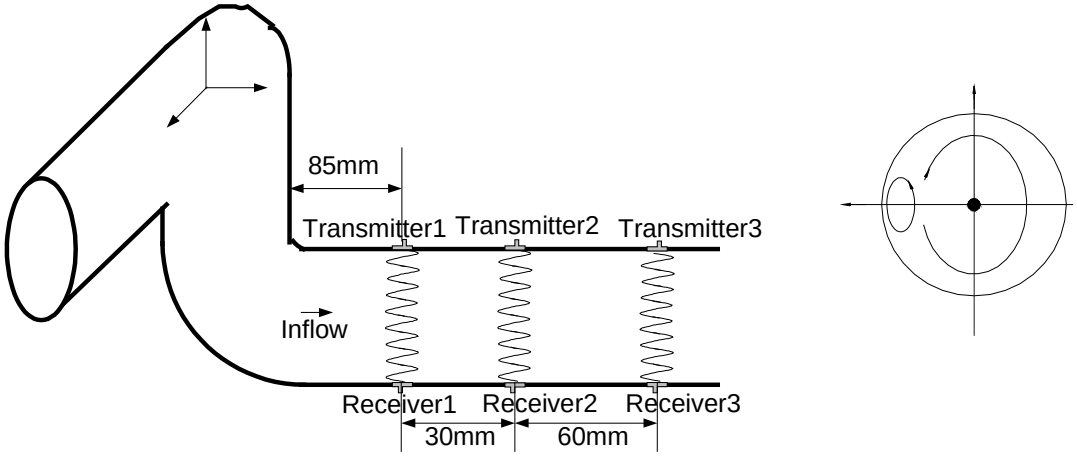

Fig. 9-4 Two 90° bends out of plane

In contrast to the 90° bend, the double bend out of plane generates a single vortex shown in Fig.9-4. Close to the bends the vortex core spirals around the pipe axis. For longer distances in straight pipes the vortex core gradually aligns with the pipe axis and the intensity of the swirl decreases. The complete decay process can extend over several ten pipe diameters.

9.4 Vortex measurement in disturbed flow

Windorfer has made some initial research in this field[12]. But what he studied was centered only on the conventional setup. This section mainly studies the vortex measurement in disturbed flow with unconventional-setup triangular bluff bodies. The conventional setup is only once described in the next to show the advantages of unconventional setup over it.

9.4.1 One bend

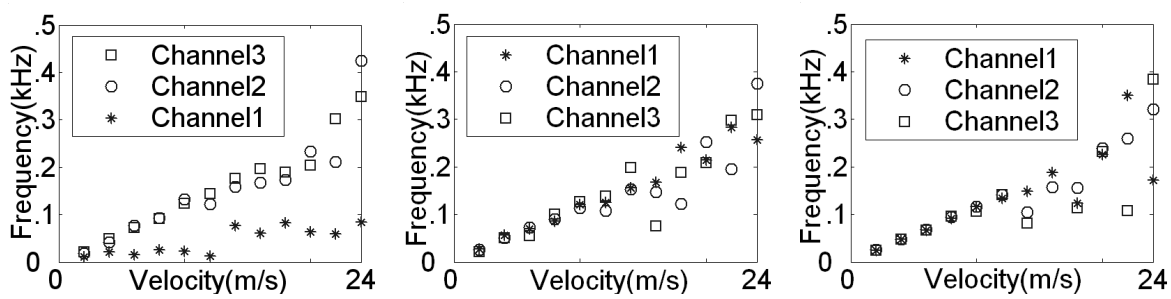

Fig.9-5 Frequency-velocity relation measured in unconventional setup one 90° bend with triangle24-72(left), triangle24-48(middle) and triangle24-24(right)

It was pointed out in [12] that velocity measurement in disturbed flow using triangle bluff bodies is impossible. This conclusion was drawn according to the conventional setup. As to unconventional setup, it can be easily seen from Fig.9-5 that triangle bluff bodies function fairly well at low velocities in disturbed flow. This can be explained by the reshaping ability of the unconventional-set triangle bluff bodies. This kind of setup has quite similarities with the V-cone described above. With the increasing velocity, the reshaping ability becomes worse because of too strong disturbance. But with these bluff bodies, the measurement result is fairly good in the velocity range which is most widely used in industry. The channel 1 of triangle24-72 does not yield good results because the channel one is only 9mm from the vortex shedding area which is not stable yet. The distance is shown in Fig.9-6.

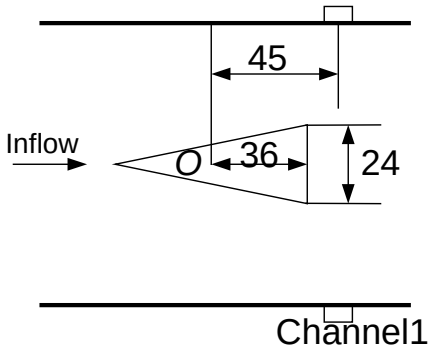

Fig. 9-6 Distance between channel 1 and the shedding point for triangle24-72

9.4.2 Two 90° bends in plane

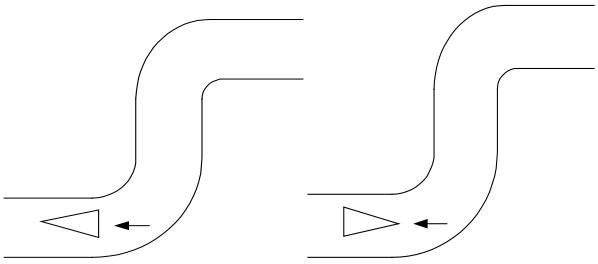

Fig. 9-7 Conventional setup(left) and unconventional setup(right) with two 90° bends in plane

The bluff body is installed directly behind the bend both in conventional setup and unconventional setup. A triangular bluff body whose width is 24mm and length is 72mm is

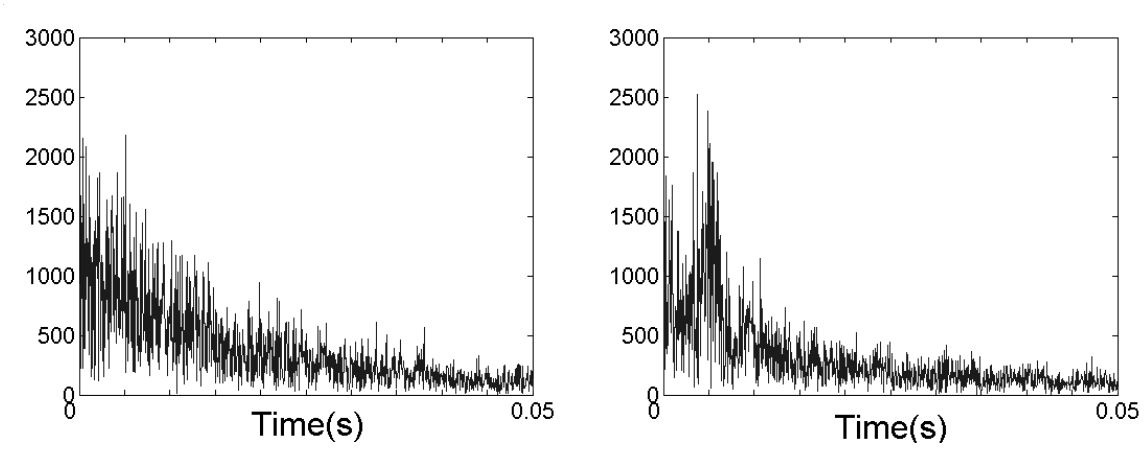

Fig. 9-8 Spectrum of signal at 10m/s in conventional setup(left) and unconventional setup(right)

first tried. Fig.9-8 shows the spectrum of the measured signal at 10m/s in conventional setup and unconventional setup. Apparently there is much more noise in conventional setup than in unconventional setup. This noise exists almost at each velocity and therefore leads to worse measurement results as shown in Fig.9-9.

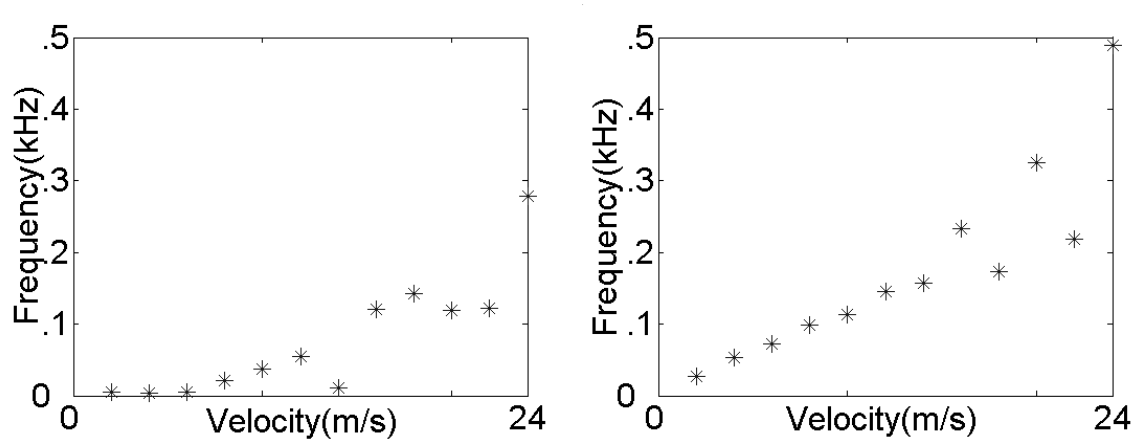

Fig. 9-9 Frequency-velocity relation in conventional setup(left) and unconventional setup(right)

The noise is generated by the singularity of the flow pipe. The velocity measurement with conventional-set triangle bluff body is almost impossible from Fig.9-9. In the case of unconventional setup, the quasi-contour-shaped surface directs the flow without impacting it against an abrupt unstreamlined surface. For this reason, the unconventional-set triangle bluff body can, to some extent, reshape the velocity profile so that it becomes closer to the fully developed flow in which the flow meter works fairly well. But even in unconventional setup, the measured result is not so ideal at high velocities due to the much too strong turbulence. The triangle bluff body is not v-cone which can reshape the rotating flow profile at high velocity. In the present case, the velocity range is from 2m/s to 15m/s which is the most widely used velocity range in flow industry.

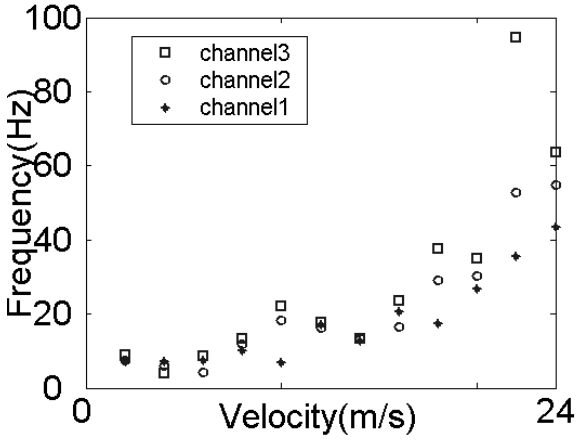

Fig. 9-10 Frequency-velocity relation in unconventional setup in plane (triangle4-12)

In addition, to reach the aim of reshaping the disturbed asymmetrical velocity profile, the bluff body must be of relatively bigger size. This conclusion is drawn from the other experiments with relatively smaller bluff bodies. A triangle bluff body with a width of 4mm is tested and is found

that this does not function in flattening the flow profile. This is displayed by Fig.9-10 where different shapes stand for measurement result through different channels which have different distances from the bend. No matter which channel is used, the characteristic line between frequency and velocity is not good. This indicates the small bluff body can not reshape the flow profile much enough so as to obtain fully or quasi-fully developed flow. The vortices generated by bluff body itself are very small relative to those caused by bend. So they are immersed into the strong disturbance so that they can't be detected. This can be seen from the different signals in fully developed flow and disturbed flow shown in Fig.9-11.

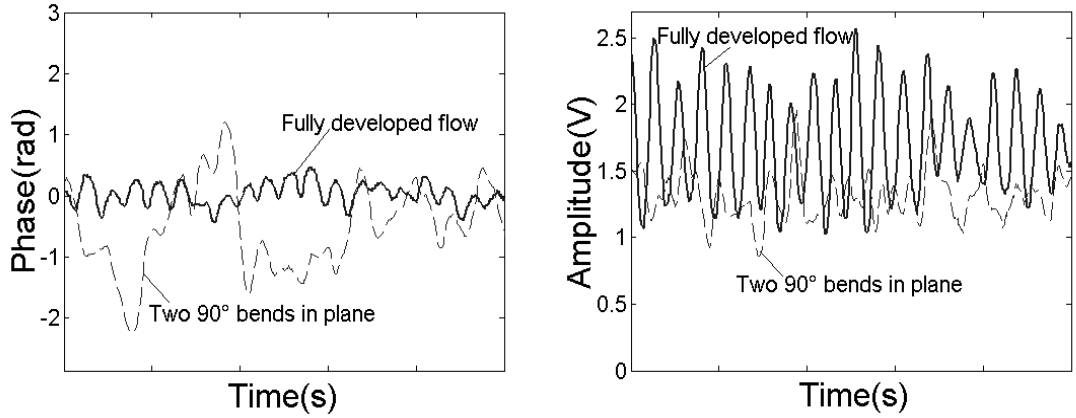

Fig. 9-11 Comparison of phase signal(left) and amplitude signal(right) in fully developed flow and disturbed flow with triangle4-12

The phase signal is severely disturbed in the disturbed flow. The smaller vortices generated by bluff body itself can not be displayed by the phase signal detected. That is, the characteristic sinusoidal signal disappeared in disturbed flow. The amplitude signal, although less disturbed, has a much smaller amplitude which can not be the real signal correctly modulated by the bluff body generated vortices. But for bigger bluff bodies, triangle24-72 for example, the signals are not disturbed so severely because of the robustness of the big vortices, see Fig.9-12. These figures also confirm the conclusion described in chapter 6. That is, smaller bluff body leads to more amplitude modulation while bigger bluff body generates more phase modulation.

Fig.9-12 shows only the signal received at velocities smaller than 15m/s. The signals at high velocities will be distorted severely resulting in no good measurement results due to the much too strong disturbance.

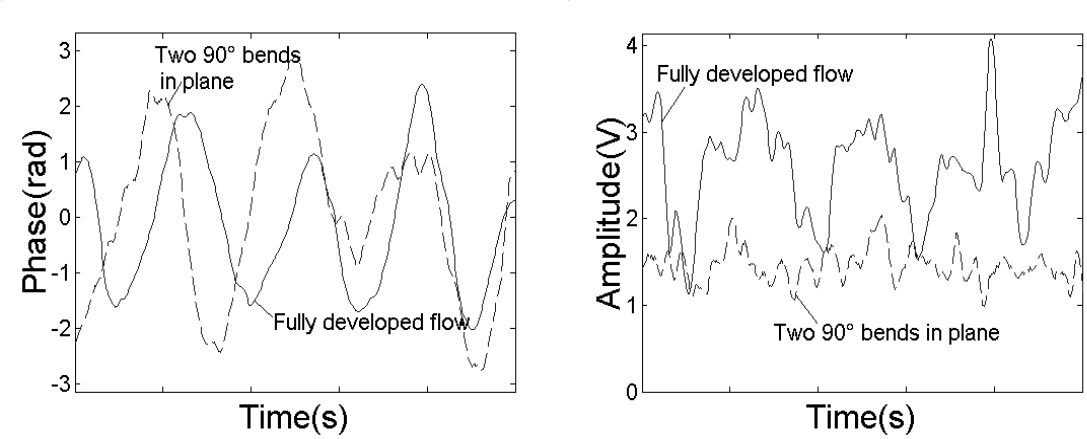

Fig. 9-12 Comparison of phase signal(left) and amplitude signal(right) in fully developed flow and disturbed flow with triangle24-72

Some other bluff bodies with the same width of 24mm but with different ratio of width to length were also investigated in order to find out the bluff body possessing the best flow profile reshaping ability which is shown in Fig.9-13.

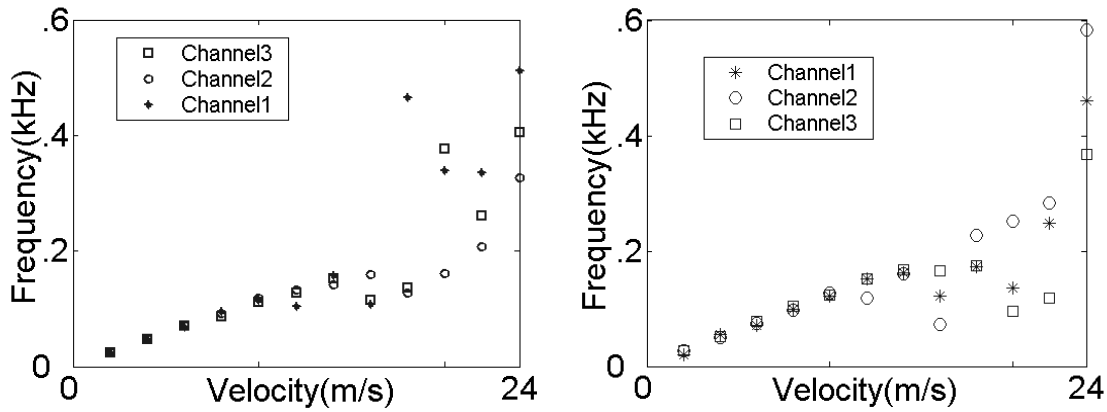

Fig. 9-13 Frequency-velocity relation in unconventional setup inplane of triangle24-24(left) and triangle24-48(right)

But from Fig.9-13, there is not a bluff body which brings out much better measurement results. All the bluff bodies investigated have the reshaping ability during the low velocity range but have no such a capability at higher velocities.

9.4.3 Two 90° bends out of plane

To avoid repeat of the content in [12], only the result of unconventional setup is described in the following. Triangle bluff bodies with the same width of 24mm but different length are studied in the disturbed flow caused by two 90° bends out of plane. The characteristic lines between the vortex shedding frequency and velocity are shown in Fig.9-14.

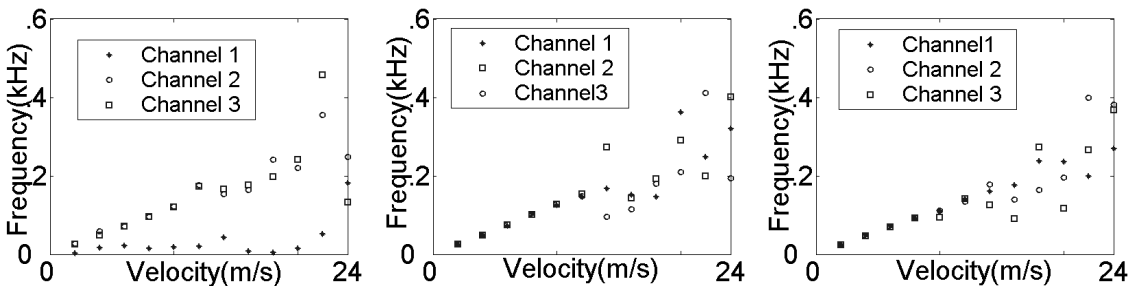

Fig. 9-14 Frequency-velocity relation measured in unconventional setup two 90° bends out of plane with triangle24-72(left), triangle24-48(middle) and triangle24-24(right)

In the disturbed vortex flow measurement, the triangular bluff body should be unconventionally set in the pipe flow so that the flow meter functions well in the low velocity range. At the same time, the size of the bluff body should be relative big. According to large amount of experiments with different bluff bodies, the width of the bluff body must not be smaller than 20mm for the pipe with a diameter of 100mm.

9.5 Cross correlation measurement in disturbed flow

9.5.1One 90° bend

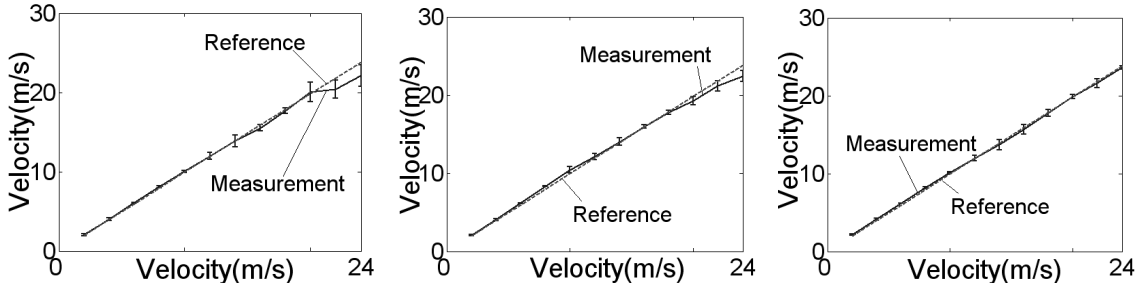

a) b) c)

Fig. 9-15 Measurement result using ccf in disturbed flow caused by one 90° bend
a)channel1,3 b)channel 1,2 c)channel 2,3

In the work of Niemann[10], the cross correlation measurement in disturbed flow is studied. Different angles of bend are thoroughly studied. This section pays more attention to the different distances between the two channels which are cross correlated. The same distance pattern is investigated combined with three pipe singularities. The first channel is installed directly behind the 90° bend. The schematic of the setup is shown in Fig.9-3. The measured velocity by means of each two channels is studied and shown in Fig.9-15.

The measured velocity corresponds with the reference velocity fairly well especially the result through channel 2 and channel 3. But with the increasing velocity, the disturbance becomes stronger, which causes the increasing error to the measurement. The linearity of the measured velocity using different pairs of channels indicates the double vortices caused by this 90° bend disappear quickly or slowly. It can be seen from Fig.9-15 the vortices disappear slowly.

9.5.2 Two 90° bends in plane

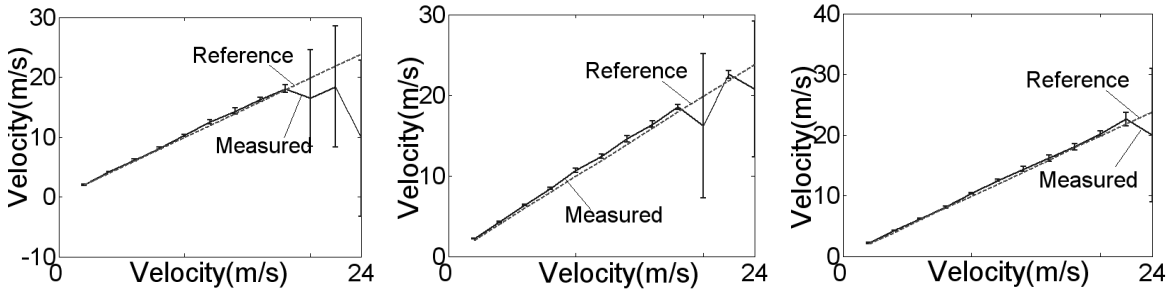

Fig. 9-16 Measurement result using ccf in disturbed flow caused by two 90° bends in plane
a)channel1,3 b)channel 1,2 c)channel 2,3

The measured results of cross correlation measurement in the disturbed flow caused by two 90° bends in plane are shown in Fig.9-16. It can be clearly seen that the disturbances are stronger than that with only one 90° bend. But this method works also fairly well in the low velocity range which is most widely used in industry.

9.5.3 Two 90° bends out of plane

Fig.9-17 shows the measured results with the cross correlation method in the disturbed flow generated by two 90° bends out of plane. Obviously, the disturbances in this case are much too strong for cross correlation method to get correct and precise measurement results.

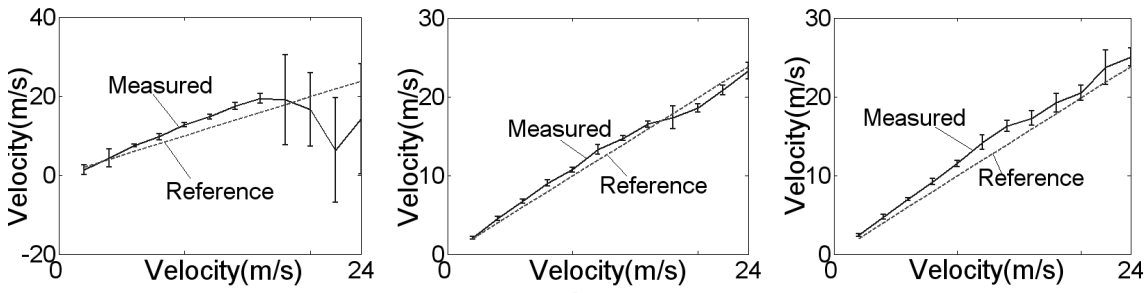

Fig. 9-17 Measurement result using ccf in disturbed flow caused by two 90° bends out of plane
a)channel1,3 b)channel 1,2 c)channel 2,3

9.6 Uncertainty analysis

The uncertainty of the corresponding measurement is illustrated in Fig.9-18 and compared with that in fully developed flow.

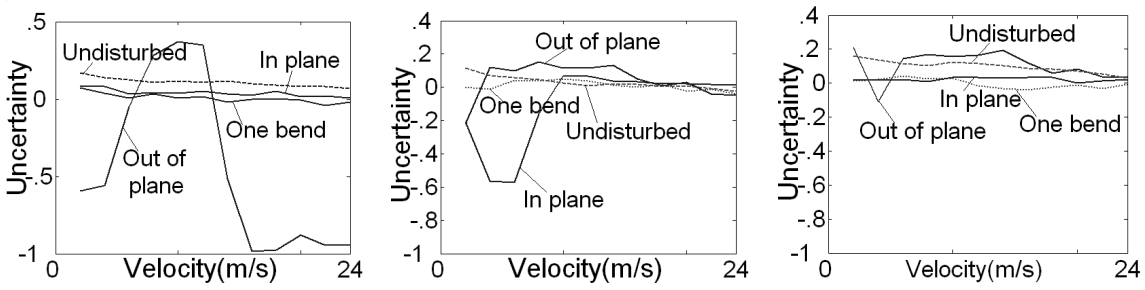

a) b) c)

Fig. 9-18 Comparison of measurement uncertainty
a)channel1,3 b)channel 1,2 c)channel 2,3

Fig. 9-18 indicates that the uncertainty of the measured velocity is dependent on the distance between the two channels from which the signals are cross correlated. Channel 1 and 3, whose distance is 90mm, results in lower uncertainty which is around 0.1 for the disturbed flow caused by one 90 degree bend and two 90 degree bends in plane. Principly, what is measured in fully developed flow is the linear velocity instead of area velocity because the ultrasonic beam travels only through the diameter. This is also one source of the systematic error. One method to avoid this error is to use multipath measurement. The other is rotating the flow. With the disturbed flow caused by the bend, the flow rotates and moves forward. This partially compensates the systematic error. Therefore the uncertainty is smaller. But for the disturbed flow caused by two 90 degree bends out of plane, the uncertainty is not lower but much higher. This kind of disturbed flow is not suitable for the cross correlation measurement independent off the distance between the two channels. The uncertainty will have more fluctuation by shortening the distance between the two channels for the disturbed flow caused by one bend and two 90 degree bends in plane. This can be seen from the lower picture in Fig.9-18 with distance of 30mm. The uncertainty provided by channel 2 and channel 3 whose distance is 60mm is also a little bit higher. This suggests 90mm is the best distance of the three for the cross correlation measurement in disturbed flow.

10 Summary

Two types of flow meter by means of ultrasonic are thoroughly researched in this work. They are cross correlation measurement and vortex flow measurment, respectively.

It aims to improve the flow measurement precision by signal processing according to the unique characteristics of cross correlation measurement and the techniques applied in vortex measurement.

Analytic signal is used to model the complex modulation based on which the Hilbert Transform is introduced. The reconstructed signals through software Hilbert Transform not only keep a good result dealing with phase modulation part but also yield fairly good results when dealing with amplitude modulation part in cross correlation measurement. It was believed that the applitude modulation signal is not applicable for measurement[10-13], which is a conclusion got in the case of the common Quadrature Amplitude Demodulation(QAD).

The other kind of demodulation method is Extended Kalman Filter. It is not only used in phase demodulation but also in amplitude demodulation. This method, taking advantage of the same information required when using QAD, yields better demodulation results with less noise and overcomes the disadvantages such as phase jumping at high velocities using QAD. Kalman Filter is applied both in fully developed flow and in disturbed flow. It shows good performance in eliminating the phase climbing problem in disturbed flow measurement. Different forms of Kalman Filter are discussed in details. More types of Kalman filter could be developed from pure mathematical viewpoint. But due to the increasing data processing burden for the computer, this method should be limited for the online measurement.

Due to the fact that the amplitude modulation is strong in vortex measurement, an analog signal processing method is produced. This method, from another view aspect, also proves the modulation characteristics in cross correlation measurement. That is, the phase modulation is more dominant in cross correlation measurement.

The combination of vortex with ccf provides a simple method to eliminate the systematic error which exists in the pure cross correlation measurement. It also provides a self-monitoring measurement system.

The inclination of bluff body in vortex flow measurment is a subject worth studying. Large amounts of experiments indicate that the inclination of bluff budy does influence the measurement although a cogent theoretical explanation has not been found yet due to the complexity of flow itself. But a general conclusion can be drawn that the conventional-set bluff body and the bigger bluff body are more robust to the inclination. The unconventional-set bluff body and smaller bluff body generate higher sensitivity but has less robustness to the inclination.

Disturbed flow measurement is always a difficult problem in flow industry. The two types of flowmeter referred to above are both studied under the disturbed flow caused by three kinds of pipe configurations. For vortex flowmeter, only large size and unconventional-set bluff body is available to measure the velocity between 2m/s to 15m/s in the disturbed flow measurement. For cross correlation flowmeter, the measurement results are good in the low velocity range in the disturbed flow formed by one 90° bend and by two 90° bends in plane. Due to the strong disturbance in the flow formed by two 90° bends out of plane, the measurement error becomes larger.

The above conclusions drawn from the research are suitable for the single phase gas pipe flow. Although a fairly large part of the fluid to be measured in practice belongs to more-phase fluid which is to be further investigated, yet this work is instructive for the single phase flow measruement. Owing to the inherent characteristics and advantages of the ultrasonic approach, no doubt ultrasonic flow measurement will have its unbeatable position in the flow measurement industry.

11 Literature

[1] DeCarlo, J.P.: Fundamentals of flow measurement, Publishers Creative Services, 1984.

[2] http://www.findarticles.com/cf_dls/m0LTJ/1_76/112984820/p1/article.jhtml

[3] http://www.nciweb.net/v-cone.htm

[4] Bentley, J.: Principles of measurement systems, Longman, 1983.

[5] Balzer, D.: Online-Demodulation stark gestörter winkelmodulierter Signale mit dem Extended Kalman-Filter, Dissertation, Universität Siegen, 1999.

[6] Upp, E. L.: Fluid, flow measurement, Gulf publishing company, 1993.

[7] Skwarek, V., Hans, V.: Multipath cross-correlation flowmeters, Proceedings of IMEKO 2000.

[8] Beck, M. S.: Cross correlation flowmeters: their design and application. Bristol/UK: IOP Publishing, 1987.

[9] Poppen, G.: Durchflußmessung auf der Basis kreuzkorrelierter Ultraschallsignale. PhD-thesis: University of Essen, Aachen: Shaker, 1997.

[10] Niemann, M.: Signalverarbeitung in der Ultraschall-Durchflußmessung, Dissertation, University of Essen, Shaker publisher, 2002.

[11] Filips, C.: Ultraschallsignalverarbeitung bei Korrelations-und Vortexverfahren zur Durchflussmessung, Dissertation, University of Essen, Cuvillier Publisher, 2003.

[12] Windorfer, H.: Optimierung von Wirbelfrequenz-meßgeräten mit demodulierten Ultraschallsignalen, Dissertation, University of Essen, Shaker Publisher, 2001.

[13] Skwarek, V.: Verarbeitung modulierter Ultraschallsignale in Ein- und Mehrpfadanordungen bei der korrelativen Durchflußmessung, Dissertation, University of Essen, Shaker Publisher,Aachen, 2000.

[14] Baker, R. C.: An introductory guide to flow measurement, Mechanical Engineering Publications Limited, London,1989.

[15] Rettich T.: Korrelative Ultraschall-Durchflußmessung auf der Basis turbulenter Strukturen. PhD-thesis: University of Essen, Düsseldorf: VDI, 1999.

[16] Randall R.B., Tech B.., B. A.: Frequency analysis. K. Larsen& S, Denmark, 1987.

[17] Hilgenstock A., Heinz M.: Numerical flow simulation as a tool for developing and calibrating ultrasonic flow meters. FLOMEKO'96, Beijing, 1996.

[18] Haykin, S.: Adaptive Filter Theory, 3rd Edition, Practice Hall Information and System Sciences Series, 1996.

[19] Walker, J.: The Vortex Meter Comes of Age. Endress+Hauser, Inc., 2000.

[20] Hans, V., Windorfer, H.: Comparision of pressure and ultrasound measurements in vortex flow meters. Measurement 33, p.121-133, 2003.

[21] Baker R.C.: Flow Measurement Handbook, University Press, Cambridge, 2000.

[22] Hans V., Poppen G., Lavante E.V., Perpeet S.: Interaction between vortices and ultrasonic waves in vortex shedding flowmeters, in: FLUCOME 97; Hayama; Proceedings, 1997.

[23] Skwarek H., Hans V.: An improved method for hardware-based complex demodulation. Measurement 29 (2) (2001) p.87-93.

[24] Hans V., Windorfer H., Perpeet S.: Influence of vortex structures on pressure and ultrasound in vortex flowmeters. Proceedings of IMEKO 2000, IC9, Wien, 2000.

[25] Hans V.: Digital processing of complex modulated ultrasound signals. ISMTII, Proceedings, p.291-296, Kairo, 2001.

[26] Otnes R.K., Enochson L.: Applied time series analysis, Wiley, New York, 1978.

[27] Bachmann W.: Signalanalyse, Vieweg, Braunschweig, 1992.

[28] Skwarek V., Hans V.: Low effort phase and amplitude detection in mixed modulated signals with hybrid demodulation techniques; Proceedings of IMEKO XV; Osaka, p. 127-134. 1999.

[29] Bernhard M.: An intelligent flowmeter fusing vortex frequency and vortex transit time measurements. IMEKO XIV Proceedings; Tampere, 1997.

[30] Stengel R. F.: Stochastic optimal control. New York, Wiley, 1986.

[31] Hans V.: Systemtheorie. Lecture manuscript, University of Essen, WS 2001/02.

[32] Hans V., Skwarek V.: Signal processing of ultrasound modulated by gas flow. IEEE Transactions on Instrumentation and Measurement, VOL. 51, No. 6, December 2002.

[33] Worch A.: A clamp-on ultrasonic cross-correlation flowmeter for two-phase flow, in 9th Int. Conf. Flow Meas. FLOMEKO, Lundt, Sweden, June 15-17, 1998, pp. 121-126.

[34] Schneider F., Peters F., Merzkirch W.: Quantitative analysis of the cross-correlation ultrasonic flow meter by means of system theory. Measurement Science and Technology, 14 (2003) 573-582.

[35] http://ccrma-www.stanford.edu/~jos/mdft/Analytic_Signal_Hilbert_Transform.html

[36] Hans V.: State and research results of ultrasonic gas flow measurement. 2nd ISIST Proceedings; Ji‘nan, China, 2002.

[37] Beck, M. S.: Powder and fluid flow measurement using correlation techniques. PhD thesis University of Bradford, 1969.

[38] Shannon, C. E.: Mathematical theory of communication – Part III. The Bell System technical Journal, pp. 623-656, vol. (27)/3, July 1948.

[39] Skwarek, V., Hans, V.: Modern principles of signal processing for analyzing properties of turbulent fluids. WISP 99, Budapest, Proceedings, 5-10, 1999.

[40] Filips C., Hans V.: Interaction between ultrasound and streaming fluid in vortex shedding flow metering. XVII IMEKO, Proceedings, Dubrovnik, Croatia, 2003.

[41] Strohrmann, G.: atp-Marktanalyse Durchfluß- und Mengenmeßtechnik (Teil 1). Atp, 36: 9-29, 7, 1994.

[42] Strohrmann, G.: atp-Marktanalyse Durchfluß- und Mengenmeßtechnik (Teil 2). Atp, 36: 9-29, 8, 1994.

[43] Williams, J.: Introduction to Fluid mechanics. PWS-Kent Publishing company, Boston, 2003.

[44] Tan S.M.: Linear Systems, The University of Auckland.

[45] Nikuradse, J.: Strömungsgesetze in rauhen Rohren. Berlin: VDI-Verlag, 1933.

[46] Palme F., Schrüfer E.: Berechnung der Signalleistung im Zeit- und Frequenzbereich. Teschnisches Messen 65,(10/98), 370-377, 1998.

[47] Wang Z.: Basic research on ultrasonic flowmeter. Dissertation. Northwestern Polytechnical University. Xi'an, 1997.

[48] Bundesamt für Wirtschaft: Erdgasimporte: Januar 2000. http://www.bawi.de/oo12bawp.html

Appendix

Matlab Code for Kalman Filter used for phase demodulation

```
function daten=EKF32func(realpart,imagpart,phase,anzahl,samplingrate)
y(1,:)=realpart;
y(2,:)=imagpart;
y(3,:)=phase;
Q=[.1 0;0 .1];
samplingrate=20000;
ny=0.158;
A=[1 samplingrate^-1;0 1];
x(:,1)=[y(3,1);0];
R=[1 0 -.1*sin(x(1,1));0 1 .1*cos(x(1,1));-.1*sin(x(1,1)) .1*cos(x(1,1)) .1];
xs(:,1)=[0 0]';
xtilde(:,1)=xs(:,1)-x(:,1);
K=(xtilde*xtilde');K(1,2)=0;K(2,1)=0;
Ainno=[x(1,1)+samplingrate^-1*x(2,1);x(2,1)];
predx(:,1)=Ainno;
predK=A*K*A'+Q;
Cinno=[cos(2*pi*ny*predx(1,1));sin(2*pi*ny*predx(1,1));2*pi*ny*predx(1,1)];
C=[-2*pi*ny*sin(2*pi*ny*predx(1,1)) 0; 2*pi*ny*cos(2*pi*ny*predx(1,1)) 0;2*pi*ny 0];
ytilde(:,1)=y(:,1)-Cinno;
G=predK*C'/[C*predK*C'+R];
predx(:,1)=predx(:,1)+G*ytilde(:,1);
K=(eye(2,2)-G*C)*predK;
Kalt=K;
x(:,1)=predx(:,1);
for n=2:anzahl-1
   x(:,n)=x(:,n-1);
   predK=Kalt;
   R=[1 0 -.1*sin(x(1,n));0 1 .1*cos(x(1,n));-.1*sin(x(1,n)) .1*cos(x(1,n)) .1];
   Ainno=[x(1,n)+samplingrate^-1*x(2,n);x(2,n)];
   predx(:,n)=Ainno;
   predK=A*predK*A'+Q;
   Cinno=[cos(2*pi*ny*predx(1,n));sin(2*pi*ny*predx(1,n));2*pi*ny*predx(1,n)];
   C=[1-2*pi*ny*sin(2*pi*ny*predx(1,n)) 0; 2*pi*ny*cos(2*pi*ny*predx(1,n)) 0;2*pi*ny 0];
   ytilde(:,n)=y(:,n)-Cinno;
   K=predK*C'/[C*predK*C'+R];
   predx(:,n)=predx(:,n)+G*ytilde(:,n);
   K=(eye(2,2)-K*C)*predK;
   Kalt=K;
   x(:,n)=predx(:,n);
end
x(:,anzahl)=x(:,anzahl-1);
daten=x(:,:);
```

Matlab Code for EKF24

```
function daten=kalmanfilter24(realpart,imagpart,anzahl,samplingrate)
y(1,:)=realpart;
y(2,:)=imagpart;
Q=[0 0 0 0;0 1 0 0;0 0 0 0;0 0 0 0.001];
R=[1 0;0 1];
ny=.158;
Fn=[1 1 0 0;0 1 0 0;0 0 1 1;0 0 0 1];
x(:,1)=[y(1,1);y(2,1);0;0];
xs(:,1)=[0 0 0 0]';
xtilde(:,1)=xs(:,1)-x(:,1);
K=(xtilde*xtilde');K(1,2)=0;K(1,3)=0;K(1,4)=0;K(2,1)=0;K(2,3)=0;K(2,4)=0;K(3,1)=0;K(3,2)=
0;K(3,4)=0;K(4,1)=0;K(4,2)=0;K(4,3)=0;%this is K(0)
Fx=[x(1,1)+1*x(2,1);x(2,1);x(3,1)+1*x(4,1);x(4,1)];
predx(:,1)=Fx;
predK=Fn*K*Fn'+Q;
Cxn=[cos(2*pi*ny*predx(1,1))+predx(3,1); sin(2*pi*ny*predx(1,1))+predx(3,1)];
C=[1-2*pi*ny*predx(1,1) 0 1 0;2*pi*ny*predx(1,1) 0 1 0];
ytilde(:,1)=y(:,2)-Cxn;
G=predK*C'/[C*predK*C'+R];
predx(:,1)=predx(:,1)+G*ytilde(:,1);
K=(eye(4,4)-G*C)*predK;
Kalt=K;
x(:,1)=predx(:,1);
for n=2:anzahl-1
   x(:,n)=x(:,n-1);
   predK=Kalt;
   Fx=[x(1,n)+1*x(2,n);x(2,n);x(3,n)+1*x(4,n);x(4,n)];
   predx(:,n)=Fx;
   predK=Fn*predK*Fn'+Q;
   Cxn=[cos(2*pi*ny*x(1,n))+x(3,n);sin(2*pi*ny*x(1,n))+x(3,n)];
   C=[-2*pi*ny*sin(2*pi*ny*x(1,n)) 0 1 0;2*pi*ny*cos(2*pi*ny*x(1,n)) 0 1 0];
   ytilde(:,n)=y(:,n+1)-Cxn;
   G=predK*C'/[C*predK*C'+R];
   predx(:,n)=predx(:,n)+G*ytilde(:,n);
   K=(eye(4,4)-G*C)*predK;
   Kalt=K;
   x(:,n)=predx(:,n);
end
x(:,anzahl)=x(:,anzahl-1);
daten=x(:,:);
```

Code for the Fast Fourier Transform realization of Hilbert Transform

```
function s = hilbert(x)
   [r_x, c_x] = size (x);
        if r_x == 1
                x = x.';
   end
        [r_x, c_x] = size (x);
        n=r_x;
        if(gcd(r_x,2)==1)
                n=r_x + 1;
   end
        sft = fft(real(x),n);
        w = [0; -i*ones(fix((n-1)/2),1); 0; i*ones(fix((n-1)/2),1)];
        sw = sft.*w;
        s = ifft(sw);
```